Mechanistic and structural analyses of different non-coding RNAs in bacteria

Dissertation

zur

Erlangung des Doktorgrades

der Naturwissenschaften

(Dr. rer. nat.)

dem

Fachbereich Pharmazie

der Philipps-Universität Marburg

vorgelegt von

Diplom-Chemikerin

Karen Köhler

aus Marburg

Marburg an der Lahn; Juli 2014

Vom Fachbereich Pharmazie

der Philipps-Universität Marburg

als Dissertation am 18.08.2014 angenommen.

Erstgutachter: Prof. Dr. rer. nat. Roland K. Hartmann

Zweitgutachter: Prof. Dr. rer. nat. Jens Wöhnert

Tag der mündlichen Prüfung am 18.08.2014

Hochschulkennziffer: 1180

Table of Contents

Summary

RNase P RNA and 6S RNA are two non-coding RNAs found in essentially all (RNase P RNA) or most (6S RNA) known bacteria. The tRNA maturation function of RNase P is highly essential but until now the catalytic mechanism is not fully understood. We started to investigate the two-metal-ion-based mechanism via dynamical NMR measurements. For this purpose, we used a shortened variant of the *Escherichia coli* (*E. coli*) RNase P RNA (~370 nt) which lacks most of the specificity domain (*E. coli* RNase P RNA catalytic domain termed Ecat) to minimize the amount of NMR signals. Furthermore, we designed several hairpin-like minimal substrates containing a 5'-leader to determine nucleotides (substrate and Ecat) that are involved in the catalytically process. Due to the fact, that Ecat lost the function to cleave a substrate alone, the *E. coli* RNase P protein (C5-protein) was essential for the reaction. Here i) the homogeneity of the Ecat variant ii) the stability of C5-protein at room temperature and iii) the cleavability of the minimal substrates was tested. Further investigations on the usability of the minimal substrates for NMR measurements were performed.

6S RNA is a bacterial small non-coding RNA with a length of approximately 200 nt. First described in *E. coli* it was later detected in all branches of the bacterial kingdom [Barrick *et al*., 2005]. Among them the well-known model organisms *E. coli* and *B. subtilis* (*Bacillus subtilis*), but also extremophilic organisms such as the *Aquificales* bacteria were predicted to harbor a 6S RNA. The function of 6S RNA remained elusive for decades. Nowadays it is known that 6S RNA is a transcriptional regulator, binding RNA polymerases (RNAP) containing the housekeeping sigma factor to inhibit gene expression upon transition into stationary growth phase [Wassarman and Storz, 2000; Beckmann, Hoch *et al.*, 2012]. Although 6S RNA is thought to compete with σ^{70} (*E. coli)* or σ^{A} (*B. subtilis*)- dependent promoters for binding to $\sigma^{A/70}$-RNAP by mimicking an open DNA promoter structure also promoters regulated by other sigma factors were found to be affected by a 6S RNA knockout [Wassarman, 2007]. When bound to RNAP 6S RNA is used as a template for the synthesis of short 'product' RNAs (pRNAs). While shorter pRNAs (~ 8-mers) dissociate from the complex, transcription of pRNAs exceeding a certain minimal length leads to a persistent rearrangement of the 6S RNA structure which results in the dissociation of 6S RNA:RNAP complexes [Beckmann and Hoch *et al.*, 2012; Steuten *et al.*, 2014].

A 6S RNA homolog was also identified in an experimental RNomics study based on a cDNA library derived from small RNAs expressed in the hyperthermophilic bacterium *Aquifex aeolicus* [Willkomm *et al.*, 2005]. *A. aeolicus* 6S RNA is predicted to form a canonical rod-shaped secondary structure with a central bulge region. The central bulge is flanked by two stem structures: i) the terminal or closing stem formed by the bases located at the 5'- and 3'-end of 6S RNA and ii) the internal stem arranged in a hairpin-like structure. Comprising only 163 nt and a G/C- ratio of ~ 61% this 6S RNA

exhibits the most stable structure among all known 6S RNAs. In this work the secondary structure of *A. aeolicus* 6S RNA and its structural change after pRNA transcription were investigated by NMR. NMR studies were performed on free 6S RNA as well as 6S RNA:pRNA hybrids, using a putative pRNA 15-mer previously found by deep sequencing analysis. Due to the fact that an maximal RNA size for NMR measurements is approx. 80 nt, the *A. aeolicus* 6S RNA was shortened either at the terminal stem (132-nt 6S RNA variant) or at both (terminal and internal) stem regions (85-nt 6S RNA variant). By analyzing these two shortened 6S RNA variants via NMR, we were able to verify formation of several predicted structural stem elements within the terminal and the internal stem, as well as predicted structural transitions upon pRNA binding. Additionally, the secondary structure of *A. aeolicus* 6S RNA was investigated by enzymatic and chemical structure probing to complement the NMR data in order to obtain a more fine-grained model of the RNA's solution structure. We could finally clarify that the free 6S RNA is formed as expected, whereas the solved structure of the 6S RNA:pRNA hybrid shows intense divergence to the prediction. First of all, we could show that the terminal stem remains solidly paired even after the pRNA-induced rearrangement of the 6S RNA structure. Moreover, hairpin formation in the 3´-central bulge (CB), which is known e.g. from *B. subtilis* 6S RNA, could not be detected. In line with the prediction we were able to prove the pRNA-mediated formation of the CB collapse helix.

Besides the structural investigation of 6S RNA we were interested in mechanistic aspects. To determine if *A. aeolicus* 6S RNA shares hallmark features with canonical 6S RNAs we employed the RNAP from *B. subtilis* which is well investigated in terms of 6S RNA binding and pRNA transcription [Beckmann *et al.*, 2011; Beckmann, Hoch *et al.*, 2012; Burenina *et al.*, 2014]. Using *B. subtilis* RNAP for *in vitro* transcription, the 6S RNA of *A. aeolicus* was demonstrated to serve as a template for pRNA transcription and to undergo the structural rearrangement upon pRNA hybridization comparable to already known 6S RNAs of *E. coli* and *B. subtilis*. However, inhibiting formation of the central bulge collapse helix leads to inefficient 6S RNA:pRNA release from the RNAP complex, in *A. aeolicus* as well as in *B. subtilis*. This observation suggests that an efficient release of 6S RNA:pRNA hybrids from the complex with RNAP can only be induced by pRNAs whose transcription is initiated at their canonical position in 5'-CB.

Zusammenfassung

RNase P RNA und 6S RNA sind zwei nicht-codierende RNAs die im Grunde in allen (RNase P RNA) oder in den meisten (6S RNA) bekannten Bakterien gefunden wurden. Die Funktion der tRNA Maturation von RNase P ist äußerst wichtig, aber bis jetzt noch nicht vollständig verstanden. Wir begannen den Zwei-Metall-Ionen-Mechanismus mittels NMR Messungen zu untersuchen. Zu diesem Zweck verwendeten wir eine verkürzte Variante der *Escherischia coli* (*E. coli*) RNase P RNA (~370 nt) welcher der größte Teil der Spezifitäts-Domaine fehlt (*E. coli* RNase P RNA katalytische Domain genannt Ecat), um die Menge an NMR-Signalen zu minimieren. Weiterhin haben wir einige Haarnadel ähnliche Minimalsubstrate entworfen, die eine einzelsträngige 5'-Leitsequence beinhaltet, um die Nukleotide (Substrate und Ecat), die an dem katalytischen Prozess beteiligt sind, zu ermitteln. Da Ecat die Funktion ein Substrat ohne die Hilfe zu binden und somit zu spalten verloren hat, musste das *E. coli* RNase P Protein (C5-Protein) zur Reaktion zugesetzt werden. Wir testeten i) die Homogenität der Struktur der Ecat Variante, ii) die Stabilität des C5-Proteins bei längerer Aufbewahrung bei Raumtemperatur und iii) die Effektivität der Spaltung der verschiedenen Minimalsubstrate. Weiter wurde auch die Verwendbarkeit der Minimalsubstrate für folgende NMR-Messungen getestet.

6S RNA ist eine bakterielle kleine, nicht-codierende RNA mit einer Länge von ca. 200 nt. Zum ersten Mal beschrieben in *E. coli* wurde 6S RNA später in allen Bereichen der Bakterienwelt gefunden [Barrick *et al.*, 2005]. Unter ihnen befinden sich die Modellorganismen *E. coli* und *B. subtilis,* aber ebenso extremophile Organismen wie *Aquificales* Bakterien wurde der Besitz einer 6S RNA vorausgesagt. Die Funktion der 6S RNA blieb jahrzehntelang unbekannt. Heutzutage ist bekannt, dass 6S RNA die Transkription reguliert, indem sie mit der RNA-Polymerase (RNAP) interagieren, die die Enzym-eigene Sigma Untereinheit enthält. Diese ist für die Genexpression beim Übergang in die stationären Phase zuständig, welche durch die Bindung an die 6S RNA inhibiert wird [Wassarman und Storz, 2000; Beckmann und Hoch *et al.*, 2012]. Obwohl angenommen wird, dass 6S RNA mit σ^{70} (*E. coli*) oder σ^{A} (*B. subtilis*) abhängige DNA-Promotoren um die Bindung an die $\sigma^{A/70}$-RNAP konkurriert, indem sie eine offene DNA Promotor Struktur imitiert, wurden auch Promotoren, die von anderen Sigma-Faktoren reguliert werden, gefunden, die durch 6S RNA Deletion beeinflusst werden [Wassarman, 2007]. Wenn 6S RNA an die RNAP gebunden ist, wird sie als Matrize zur Transkription kurzer ´Produkt' RNAs (pRNAs) verwendet. Während kürzere pRNAs (~ 8-mere) vom Komplex dissoziieren, erreicht die pRNA während der Transkription durch Zugabe frischem Mediums (erneute exponentielle Phase) eine minimale Länge, die zu einer Umlagerung der 6S RNA Struktur führt. Diese wiederum initiiert die Ablösung der 6S RNA:pRNA Hybridstruktur aus dem 6S RNA:RNAP Komplexes [Beckmann und Hoch *et al.*, 2012; Steuten *et al.*, 2014].

Ein 6S RNA Homolog wurde in einer in einer cDNA Bibliothek kleiner RNAs basierend auf einer experimentellen RNomics Studie in dem hyperthermophilien Bakterium *Aquifex aeolicus* identifiziert [Willkomm *et al.*, 2005]. Diese 6S RNA weist Berechnungen zur Folge die kanonische stäbchenartige Sekundärstruktur mit dem zentralen Bauch-Bereich auf. Der zentrale Bauch-Bereich ist von zwei

Stammstrukturen flankiert: i) der terminale oder Schluss-Stamm, der durch Basen des 5‘- und 3‘-Endes der 6S RNA geformt wird und ii) der interne Stamm mit einer Haarnadel ähnlichen Struktur. Mit nur 163 nt und einem G/C-Gehalt von ~ 61% dieser 6S RNA, weist die stabilste Struktur aller bekannten 6S RNAs auf. Diese Arbeit wurde durchgeführt um die Sekundärstruktur der freien *A. aeolicus* 6S RNA als auch die umgelagerte Struktur nach der 6S RNA:pRNA Hybridisierung mittels NMR zu bestimmen. Es wurden NMR Messungen an der freien 6S RNA als auch an der 6S RNA:pRNA hybridisierten Struktur durchgeführt. Dafür haben wir eine 15-nt pRNA gewählt, deren Sequenz wir in einer mittels Deep Sequencing identifiziert haben. Um eine möglichst kleine RNA (~80 nt; Größenlimit für NMR Messungen) vermessen zu können, wurden zwei durch Mutation verkürzte Varianten der *A. aeolicus* 6S RNA verwendet (132-nt Variante: Verkürzt durch Mutation des terminalen Stamms; 85-nt Variante: Verkürzt durch Mutation des terminalen und des internen Stammes). Wir konnten durch Vermessung dieser 6S RNA Varianten verschiedene vorhergesagte Stammregionen im terminalen und internen Stammbereich verifizieren und ebenso strukturelle Übergänge durch die pRNA Bindung. Zusätzlich haben wir zur Sekundärstrukturaufklärung enzymatischen und chemischen Sonden Experimenten durchgeführt, zum komplettieren der NMR Daten um ein fein-strukturiertes Model zu erhalten. Abschließend konnten wir klären, dass die freie 6S RNA Struktur geformt ist, wie zuvor *in* silico berechnet. Einige Ergebnisse wichen jedoch immens von den berechneten Vorhersagen ab, wie die Struktur des terminalen Stamms, der nach der pRNA-induzierten Umlagerung weiterhin geschlossen vorliegt. Außerdem konnte keine Ausbildung einer Haarnadelstruktur am 3‘-zentralen Bauch (CB) in der Hybridstruktur, bekannt von z.B. *B. subtilis* 6S RNA, aufgedeckt werden. In Einklang mit der Berechnung konnten wir den pRNA vermittelten Kollaps des zentralen Bauch-Bereiches (CBC) mit einhergehender Bildung der CBC-Helix bestätigen.

Neben der Strukturaufklärung waren wir ebenfalls an der Funktion dieser 6S RNA interessiert. Um herauszufinden, ob die *A. aeolicus* 6S RNA die typischen Funktionen einer kanonischen 6S RNA aufweist, verwendeten wir die in Hinsicht auf 6S RNA Bindung und pRNA Transkription gut untersuchte *B. subtilis* RNAP [Beckmann *et al.*, 2011; Beckmann, Hoch *et al.*, 2012; Burenina *et al.*, 2014]. Durch Verwendung der *B. subtilis* RNAP konnte gezeigt werden, dass *A. aeolicus* 6S RNA (132 nt) als Matrize zu pRNA Transkription dient und eine strukturelle Umlagerung vergleichbar zu bekannten 6S RNAs von *E. coli* und *B. subtilis* induziert wird. Indes führt die Inhibition der CBC-Helix-Bildung sowohl in *A. aeolicus* als auch in *B. subtilis* zu einer ineffizienten Ablösung des 6S RNA:pRNA Hybrids von der RNAP. Diese Beobachtung suggeriert, dass eine effektive Ablösung des 6S RNA:pRNA Hybrids aus dem Komplex mit RNAP nur durch pRNAs induziert werden kann, deren Transkription an der kanonischen Position des 5‘-CB gestartet wird.

1. Introduction

1.1 Macromolecules of life

Biological macromolecules include the classes of polysaccharides, lipids, deoxyribonucleic acid (DNA), ribonucleic acid (RNA) and proteins. These molecules fulfill functions in all living organisms. While DNA stored and encodes the genetic information, RNA is known to form manifold structures and fulfills reams of functions. Proteins catalyze sumless biochemical reactions e.g. utilize chemical energy to carry out mechanical work, to sustain neural functions, vision and many other processes [Berg, Tymoczko and Stryer, 2007].

1.2 RNA

The primary function of RNA is the transcription of the encoded information given by DNA into RNA to be able to translate this information into proteins. But also transfer, ribosomal, regulatory and catalytically RNAs and many more are present in all organisms. Because of the normally single strand nature of RNA, they are able to form an enormous number of secondary and three-dimensional structures, which are often responsible for the function of the specific RNA.

1.3 Non-coding RNAs in Bacteria

Functional RNA molecules that are not translated into proteins are called non-coding RNAs (ncRNAs). The term small RNAs (sRNAs) is often used for short bacterial ncRNAs. To the group of these ncRNAs belong functionally important RNAs such as transfer RNAs (tRNAs; adaptor molecule between mRNA and protein) and ribosomal RNAs (rRNAs; catalyzing the translation of a nucleotide sequence into its encoded protein) as well as e.g. snoRNAs, microRNAs, siRNAs as well as the almost ubiquitous RNase P RNA. This results in a heterogeneous group of RNAs which act by diverse mechanisms to regulate eukaryotic and bacterial cell physiology. In bacteria, external influences like thermal differences or lack of nutrients necessitate an adaption of intracellular reactions to ensure cell survival. The majority of bacterial sRNAs affect cell viability via acting on transcriptional and translational initiation or by regulating post-transcriptional events such as RNA decay [Waters and Storz, 2009; Repoila and Darfeuille, 2009]. CRISPR RNAs take part in innate immunity responses to protect prokaryotic cells from infection e.g. by viruses [Karginov and Hannon, 2010]. Other ncRNAs form chimeras with protein-coding sequences for example riboswitches that are regulatory segments of mRNAs that bind small ligands to directly regulate their own activity in RNA metabolism [Vitreschak *et al.*, 2004]. Another group of ncRNAs

binds in *cis* (acting from the same molecule; intramolecular) as antisense transcripts to their target RNAs, whereas other ncRNAs, e.g. RNase P, are transcripts that act in *trans* to regulate or process other target RNAs. Nevertheless some ncRNAs like 6S RNA interact directly with proteins in this case RNAP.

1.4 RNase P

RNase P is a ribonucleoprotein consisting of a single catalytic RNA subunit and one or more protein components. The ratio of RNA to protein depends on the domain of life (Bacteria, Archaea or Eukarya) (Figure 1. 1). In 1971 RNase P was first isolated from *E. coli* [Altman and Smith, 1971]. Bacterial RNase P consists of one RNA subunit with a size of approx. 400 nt (~130 kDa) and one protein subunit of approx. 120 amino acids (~13.5 kDa), which are encoded by the genes *rnpB* and *rnpA*, respectively. Archaeal RNase P RNA is associated with four to five proteins, whereas eukaryotic RNase P RNA forms a complex with nine to ten proteins. Interestingly, also protein-only variants of RNase P have been found. The first was identified in human mitochondria and is composed of three proteins [Holzmann *et al.*, 2008]. More recently, a single-polypeptide RNase P enzyme (PRORP) was found in Ar*abidopsis thaliana* [Gobert *et al.*, 2010].

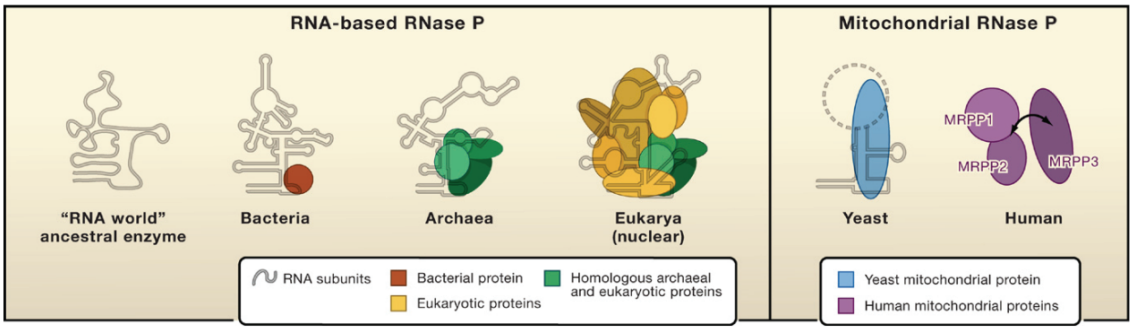

Figure 1. 1 The Evolution of RNase P. Starting from a hypothetical "RNA world" where RNase P is formed exclusively of RNA, increased numbers of protein are found for the RNase P holoenzyme from Bacteria to Archaea to Eukarya, accompanied with the more complex set-up of the organisms (left). The "RNA world" RNase P structure is unknown, but depict to be composed of the structural elements conserved in all forms of RNase P RNA. The composition of the mitochondrial RNase P for yeast (*Saccharomyces cerevisiae*) is shown. In various yeast mtRNase P enzymes also structural conserved elements of the RNA subunit are present. The dashed line indicates areas of the RNA structure which are not well defined. The protein-only human mitochondrial RNase P consists of the three proteins MRPP1, MRPP2 and MRPP3. (adapted from Walker and Engelke, 2008).

RNase P is responsible for the 5'-maturation of precursor tRNAs (ptRNAs), which is one of a number of post-transcriptional processes leading to functional tRNAs. The 5'-leader of ptRNAs is cleaved off in a hydrolysis reaction of the phosphodiester bond between nucleotides -1 and +1, resulting in cleavage products with 5'-OH and 3'-phosphate termini (Figure 1. 2).

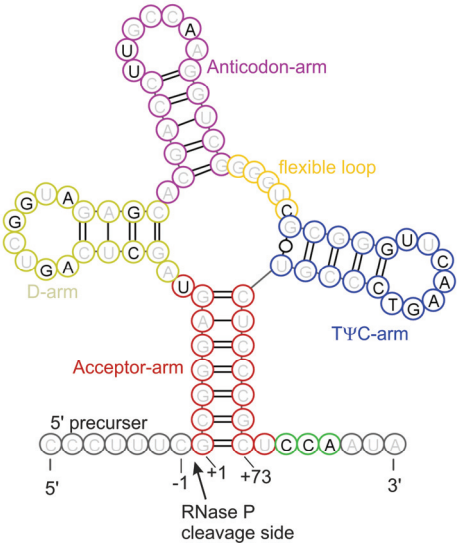

Figure 1. 2 Example of a precursor tRNA structure. Nucleotide +1 depicts the first nucleotide of the mature tRNA. The nucleotides marked in black indicate base conservation. Areas highlighted in different colors mark the different arms and loop regions of the tRNA.

Additionally other substrates like viral RNAs [Bothwell *et al.,* 1976; Mans *et al.*, 1990, Forti *et al.*, 1995; Hartmann *et al*. 1995], p4.5S RNA [Peck-Miller and Altman, 1991], a few mRNAs [Alifano *et al.*, 1994; Li and Altman, 2003], some riboswitches [Altman *et al.*, 2005] and some small hairpin model RNAs [Kufel and Kirsebom, 1998; Sinapah *et al.*, 2011] are processed by RNase P.

Since 1983 it is known that the RNA subunit is the catalytically active component of RNase P [Guerrier-Takada *et al.*, 1983]. The RNase P protein is involved in the recognition and binding of the 5'-leader of the ptRNA and in structuring the binding sites for catalytic metal ions of the RNA [Stams *et al.*, 1998; Reiter *et al.*, 2010].

1.5 Bacterial RNA subunit

The catalytic activity of the bacterial RNA subunit has been shown under high salt conditions *in vitro* in the absence of the protein subunit [Guerrier-Takada *et al.*, 1983]. The RNA subunit is built up of a specificity domain (S-domain) and a catalytic domain (C-domain). The S-domain (helices P7-P14) is important for substrate recognition to confer specificity for tRNA molecules by contacting the T-arm [Pan *et al.*, 1995; Loria and Pan, 1998]. The C-domain, composed of helices P1-6 and P15-18, contains universally conserved residues and recognizes the tRNA acceptor stem as well as the tRNA 3'-CCA end. All structural elements needed for catalysis are located within the C-domain, including the catalytically relevant metal ion binding sites. Only about 40 of the ~400 nt in bacterial RNase P RNAs are conserved based on the known

sequences, all of which are concentrated in the vicinity of the pre-tRNA binding interface [Haas and Brown, 1998].

Three structural RNase P RNA types can be distinguished. Most RNase P RNAs belong to the structural type A (ancestral) such as *E. coli* RNase P RNA. In gram-positive bacteria with a low G/C content, e.g. *B. subtilis*, type B RNase P RNAs are found [Haas *et al.*, 1996]. An intermediate structure (type C) is found in green non-sulfur bacteria [Haas and Brown, 1998].

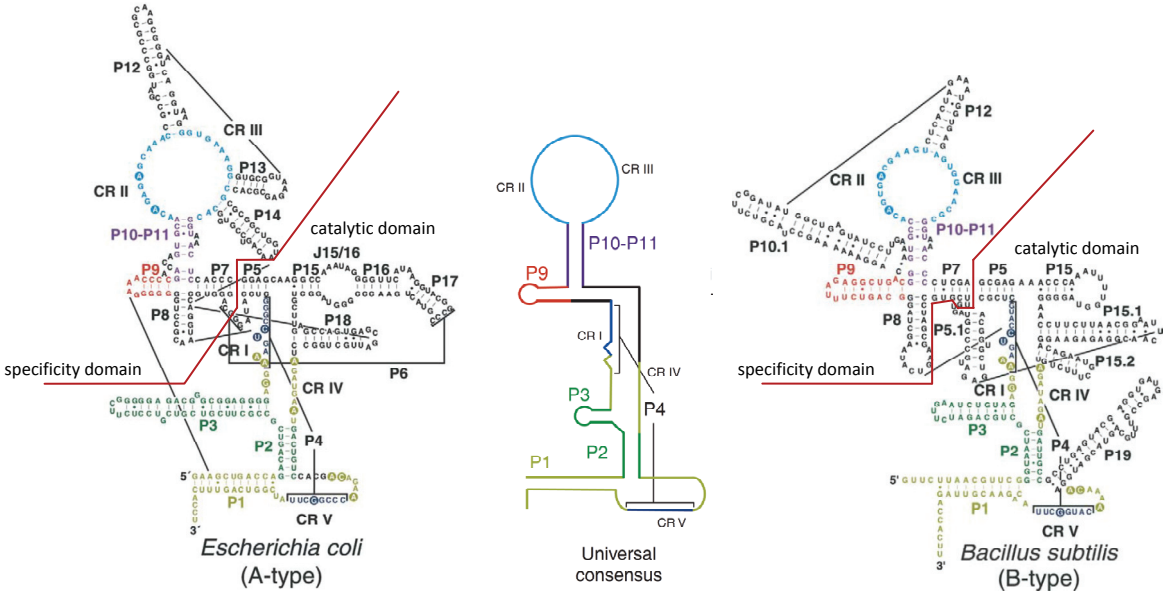

Figure 1. 3 Type A and type B form of bacterial RNase P RNAs (RPRs), in addition to the universal minimum consensus structure. The universal minimum consensus structure contains only structural elements that are conserved in all known RPRs. Colors illustrate structural elements corresponding found in representative RNAs, whereas non-conserved elements are shown in black. The labeling of elements is as follows: 'P' for paired region, 'L' for loops and 'J' for joining regions, numbering in 5'-3' direction. Brackets depict long-range tertiary interactions (e.g. base-pairing in helix P4). The five conserved regions are marked as CRI-V. The two different domains (specificity domain and catalytic domain) are separated by the dark red lines. (adapted from Evans *et al.*, 2006).

There are some structural differences between type A and type B RNase P RNA (RPR), mainly caused due to the absence/presence of helical elements or variation in the lengths of helices, loops and joining regions. However, the overall structure of RNase P RNAs is highly conserved (Figure 1. 3) [Evans *et al.,* 2006].

1.6 Bacterial RNase P: three-dimensional structure

Recently, the first high-resolution crystal structure of the *Thermotoga maritima* RNase P holoenzyme was solved which was in good agreement with previously known three dimensional models of the holoenzyme [Tsai *et al.*, 2003; Buck *et al.*, 2005; Niranjanakumari *et al.*, 2007] or the RNase P RNA [Massire *et al.*, 1998], and

with X-ray structures of RNase P RNA or RNase P protein subunits alone [Reiter *et al.*, 2010]. The analyzed crystals contained the *T. maritima* RNase P RNA (338 nt, 110 kDa) and protein subunit (117 amino acids, 14.3 kDa) in complex with mature $tRNA_{Phe}$ (76 nt, 26 kDa; marked in red within Figure 1. 4 a/b). In addition, a 5'-leader fragment was soaked into the crystals.

To generate stabilizing contacts between RNase P holoenzyme complexes in the crystal lattices, nucleotide extensions were introduced into the tRNA anticodon arm and the RNase P RNA S-domain (marked in gray in Figure 1. 4 a/b). The two different domains of the RNA subunit are shown in blue, termed the catalytic domain (C-domain, dark blue Figure 1. 4) and specificity domain (S-domain, light blue Figure 1. 4). The C-domain contains the catalytic site and harbors multiple interaction sites with the tRNA moiety. It could be shown that the highly conserved TΨC and D loop regions of the tRNA interact with the S-domain of RPR. The acceptor stem extends from the S-domain into the C-domain and is thereby crossing the main P1/P4/P5 coaxial stem (Figure 1. 4 b and Figure 1. 5 a). The 5'-end (nucleotide +1) of the mature tRNA lies centrally in the active site of the RNase P RNA. The important recognition of the tRNA 3'-CCA end involves, as previously demonstrated by several biochemical studies [Hartmann *et al.*, 2009, for review], base pair formation with nucleotides in the L15-loop (G254, G255; U256; Figure 1. 5 d). These elements are further surrounded by the P6/P15/P16/P17 regions. The RNase P protein (RPP) (marked in green; Figure 1. 4) is located close to the active site and binds the 5'-leader region of the pre-tRNA substrate. These different binding motifs result in a much higher binding affinity of the pre-tRNA to the RNase P holoenzyme in comparison to the mature tRNA which leads to the release of the mature tRNA and the cleaved 5'-flank from the complex. Contact regions between the P RNA and the P protein are the P15 stem, the CR-IV and CR-V regions and the P2/P3 helices (regions indicated in Figure 1. 5 a).

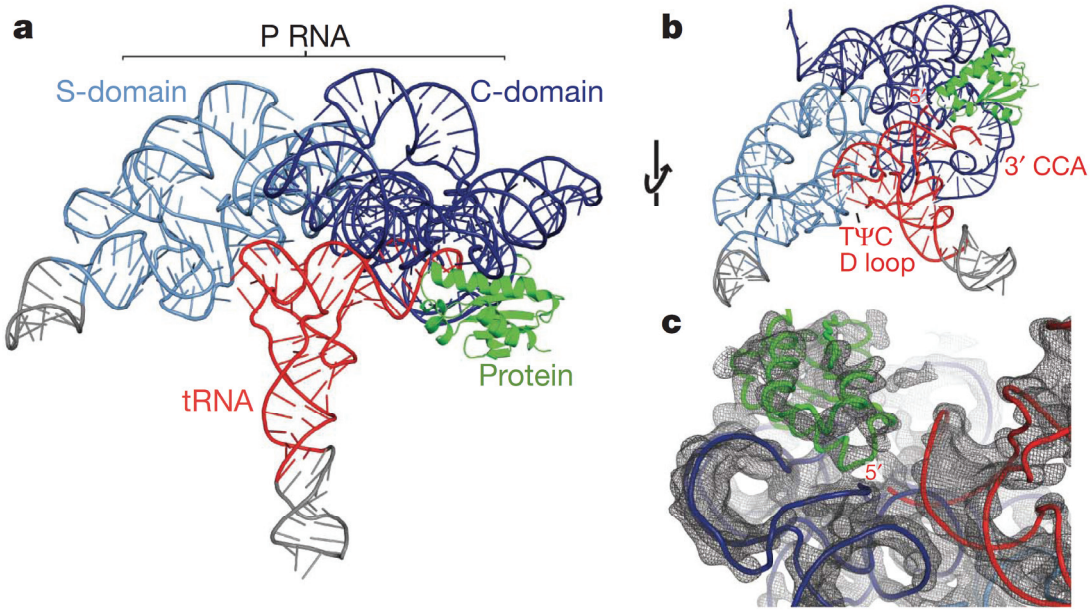

Figure 1. 4 Crystal structure of the *T. maritima* RNase P holoenzyme in complex with tRNA. a) and b), skewed views of the bacterial RNase P structure. The RNA component contains two domains, termed the catalytic domain (C-domain, blue) and the specificity domain (S-domain, light blue). The RNase P protein (green) binds the 5'-leader region of the pre-tRNA substrate. tRNA recognition regions: the 5'-end where catalysis occurs, the 3'-CCA end, and the highly conserved TΨC and D loop regions. To generate a crystal lattice, a tetraloop was inserted into the P12 loop (L12) of RNase P RNA and a tetraloop-receptor into the anticodon stem of the tRNA (gray) c) View of the 4.1 Å experimental electron density map centered on the 5'-end of tRNA (figure according to Reiter *et al*., 2010).

1.7 Substrate recognition

The catalytic site of the RNase P RNA C-domain is responsible for the cleavage of various substrates (see chapter 1.5) without an obvious preference for certain 5'-leader sequences. It has been shown in previous studies that the three-dimensional structural properties of tRNAs are recognized by RNase P (Altman *et al*., 1993). However, recognition elements near the cleavage site are redundant, such that truncated substrates lacking the anticodon and D arm and thus deviating from the tRNA L-shape (e.g. acceptor stem-T arm mimics) are still recognized and cleaved by the enzyme.

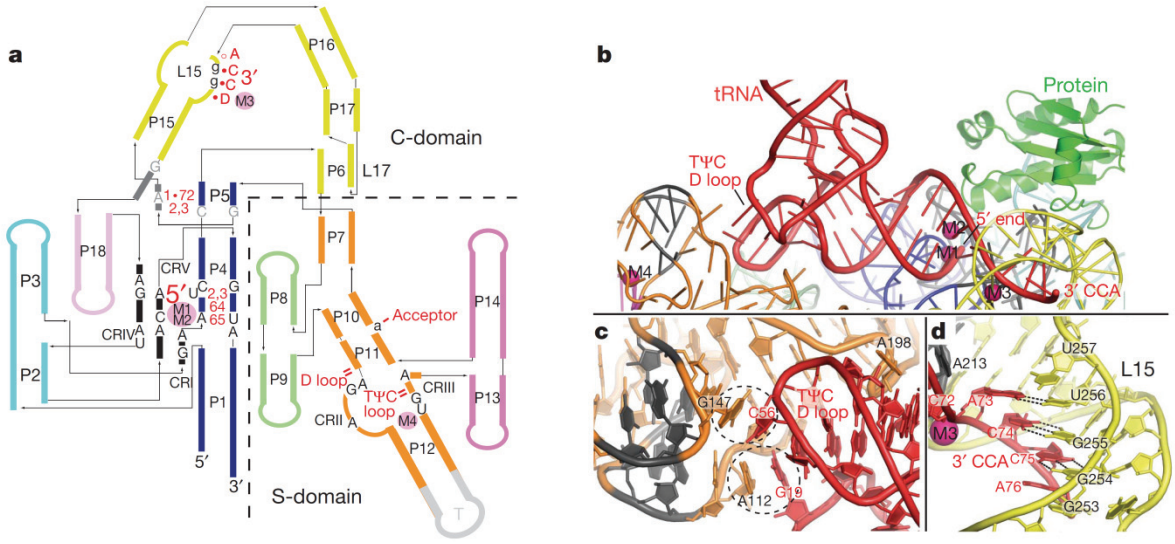

Figure 1. 5 tRNA recognition mediated by RNA–RNA interactions. a) Schematic P RNA secondary structure illustrating the tRNA–P RNA contacts observed in the crystal structure. The tRNA nucleotides (1•72, 2, 3, 64 and 65) and regions (5′-end, 3′-end, TΨC loop, D loop and acceptor stem) involved in direct interactions are shown in red. P RNA nucleotides that are universally conserved (black, uppercase), conserved among all bacteria (grey, uppercase), or highly conserved in bacteria (black, lowercase) are indicated. Metal ions are shown as filled pink spheres. All identified tRNA–P RNA contacts are within 4 Å. The crystallized *T. maritima* P RNA consists of eighteen paired helices (P), five universally conserved regions (CR-I to CR-V) (black), two junctions containing conserved nucleotides in bacteria (dark grey), several loop (L) regions, and an engineered tetraloop region (T, light grey). The coaxial P1/P4/P5 stem is shown in blue, P2/P3 stems in cyan, P6/P15-17 and L15/L17 in yellow, P7 and P10/P11/P12 in orange, P8/P9 in light green, and P13/P14 in pink. b) tRNA recognition by the P RNA. The acceptor stem of tRNA (red) docks onto the P RNA (colored as in a) resulting in a series of interactions, including base stackings between in the TΨC/D loops of tRNA and the S-domain, an A-minor interaction, and base pairing, ribose zipper and stacking interactions between the 5′-and 3′-ends of tRNA and the C-domain. The protein (green) makes no direct contacts with mature tRNA. c) tRNA recognition by the S-domain. Two universally conserved P RNA regions (CR-II and III, dark grey) facilitate base stacking interactions with unstacked bases in the structurally conserved TΨC and D loops of tRNA. d) Recognition of the tRNA 3′-CCA by the C-domain. Intermolecular base pairs form between the tRNA 3′-DCCA and the L15 loop (5′-GGU) of P RNA. This interaction is stabilized by a structural metal (M3, magenta sphere) and an L15 ribose zipper conformation (according to Reiter *et al*., 2010).

The RNA-RNA interaction between tRNA T loop (TΨC) and D loop and the P RNA S-domain is mediated by base stacking (Figure 1. 5 c). The tRNA acceptor stem, which is 7 bp long in the most natural tRNA molecules, is connected through its minor groove to the highly conserved A198 within the P11 stem (Figure 1. 5 a, b, c). Nevertheless, the contacts with the acceptor stem are mainly mediated by the C-domain of the RNA subunit (Figure 1. 6a). The length of the acceptor stem and its primary structure is thought to be the major determinant for cleavage site selection [Holm and Krupp, 1992; Kirsebom and Svärd, 1992]. At least the canonical base pairing interaction between the tRNA 3′-DCCA (D indicates the discriminator base) motif and the nucleotides 254-256 of the L15 loop is important for substrate binding (Figure 1. 5d, Figure 1. 6).

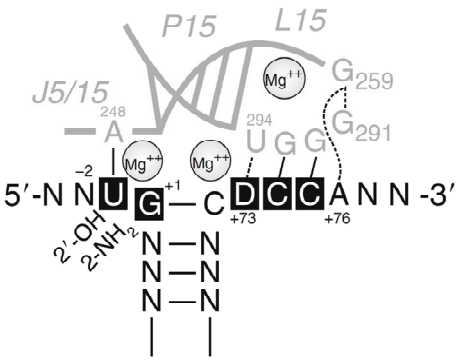

Figure 1. 6 Contacts between the C-domain of *E. coli* RNase P RNA (gray) with pre-tRNA at and near the cleavage site (between nucleotide -1 and +1). Multiple Mg^{2+} ions are involved in this interaction, although their exact position is unknown (figure adapted from Hartmann, 2009).

This interaction is conserved in probably all bacterial and most archaeal RNase P ribozymes. However, the interaction is not conserved in organisms where the CCA motif is added post-transcriptionally [Hartmann *et al.,* 2009]. Most non-tRNA substrates of RNase P mimic the coaxially stacked acceptor stem and T stem [Forster and Altman, 1990; Peck-Miller and Altman, 1991]. Beside these features several base identities close to the cleavage site seem to be important for the recognition and positioning of the substrate (Figure 1. 6). For example, in more than 80% of the characterized tRNAs a guanosine is found at position +1 [Sprinzl *et al.*, 1998]. In 1998, it was also shown that a small artificial hairpin substrate, termed pATSer, can be efficiently cleaved by *E. coli* RNase P (Figure 1. 7). Cleavage is dependent on the 3'-DCCA-P RNA interaction. Additionally, coordination of the Mg^{2+}-ion at this position strongly affects cleavage [Kufel and Kirsebom, 1998].

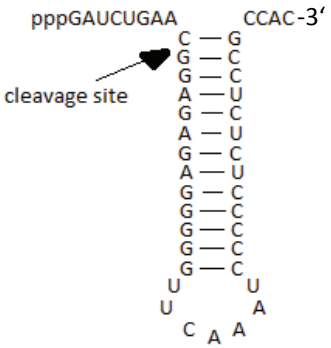

Figure 1. 7 An illustration of the secondary structure of pATSer. The arrow indicates the cleavage site [Kufel and Kirsebom, 1998].

1.8 The protein subunit

The single protein subunit (about 120 aa) of the bacterial RNase P contributes around 1/10 to the mass of the holoenzyme. It adopts a highly conserved tertiary structure (despite low primary sequence conservation), which explains the exchangeability of protein subunits between different bacteria [Guerrier-Takada *et al.*, 1983; Pascual and Voique, 1996; Gößringer and Hartmann, 2007]. Also, the protein is required for efficient tRNA processing *in vivo* under physiological salt conditions [Guerrier-Takada *et al.*, 1983; Kurz *et al*. 1998; Kurz and Fierke, 2002]. Based on the crystallization of the *T. maritima* RNase P structure in complex with tRNA, the P proteins location could be mapped close to the end of the mature tRNA, but at a distance of more than 6 Å and thus not close enough for direct contacts. It is positioned between the stems P15 and P3 and the conserved regions CR-IV and CR-V of the P RNA (Figure 1. 8) [Reiter *et al.*, 2010]. Based on biochemical and genetic analyses as well as phylogenetic conservation, three RNA binding motifs within the P protein were identified and are in good agreement with the solved crystal structure. i) the RNR motif, a conserved stretch of approx. 11 aa (Altman, 1989; Pace and Brown, 1995) (Figure 1. 8), ii) a metal ion binding loop connecting β sheet 2 and 3 (Stams *et al.*, 1998), iii) conserved cleft formed by an α-helix and a four-stranded β-sheet (Figure 1. 8).

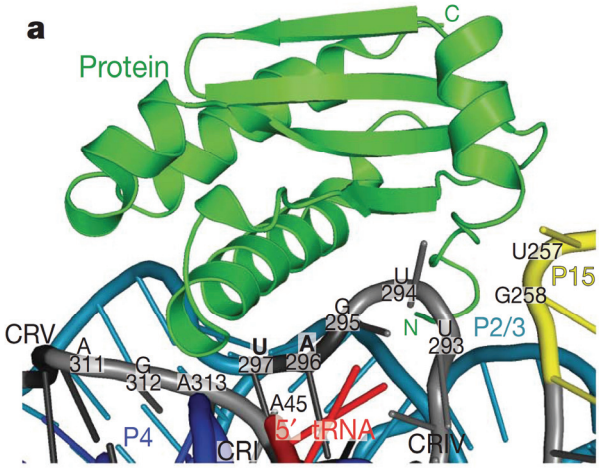

Figure 1. 8 Protein–RNA contacts within the RNase P holoenzyme. The protein (green, shown as ribbons) contacts the P RNA surface by CRI, IV and V, at the L15/P15 junction, and at helices P2/3 (P RNA colored as in Figure 1. 4). Labeled P RNA nucleotides make protein contacts (within 4 Å). Nucleotides highlighted in bold are universally conserved (figure adapted from Reiter *et al.*, 2010).

The 5'-leader of pre-tRNA interacts with the conserved cleft of the P protein mainly at residues Phe17, Phe21, Lys51, Arg52 and Lys90 and presumably Ser26, Gln28, Lys56 and Arg89, whereas the RNR motif and the metal ion binding loop mainly interact with the P RNA (Figure 1. 8) [Niranjanakumari *et al.*, 1998; Biswas *et al.*, 2000;

Sharkady and Nolan, 2001; Reiter *et al.*, 2010]. Additionally, it can be seen in the crystal structure that the 3'-end of the leader is located nearby the 5'-end of the tRNA and in close vicinity of the two conserved residues Arg52 and Lys56 of the P protein (Figure 1. 9). These findings point out the importance of the P protein for positioning the leader of the pre-tRNA in enzyme-substrate complexes. The protein-leader interaction enhances the affinity of pre-tRNA relative to mature tRNA, which is thought to accelerate pre-tRNA processing and to prevent inhibition of RNase P by excess amounts of mature tRNA in living cells [Kurz et al., 1998].

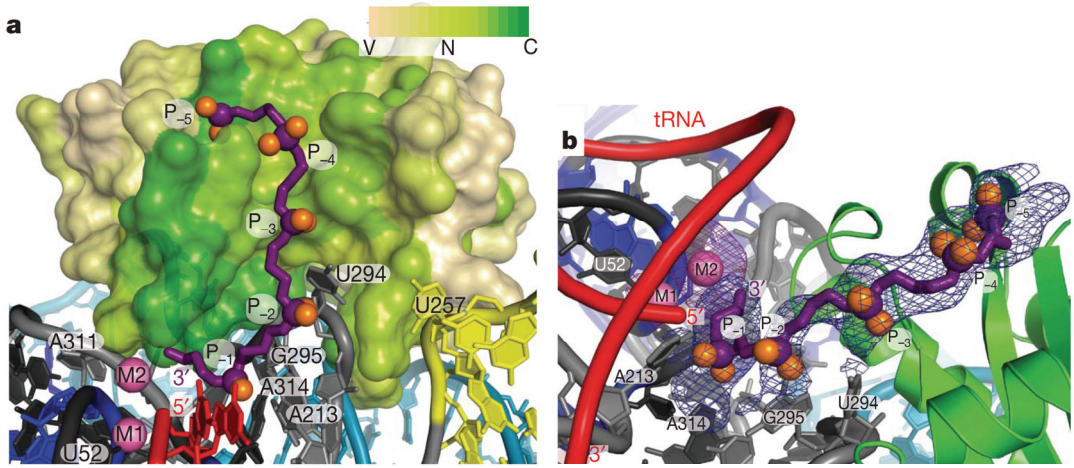

Figure 1. 9 Different views at the pre-tRNA leader–protein interactions in the RNase P holoenzyme. Surface of the RNase P protein colored by sequence conservation (variable (V), tan; neutral (N), light green; conserved (C), green). The pre-tRNA 5'-leader (purple) was modeled as a polyphosphate chain with five phosphates (P_{-1} to P_{-5}). It follows a highly conserved patch in the protein cleft, extending from the 5'-end of the mature tRNA (red) and away from the P RNA subunit. Soaking of crystals with a 5'-leader together with Sm^{3+} ions revealed a second metal ion binding site (M_2) (according to Reiter *et al.*, 2010).

1.9 Active site structure

The essential pre-tRNAs processing reaction catalyzed by RNase P (Figure 1. 10) generates 3'-OH and 5'-phosphate termini.

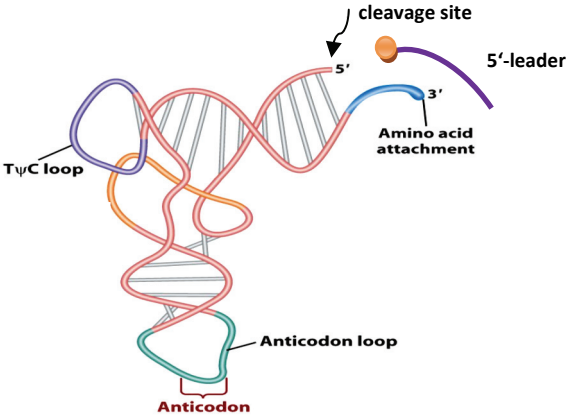

Figure 1. 10 Tertiary structure of tRNA with the cleaved off 5'-leader. The cleavage site of RNase P is marked by the black arrow.

A solvent hydroxide is thought to act as the nucleophile in an S_N2 in-line displacement mechanism (Figure 1. 11) [Guerrier-Takada *et al.*, 1986; Smith and Pace, 1993; Warnecke *et al.*, 1996; Chen *et al.*, 1997]. The proposed two-metal ion mechanism shows the stabilization and activation function of the metal ions. The phosphate group is coordinated by Me_A^{2+} and Me_B^{2+}. Me_A^{2+} additionally activated the solvent hydroxide.

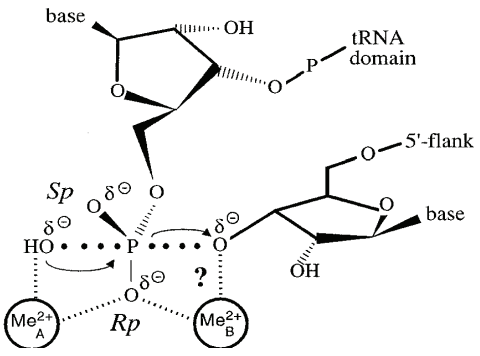

Figure 1. 11 Proposed catalytic mechanism of the pre-tRNA cleavage reaction catalysed by RNase P. (figure adapted from Warnecke *et al*., 1996).

The 2'-substituent at the scissile phosphodiester bond (nt -1/+1) was also observed to be important for catalytic efficiency (Figure 1. 12) [Persson *et al.*, 2003]. A 2'-OH group

mediates to the highest cleavage rates [Smith and Pace, 1993]. Particularly the H-bond donor function of the 2'-OH group is thought to be required to form an H-bond to a metal-ion bound water molecule. This may facilitate proton transfer from this water molecule to the 3'-oxyanion leaving group.

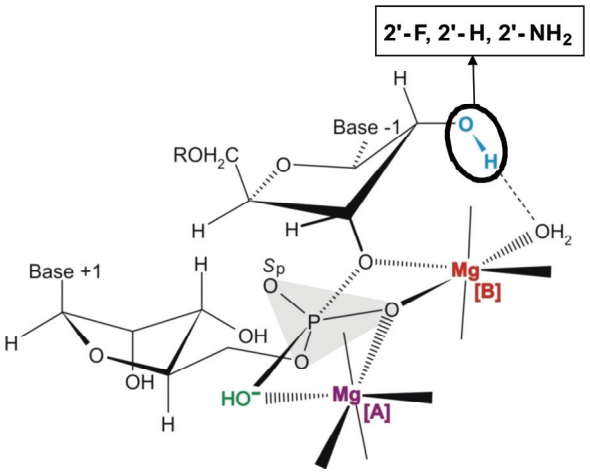

Figure 1. 12 Effect of the 2'-group on the metal-ion induced cleavage reaction of RNase P (according to Cuzic and Hartmann, 2005).

A 2'-F group is less efficient than a 2'-OH but more effective than a 2'-H substituent possibly due to combining a (weak) H-bond acceptor function with an enhanced inductive effect on the 3'-oxyanion leaving group. A 2'-NH_2 group at this location resulted in miscleavage between nt -2/-1 below pH 6. This indicated that the protonated amino group leads to repulsion of the adjacent Me^{2+} [Persson *et al.*, 2003; Cuzic and Hartmann, 2005]. Furthermore, a Cd^{2+} dependence analysis of RNase P RNA-catalyzed cleavage of an R_p-diastereomeric pre-$tRNA^{Gly}$ (termed Hill analysis) suggested that two metal ions (M_A and M_B) are primarily involved in the cleavage reaction [Warnecke *et al.*, 1996]. These findings were confirmed by the identification of two electron density areas in the solved crystal structure [Reiter *et al.*, 2010], which were assigned to metal ions within the active site (M1 and M2; Figure 1. 13).

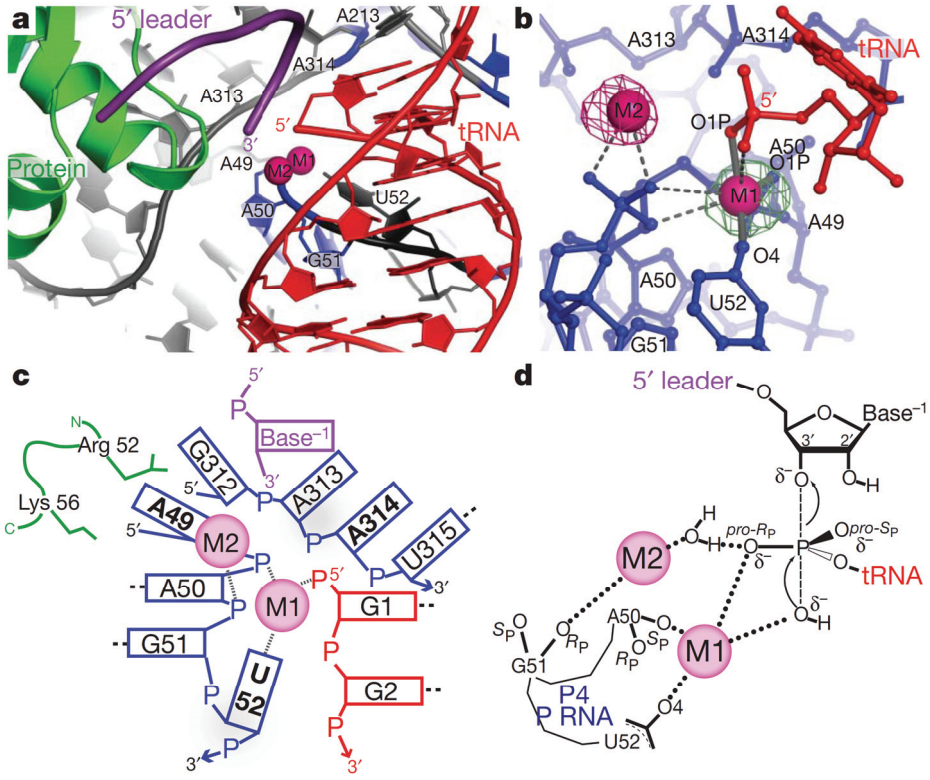

Figure 1. 13 Structure of the RNase P active site environment. Mature tRNA (red), the leader (purple), the protein component (green), the P RNA (blue and grey) and two metal ions (magenta spheres). a) The active site is inferred from the location of the mature 5'-end of tRNA. A group of conserved P RNA nucleotides (A49–U52, A213, A313 and A314) form part of the active site. b) The two active site metal ions (M1 and M2) are within 4 Å of the 5' phosphate of tRNA and the M1–M2 metal–metal distance is 4.8 Å. The M1 metal makes contacts (2.1 Å, solid grey bonds, labeled) with tRNA (G1 O1P) and P RNA (A50 O1P and U52 O4) oxygens. Other possible ligands within 3.5 Å of M1 or M2 are represented by dashed grey lines. The second metal is clearly visible only when the leader is present. c) Schematic diagram of the interactions around the active site. d) Proposed reaction mechanism for the cleavage of pre-tRNA by RNase P based on the structure of the enzyme–product (E–P) complex and previous mechanistic studies [Chen *et al.*, 1997; Warnecke *et al.*, 1996] (figure adapted from Reiter *et al.*, 2010).

The crystal structure revealed that the negatively charged phosphate backbone of the first three tRNA nucleotides (+1 to +3; Figure 1. 13c (red)) are placed on the major groove of the P4 stem (A50, G51, U52; Figure 1. 13c (blue)). The 5'-end of the mature tRNA is in close vicinity to the P4 stem phosphate backbone, whereas the nucleotide U52 is directed to the tRNA 5'-end. Furthermore, the phosphate backbone of nucleotides A313 and A314 are also located near the mature tRNA 5'-end. The conserved nucleotide A213 stabilizes the tRNA 1•72 base pair (Figure 1. 13a). The two metal ions are coordinated by the nucleotides A50, G51 and U52, whereas the M1 ion is directly coordinated by the O4 oxygen of U52 and the S_p oxygen of A50 (Figure 1. 13d). Further, the M1 ion is proposed to coordinate a solvent hydroxide that serves as the attacking nucleophile (Figure 1. 13d). Finally, a direct contact between the M1 ion and the phosphate pro-R_p oxygen is considered in this model (Figure 1. 13d). Also a direct contact could be observed between the M1 ion and the pro-R_p oxygen of the phosphate group (Figure 1. 13d). The M2 ion is shown to contact nucleotide G51 via

its non-bridging R_p oxygen and to form an outer-sphere contact to the pro-R_p oxygen of the tRNA phosphate group (Figure 1. 13d). M2 also is located in a short distance to the 3'-oxygen of the 5'-leader -1 nucleotide, but a fully occupied electron density for the M2 ion is only observed in the presence of the 5'-leader sequence. This indicates a local metal-induced conformational change occurring during substrate binding, which localize the 5'-leader close to the P RNA-P protein interface and therefore a formation of a catalytically competent RNase P:pre-tRNA complex [Hsieh *et al.*, 2010]. The distance between the metal ions and the tRNA 5'-phosphate was determined to be 4 Å, whereas M1 and M2 have a distance of 4.8 Å to each other. The nucleophilic attack by the solvent hydroxide occurs according to an in-line S_N2 reaction mechanism which goes along with an inversion of the configuration of the phosphorus atom between -1 and +1.

1.10 6S RNA in Bacteria

6S RNA as well as many other ncRNAs had been found long time before their function was revealed. In 1967, Hindley first described a 6S RNA found in *E. coli* cell extracts, followed by a proposal of its secondary structure four years later [Hindley 1967; Brownlee, 1971]. Only about 30 years later insight into its function and regulatory importance could be gained [Wassarman and Storz, 2000]. One of the reasons for this lack of understanding of 6S RNA function might be that under conventional laboratory conditions (temperature, pH value, salt conditions) no notable phenotype could be observed [Lee *et al.*, 1985]. Comparison of *E. coli* wild-type cells with *ssr1* cells lacking 6S RNA revealed binding of the major portion of cellular RNAP bound to DNA during exponentally growth for both cell types, whereas only in *ssr1* cells the major fraction of RNAP was still bound to DNA during stationary phase. Anyway, no increase in total cellular protein levels in the *ssr1* cells could be observed [Wassarman and Storz, 2000]. Further analyses revealed that in 6S RNA-deficient cells growing to mid-log or early stationary phase, 245 (exp. growth phase) and 273 (early stationary phase) genes are $\geq$ 1.5-fold up- or downregulated. These genes include many transcriptional regulators, stress-related proteins, transporters and several enzymes involved in purine metabolism. Noteworthy, a significant reduction of rRNAs was observed and, as a result, a generally reduced expression of the translation machinery. Thus, these analyses indicate an effect of 6S RNA on the basal ppGpp level, which in turn is known to affect growth adaption and ribosome biogenesis. This indicates that 6S RNA contributes to balancing the translational capacity of the cells [Neusser *et al.*, 2010, Steuten *et al.*, 2014]. For the *B. subtilis* model system, a growth phenotype of strain 168 was found, where outgrowth was delayed when 6S-1 RNA (*ΔbsrA*) is lacking but 6S-2 RNA is still present. This phenotype also shows a faster exhaustion of nutrients and therewith an earlier sporulation of these cells in comparison to the wild type. This indicates that 6S-1 RNA plays a role in economical utilization of nutrients and metabolites, similarly as described for *E. coli* 6S RNA

[Cavanagh *et al.*, 2012]. In *Legionella pneumophila,* 6S RNA could be shown to regulate expression of genes encoding type IVB secretion system effectors and stress response genes such as *groES* and *recA*. Also expression of many genes involved in acquisition of nutrients and genes with unknown or hypothetical functions are positively regulated by this 6S RNA. In protist and mammalian host cells, a deletion of 6S RNA significantly reduced intracellular multiplication, but had no detectable effect on growth in rich media [Faucher *et al.*, 2010]. It is now accepted that 6S RNA is an important regulator of RNA polymerase in all bacterial branches [Barrick *et al.*, 2005].

Of note, 6S RNA binds to the RNA polymerase holoenzyme (consisting of the subunits: σ, α_1, α_2, β, β' and ω), especially to the housekeeping σ-factor (Figure 1. 14) [Gruber and Gross, 2003]. The colored regions of 6S RNA (Figure 1. 14) indicate sites of RNA hydrolysis owing to FeBABE moieties conjugated to single cysteines of functional *E. coli* σ^{70}-variants [Steuten *et al.*, 2013].

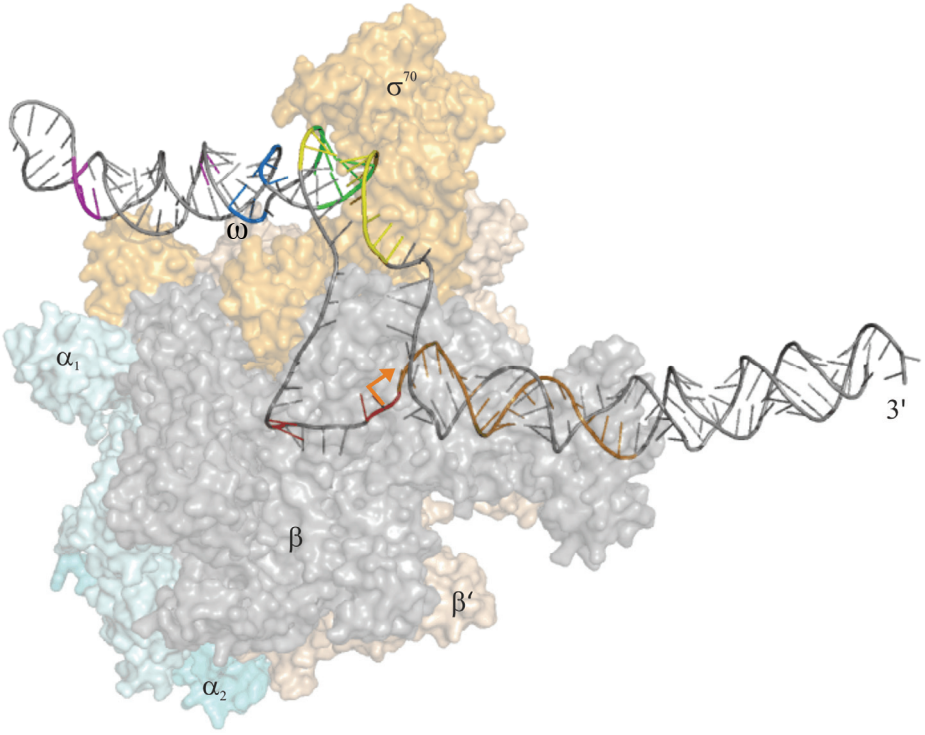

Figure 1. 14 Three-dimensional model of 6S RNA bound to the *E. coli* σ^{70}-RNA polymerase holoenzyme. The surface structure of the RNA polymerase (RNAP) is displayed, with the subunits colored as follows: α_1 in light blue; α_2 in turquoise; β in grey; β' in tan; σ^{70} in orange. The modeled three-dimensional structure of 6S RNA is colored according to the FeBABE study [Steuten *et al.*, 2013]. Colors refer to the amino acid position at which the FeBABE "nuclease" was attached to σ^{70}: K376C: $\sigma^{70}_{2.1}$ in green; R4226C: $\sigma^{70}_{2.3}$ in yellow; K496C: $\sigma^{70}_{3.1}$ in blue; S517C: $\sigma^{70}_{3.2}$ in red; D581C: $\sigma^{70}_{4.2}$ in purple. The orange arrow depicts the pRNA transcription starting nucleotide U44.

When 6S RNA is bound to the housekeeping RNAP holoenzyme (σ^{70}-RNAP in *E. coli,* σ^{A}-RNAP in *B. subtilis*), the enzyme is blocked for transcription at DNA promoters. Noteworthy, it could be unveiled that 6S RNA serves as a template for transcription

of short so-called product RNA (pRNA) when bound to RNAP (Figure 1. 14; pRNA transcription start site is indicated by the orange arrow). Thus, pRNA transcription converts RNAP to an RNA-dependent RNA polymerase. As displayed in Figure 1. 15 cellular 6S-1 RNA concentration in exponential phase is low, only small amounts of pRNAs are synthesized and the housekeeping RNAP is mainly involved in gene transcription from DNA templates. Subsequently, 6S-1 RNA levels rise in late exponential and stationary phase, such that a large fraction σ-RNAP becomes sequestered in complexes with 6S RNA (here 6S-1 RNA of *B. subtilis*). At this point 6S RNA temporary converts the DNA-dependent RNAP to an RNA-dependent RNAP which results in the transcription of short product RNAs whereas 6S RNA serves as template. Owing to the lack of nutrients (including NTPs) at this growth stage, primarily short abortive transcripts (≤ 10 nt) are synthesized that dissociate from the 6S RNA:pRNA complex instead of being elongated to longer pRNAs. The short pRNAs cannot induce a structural rearrangement of 6S RNA which leads to RNAP release. It is predicted that 6S-1 RNA molecules oscillate between their ground state and the transiently rearranged structure during stationary phase. Now, when the amount of nutrients in cellular environment again increases, a new exponential growth phase is initiated (termed outgrowth phase), and the average length of synthesized pRNAs increases. Such longer pRNAs (approx. 14 nt for *B. subtilis* 6S-1 RNA) are able to persistently rearrange the RNA's structure which triggers dissociation of the 6S RNA:pRNA hybrid structure from RNAP (Figure 1. 15 c). The fully rearranged 6S-1 RNA structure is illustrated in Figure 1. 15 c (bottom left), although the orientation of the helical elements is not known until now. The fate of 6S-1 RNA:pRNA hybrids after dissociation from RNAP is also unknown, but it is proposed that as soon as the complex dissociates, the 6S RNA:pRNA hybrid structure becomes susceptible to degradation by RNases within the bacterial cell [Wassarman and Saecker, 2006; Beckmann and Hoch *et al.*, 2012; unpublished data].

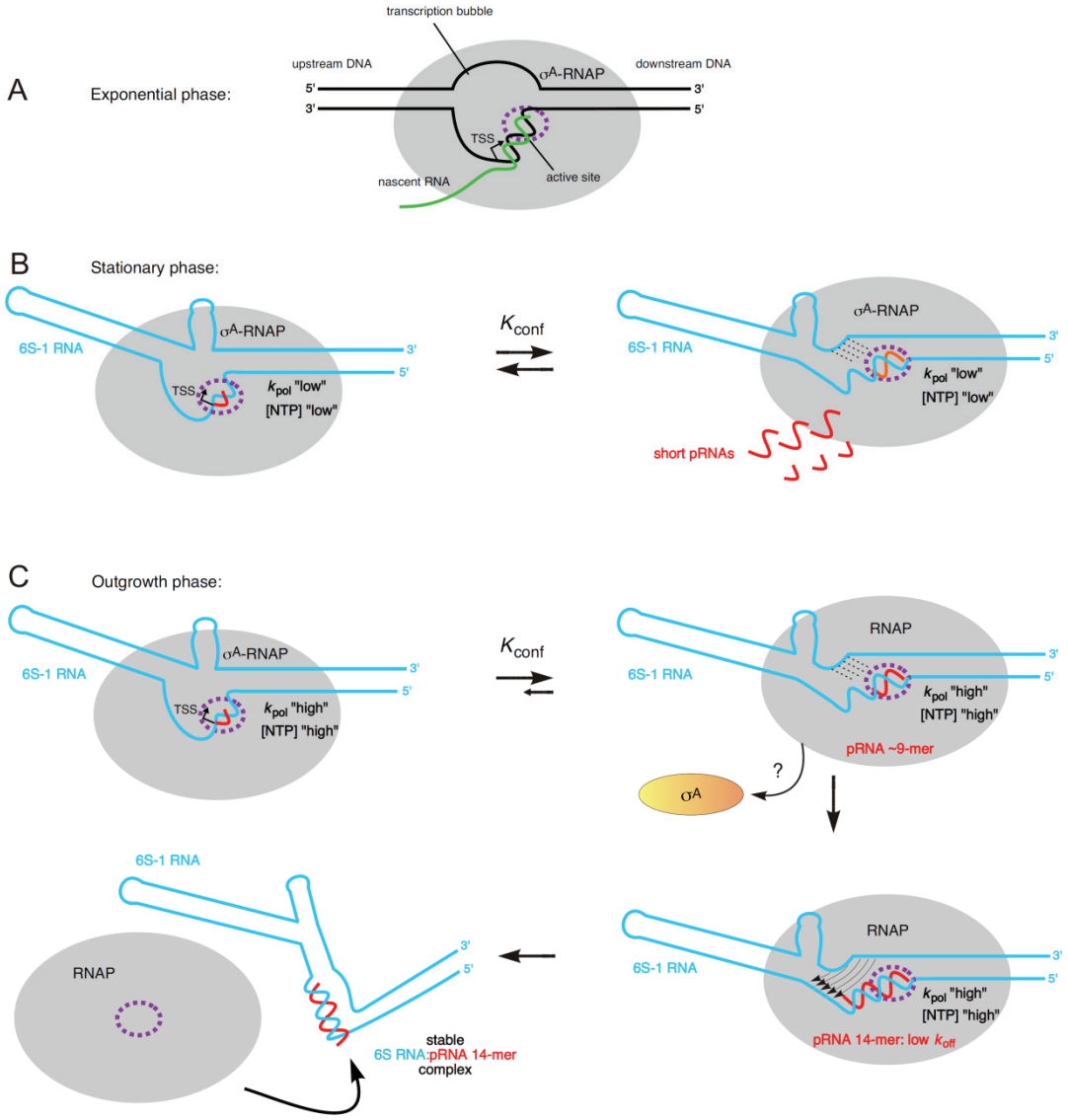

Figure 1. 15 Model of the pRNA length-controlled structural rearrangement of *B. subtilis* 6S-1 RNA and its release from σ^A-RNAP, including mechanistic components inferred from the *E. coli* system. (A) In exponential phase, cellular 6S-1 RNA concentrations are low, only small amounts of pRNAs are synthesized and σ^A-RNAP is predominantly involved in gene transcription. The sketch illustrates a complex of RNAP and open promoter DNA; the latter is thought to be mimicked by 6S RNA. (B) 6S-1 RNA levels raise in late exponential and stationary phase and a larger fraction of σ^A-RNAP is sequestered in complexes with 6S-1 RNA. In late stationary phase, nutrients including NTPs are scarce and abortive transcripts/short pRNAs dissociate instead of being elongated to longer pRNAs because the rate constant for nucleotide addition is relatively slow (k_{pol} "low"). Here, 6S-1 RNAs begin to transiently rearrange their structure (right panel), but fall back to the ground state (left panel) owing to pRNA dissociation; it is predicted that 6S-1 RNA molecules oscillate between their ground state and the transiently rearranged structure; if this also involves σ^A release and rebinding to RNAP (depicted in panel (C) as suggested for the *E. coli* system upon pRNA 9-mer synthesis, remains to be seen. (**C**) In a newly initiated exponential growth phase (outgrowth), nutrients are resupplied and NTP levels increase. As a consequence, k_{pol} increases (k_{pol} "high") and the fraction of longer pRNAs rises (12 to 14-mers), which stably rearrange 6S-1 RNA structure and trigger release of RNAP. An increase in the fraction of longer pRNA ~14-mers during outgrowth in vivo has been detected by dRNA-seq. Since the sigma factor dissociates from RNAP upon synthesis of a pRNA 9-mer in the *E. coli* system, we have

tentatively included this mechanistic element also for the *B. subtilis* system. An open question is if the 6S-1 RNA rearrangement is already complete after synthesis of a pRNA 9-mer (as in the *E. coli* system) or incomplete until a stable RNAP:pRNA ~14-mer complex is formed. In the first three sketches, the hairpin in the 3'-CB is shown with a curved stem to indicate its equilibrium with an open structure. The two helical arms are shown as slightly bent to consider that formation of the hairpin constricts this side of the central bulge. In the top sketch on the right, stippled lines depict the progressive disruption of helix P2; thin arrows in the bottom sketch on the right illustrate formation of the central bulge collapse helix. The fully rearranged 6S-1 RNA structure is depicted in the bottom sketch on the left; the orientation of the helical elements is not known and thus arbitrary (adapted from Steuten *et al.,* 2014).

1.11 6S RNA in *E. coli*

The secondary structure of 6S RNA (illustrated for *E. coli* in Figure 1. 16; termed Eco 6S RNA) was first investigated for the RNA from *E. coli*. Both, the ground state and the predicted structure after pRNA-induced rearrangement, are displayed in the figure below (Figure 1. 16). The structurally important central bulge in the middle of the 6S RNA structure is highlighted in blue. The pRNA transcription start site (U44) is located within the central bulge. When a pRNA (here a 13-mer shown in orange) is bound to 6S RNA, the P2 helix (in purple) opens up and a hairpin between the 3'-central bulge and the 3'-region of the P2 helix forms (Figure 1. 16) [Panchapakesan and Unrau, 2012; Wagner *et al.*, 2013]. The central bulge is thought to mimic an open DNA promoter to inhibit transcription [Trotochaud and Wassarman, 2005; Barrick *et al.*, 2005].

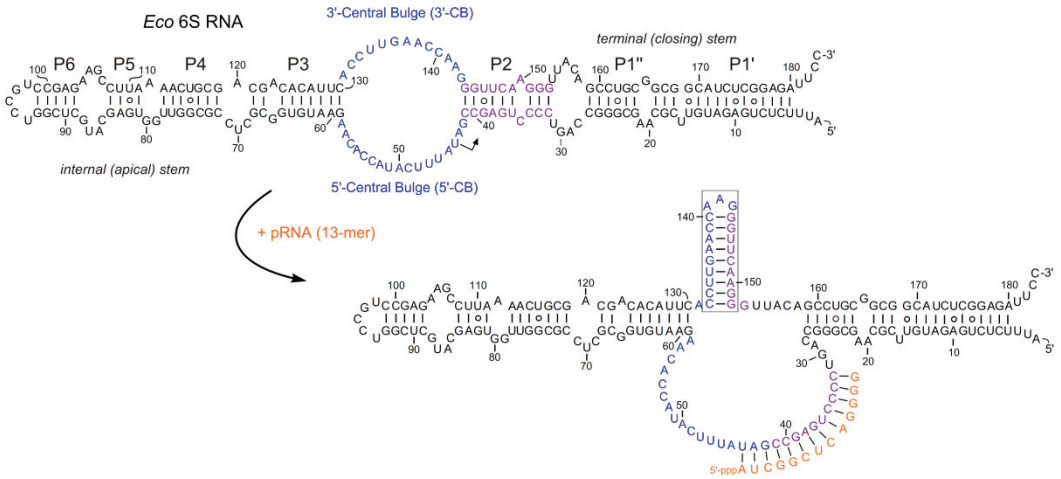

Figure 1. 16 Illustration of the ground state structure of *E. coli* 6S RNA and of the predicted pRNA-induced structural rearrangement. In *E. coli* (*Eco*) representing the γ-proteobacteria, pRNA-induced disruption of 6S RNA structure triggers formation of an extended hairpin in the 3'-CB (boxed) (figure adapted from Steuten *et al.*, 2014).

E. coli 6S RNA binds to the σ^{70}-RNAP holoenzyme via intimate contacts to the σ^{70}-subunit [Cavanagh *et al.,* 2008; Steuten *et al.*, 2013], leading to inhibition of transcription from a subset of σ^{70}-dependent promoters. This may result in activation of transcription from σ^{S}-dependent promoters [Wassarman and Storz, 2000; Trotochaud and Wassarman, 2004].

E. coli 6S RNA is transcribed from two tandem promoters, *ssrS* P1 and *ssrS* P2. Transcription from promoter P1 generates a short transcript with an extra 9-nt leader at the 5'-end of 6S RNA. 6S RNA primary transcripts initiated at the P2 promoter carry a 224 nt long 5'-extension [Kim and Lee, 2004]. P1 is a canonical σ^{70}-dependent promoter, while P2 is σ^{70}- and σ^{S}-dependent. Transcription is terminated by the Rho factor approximately 90 nt downstream of the mature 6S RNA 3'-end [Chae *et al.*, 2011]. Mature 6S RNA is generated by RNase E/G cleavage which removes the extra 3'- and 5'-sequences, respectively [Chae *et al.*, 2011; Kim and Lee, 2004].

The importance of the -35 region of the promoter sequence for RNAP inhibition by 6S RNA was substantiated in 2009 by a study using a series of σ^{70}-mutants [Klocko and Wassarman, 2009]. The authors demonstrated competition between 6S RNA and the -35 region of the DNA promoter for binding to σ^{70}-RNAP within the protein's 4.2 region. The helix-turn-helix DNA-binding domain of the 4.2 region is overlapped by a positively charged stretch of amino acids which were shown to be important for 6S RNA binding. A weak -35 promoter element was shown to be a determinant of 6S RNA-sensitive promoters [Trotochaud and Wassarman, 2004].

1.12 6S RNA in other Bacteria

In 2005, a structure-based bioinformatic screen detected 6S RNA gene homologs in all branches of the bacterial phylogenetic tree [Barrick *et al*., 2005]. In addition, two 6S RNA paralogs (named 6S-1 and 6S-2 RNA) were biochemically identified in *B. subtilis*, the second major model system in 6S RNA research (Figure 1. 17; structure of *B. subtilis* 6S-1) [Trotochaud and Wassarman, 2005].

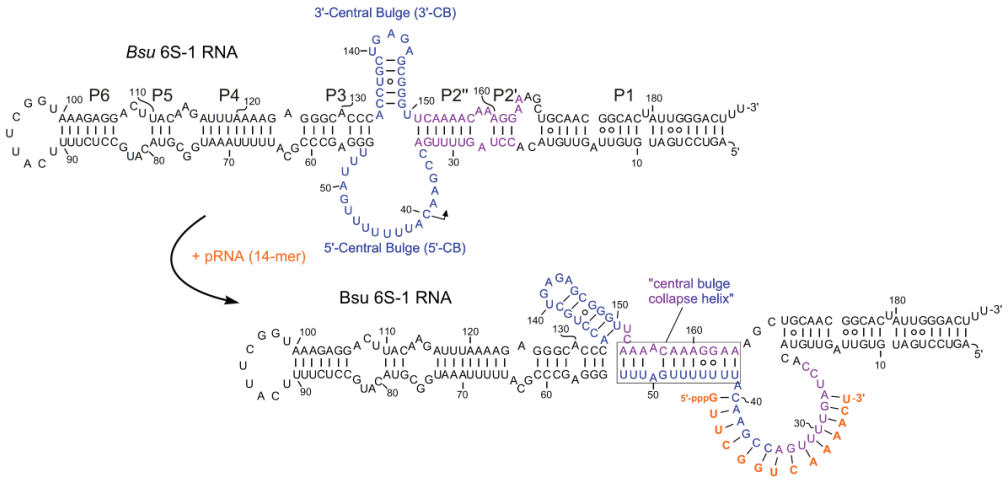

Figure 1. 17 Illustration of the ground state structure *B. subtilis* (*Bsu*) 6S RNA and of the predicted pRNA-induced structural rearrangement. *B. subtilis* 6S-1 RNA represents a group of 6S RNAs for which a hairpin can form (at least transiently) in the 3'-CB already in the free RNA; in this type of 6S RNA, the structural rearrangement is achieved by formation of a central bulge collapse helix (boxed) (figure adapted from Steuten *et al.*, 2014).

Using an experimental RNomics approach, a 6S RNA homolog was also identified in the hyperthermophilic bacterium *Aquifex aeolicus* (Figure 1. 19) [Willkomm *et al.*, 2005]. The constantly growing number of sequenced bacterial genomes combined with improved *in silico* approaches, using trained covariance models, has led to the recent identification of more 6S RNA candidates (Figure 1. 18).

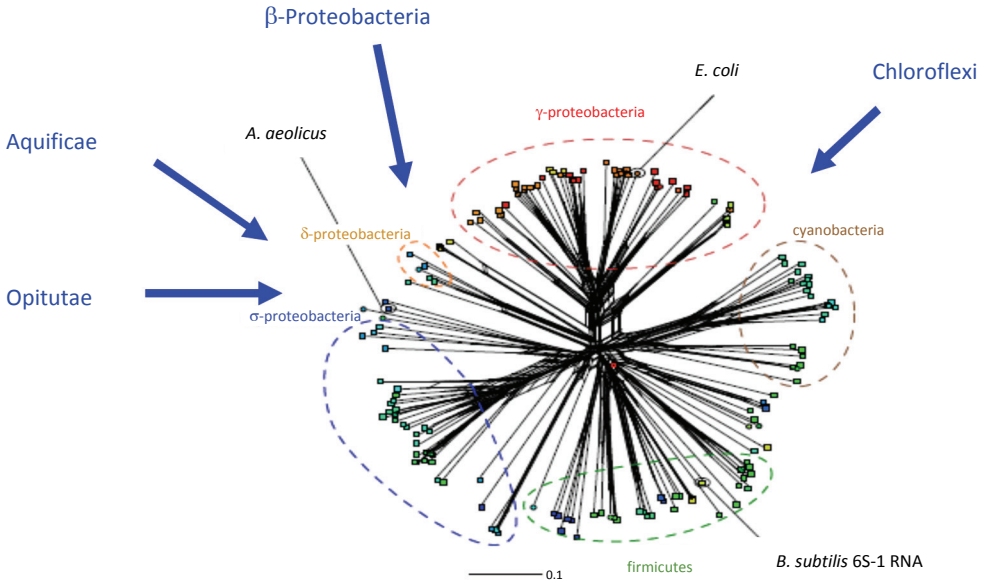

Figure 1. 18 Illustration of the phylogenetic tree of 6S RNAs in bacterial branches (Lechner and Marz, unpublished).

The common conserved feature of all 6S RNAs is their rod shape with a central bulge surrounded by two imperfect helical stems. However, 6S RNAs share little similarity on the sequence level [Willkomm and Hartmann, 2005]. In the meantime, additional 6S RNA homologs have been experimentally verified in *Synechococcus sp.*, *Salmonella typhimurium*, *Sinorhizobium meliloti*, *Staphylococcus aureus* and *Heliobacter pylori* (Watanaba *et al.*, 1997; Sittka *et al.*, 2008; Schlüter *et al.*, 2010; Pichon and Felden, 2005; Sharma *et al.*, 2010]. The latter 6S RNA was shown to serve as template for two different pRNA types, each transcribed from one side of the central bulge, approximately 70 nt apart from each other [Sharma *et al.*, 2010].

1.13 6S RNA in *A. aeolicus*

The 6S RNA from the hyperthermophilic bacterium *A. aeolicus* (Figure 1. 19), about 160 nt in length, belongs to the shortest known 6S RNAs, which usually have sizes of about 200 nt. This correlates with the minimized genome size (1.6 Mbp) of *A. aeolicus*. On the other hand, the presence of a 6S RNA in such an organism with an extremely reduced genome size highlights the importance of 6S RNA in regulating the dynamics of bacterial transcriptomes. The secondary structures of the free 6S RNA and the 6S RNA:pRNA hybrid structure were predicted by *in silico* methods and seem to be one of the most stable among known 6S RNAs due to its high GC content [Willkomm *et al.*, 2005]. The rod-shaped minimal free energy (MFE) structure is calculated to have a free enthalpy ΔG of −96 kcal/mol (*E. coli* 6S RNA (184 nt) ΔG= −80 kcal/mol; *B. subtilis* 6S-1 RNA (190 nt) ΔG= -63 kcal/mol) [Steuten *et al.*, 2014]. Furthermore, with a shortened variant of *A. aeolicus* 6S RNA (132 nt) it was possible to crystallize a part of the G/C-rich structure. RNA hydrolysis within the crystallization droplet produced a fragment representing the last 12 bp of the terminal stem of this 6S RNA. This fragment diffracted at 2.6 Å, showing a regular A-form duplex containing three G•U wobble-type base pairs. One G•U base pair was involved in an intermolecular interaction through a ribose-zipper motif at the crystal-packing interface [Kondo *et al.*, 2013].

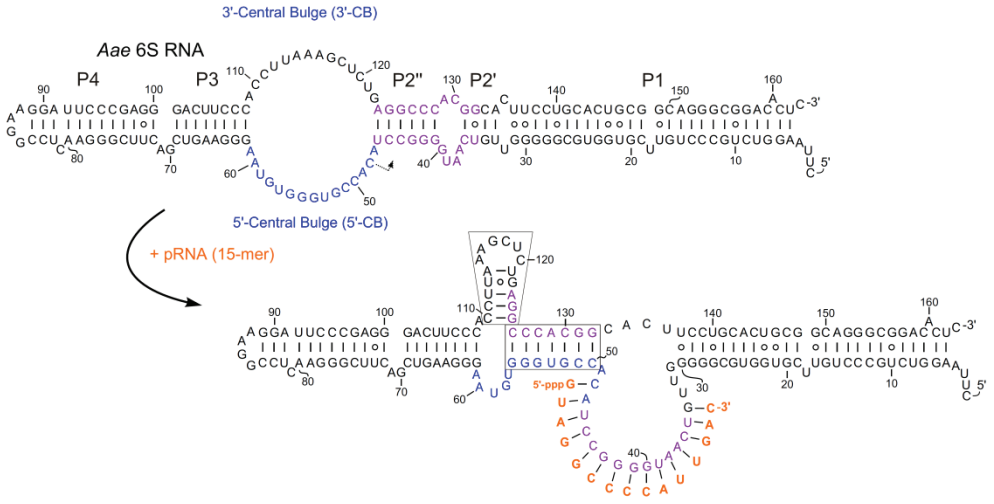

Figure 1. 19 Illustration of the secondary structure of *A. aeolicus* 6S RNA and of the predicted pRNA-induced structural rearrangement. *A. aeolicus* 6S RNA may involve both mechanistic components in its pRNA-induced rearrangement, hairpin formation in the 3'-CB and formation of a central bulge collapse helix (boxed elements) (figure adapted from Steuten *et al.*, 2014).

1.14 Future questions to be addressed

The physiological role of 6S RNAs is at present only partially understood. A key to understanding 6S RNA function was the observation that 6S RNA forms a complex with RNAP with a strong preference for binding to the housekeeping sigma-holoenzyme [Lee *et al.*, 1978; Wassarman and Storz, 2000; Trotochaud and Wassarman, 2005; Gildehaus *et al.*, 2007]. It could be shown that promoters with an extended -10 motif or promoters lacking a -35 consensus sequence are mainly affected by 6S RNA. Nevertheless, the criteria for the prediction of promoters that are affected by 6S RNA, and to what extent, need further refinement [Gildehaus *et al.*, 2007; Cavanagh *et al.*, 2008; Neusser *et al.*, 2010].

It has been suggested that 6S RNA has a general function in transcriptional adaptation during post-exponential or stationary phase, where its levels are usually highest [Trotochaud and Wassarman, 2005; Faucher *et al*, 2010]. However, the manifold adaptation is not necessarily focused on the stationary phase where cells reduce and modify transcription. Notwithstanding, a large number of genes whose expression is under the control of 6S RNA has been identified with genome-wide transcriptome analyses [Neusser *et al.*, 2010].

Apart from the finding that 6S RNA can serve as a template for transcription of short product RNAs, thereby dissociating the complex with RNAP to relieve transcriptional inhibition, the question arises if removal of transcriptional inhibition is the only biological effect or if the generated product RNAs themselves have further functions

in the cell [Wassarman and Saecker, 2006; Gildehaus *et al.*, 2007; Kugel and Goodrich, 2007].

For *E. coli* 6S RNA it could be shown that 5'-end maturation is mainly caused by RNase G and RNase E, when transcribed from *ssrS* P1 promoter, and by RNase E when transcribed from *ssrS* P2 promoter. The details of 3'-end maturation are less understood [Kim and Lee, 2004].

Moreover, the degradation of 6S RNA and of the 6S RNA:pRNA hybrid is not fully understood until now and needs further investigation. However, 6S-1 RNA of *B. subtilis* is cleaved in its apical loop during extended stationary phase, which may initiate RNA decay in this bacterium [Beckmann *et al.*, 2011]. It remains to be seen if 6S RNA decay pathways are similar in different bacteria.

The molecular basis for RNAP recognition of 6S RNA versus open DNA promoters is also unclear. No common functional groups of DNA promoter consensus sequences and nucleotides of the 6S RNA structure could be identified so far. For 6S RNA, a defined pattern of helical elements, bulges and internal loops as well as nucleotide identities or sequence patterns seem to be important for affinity [Steuten *et al.*, 2013]. Furthermore, how the inhibition of RNAP leads to differential down-regulation of cellular transcription units sequentially how this regulation affects other regulatory pathways has to be refined [Hansen *et al.*, 2008].

In a genome-wide transcriptome analysis using an *E. coli* strain lacking 6S RNA, a high amount of differentially expressed genes were identified to be affected by 6S RNA, either directly or indirectly. Mainly a significant increase in the level of ppGpp was observed, which is known as a global regulator of stringent response and growth rate regulation, resulting in a reduction of rRNAs and other components of the translation apparatus at early stationary phase. Thus, 6S RNA is indicated to be essential for the cellular capacity to adapt gene expression to changing environments. The effect of 6S RNA on ppGpp is in line with the assumption that 6S RNA is involved in stress adaptation. *E. coli* cells lacking 6S RNA could be shown to have a disadvantage in survival under conditions of long-term stationary phase, while they are more vital at higher pH. This can be attributed to enhanced *pspF* expression in the absence of 6S RNA. PspF acts in response to extracytoplasmic stress conditions that impair the integrity of the inner membrane [Jovanovic *et al.*, 2010]. Moreover, the cold shock protein CspA, the general stress proteins UspG and UspF and FNR (global transcriptional regulator under anaerobic growth conditions) are affected by 6S RNA [Trotochaud and Wassarman, 2004; Trotochaud and Wassarman, 2006; Jovanovic *et al.*, 2006; Neusser *et al.*, 2010; Geissen *et al.*, 2010]. These findings suggest that 6S RNA plays an important role in regulation of cell metabolism especially when resources become scarce or during other forms of stress cells are confronted with.

For *E. coli* 6S RNA, a dissociation of the sigma subunit during pRNA transcription could be determined at a pRNA length of 9 nt. After sigma dissociation, the remaining core enzyme elongates the pRNA to a length of 13 nt which then persistently induces the structural rearrangement and causes the 6S RNA:pRNA duplex to eventually dissociate from core RNAP [Panchapakesan and Unrau, 2012]. Until now, it could not be clarified if the same mechanism takes place within *B. subtilis*. The fact that a high amount of pRNAs with 8 to 10 nt, transcribed from 6S-1 RNA, were found *in vivo* would be consistent with a similar process of sigma RNAP binding and dissociation in *B. subtilis* [Beckmann *et al.*, 2011]. Thus, future studies have to clarify if σ^A could rebind to core RNAP when pRNAs (8 to 10-mers) dissociate to initiate a new pRNA transcription round.

Furthermore, the tertiary structures of a complete 6S RNA in its ground state (alone or in complex with σ^A-RNAP) and after pRNA-induced rearrangement await elucidation in the future.

2. Goal

RNase P project

Investigations about the 5' maturation reaction of the precursor tRNAs (ptRNAs) catalyzed by the ribonuclease P (RNaseP) led to a proposed two metal ion in-line SN_2 cleavage reaction. Therefore the two metal ions coordinated to the RNase P RNA subunit are connected to the tRNA phosphate between the nucleotides -1 and +1 either directly or indirectly via a water molecule and the M1 ion is responsible for the activation of an additional water molecule which led to the nucleophilic attack of the phosphorus atom. *In vivo t*he P protein subunit (single protein) of bacterial RNase P is important for the leader sequence binding.

To find out more detailed information about the RNase P cleavage reaction the shortest RNase P cleavable substrate and the shortest catalytically active form of the RNase P RNA (*E. coli* RNase P RNA C-domain termed Ecat) in combination with the P protein should be measured via NMR to get dynamic reaction information. Therefore different NMR spectra should be collected of the substrate alone, the C-domain (Ecat) alone and in combination with the P protein and of all three components. Afterwards the titration of different metal ions (Mg^{2+}, Mn^{2+}, Ca^{2+}) should lead to different NMR spectra. Ca^{2+} ions should lead to metal ion binding which may goes along with a conformational change but could not catalyze the cleavage reaction. The Mg^{2+} ion induced cleavage reaction should be detected. With the titration of the $^{55}Mn^{2+}$ ion a specific wider chemical shift range should be detectable within the NMR spectra so the nucleotides connected to the metal ions may be able to be identified. These measurements should gain insight to the dynamic time-solved RNase P cleavage reaction process including the involved P RNA nucleotides, mini substrate nucleotides and if possible to detect the participating P protein residues.

***Aquifex aeolicus* 6S RNA project**

Main research affords, to solve 6S RNA function, were performed in *E. coli* and *B. subtilis.* After 6S RNA homolog was found in *A. aeolicus* and were predicted to be the most stable homolog of the currently known 6S RNAs its secondary and tertiary structure should be investigated by NMR measurements. Hence, different length variants of *A. aeolicus* 6S RNA should be used to get in balance between structure stability and structural dissolvability. Also a shortened variant of *B. subtilis* 6S RNA should to be measureable by NMR. Simultaneously chemically secondary structure experiments already performed for *B. subtilis* 6S RNA [Beckmann and Hoch *et al.*,

2012] should be performed for *A. aeolicus* 6S RNA to reveal additional structure information.

To check the hallmark function abilities of *A. aeolicus* 6S RNA, RNAP binding experiments with the *B. subtilis* RNAP as well as release experiments with influence of different pRNA oligonucleotides should be performed. If RNAP:6S RNA complex formation can be reported, the competence to serve as template for *in* vitro pRNA transcription by RNAP should be set out. Additionally the minimal pRNA length required to induce structural rearrangement should be discovered *in vitro* by electrophoretic mobility shift assay.

The tertiary structure of 6S RNA seems to play a key role in RNAP binding and inhibition. Therefore different methods could be used. After the crystallization of the full length 6S RNA structure wasn't successful, another method for dynamic structural solution should be tested. Pf1 Phage DNA should orient the 6S RNA molecules within the magnetic field of the NMR device, which should reveal information about the orientation of the two helical stems of 6S RNA and the angle between them.

3. Materials and Methods

3.1 Bacterial cell culture

To avoid contamination, all buffers, media, glass pipettes, pipette tips, flasks and tubes used for bacterial cell culture were autoclaved for 20 min at 121°C and 2 bar or were sterile-filtered if heat-labile. To avoid contamination by heat-resistant RNases, glassware was additionally baked at 140°C for at least 4 h.

3.1.1 Bacterial cell culture in liquid medium

Table 3. 1 Composition of lysogeny broth medium

LB-medium	1 L
Yeast extract	5 g
Pepton/Bactotrypton	10 g
NaCl	10 g
ddH_2O	Ad 1 L

pH was adjusted to 7.5 with NaOH

Table 3. 2 Composition of terrific broth medium

TB-medium	1 L
Yeast extract	24 g
Pepton/Bactotrypton	12 g
Glycerol	4 mL
ddH_2O	Ad 900 mL

The medium was sterilized by autoclaving as described above and supplemented with 100 mL of a sterile-filtered solution of 0.17 M KH_2PO_4 and 0.72 M K_2HPO_4 (pH 7.5) prior to use.

E.coli cells were grown either in LB- or in TB-medium (Table 3. 1, Table 3. 2), depending on the desired amount of plasmid DNA, at 37°C under continuous shaking (200-220 rpm) in an erlenmeyer flask if not stated otherwise. The medium was supplemented with ampicillin (c_{end}: 100 µg/µL) for strain selection (puc18/19 and derivatives containing an amp resistance cassette). The bacterial cell culture was either used for recombinant DNA or protein production.

3.1.1.1 Recombinant DNA production and long term DNA storage

For cell growth, a small 3 mL culture of LB/TB-medium (Table 3. 1, Table 3. 2), supplemented with the appropriate antibiotic, was inoculated either directly from a glycerol stock or with a single colony from an agar-plate. These cultures were incubated (200-220 rpm, 37°C) overnight and were used directly for 'Mini-prep' plasmid DNA purification as described in chapter 3.3.1. For preparation of larger plamid quantities volumes of 100 mL-500 mL of medium (depending on the desired plasmid amount) were inoculated from the 3 mL culture after 8 h of growth followed by incubation overnight (200-220 rpm, 37°C).

For long-term storage 500 µL fresh bacterial culture was mixed with 500 µL Glycerol (99%) and immediately frozen in liquid nitrogen. The glycerol stocks were then stored at -80°C.

3.1.1.2 Recombinant protein production

For recombinant protein production a volume of 500 mL of LB/TB-medium (Table 3. 1, Table 3. 2) was inoculated with a 25 mL culture of LB/TB-medium overnight grown supplemented with antibiotic as described above. To initiate recombinant protein production plasmids with an inducible promoter system (in this case: lac-operon) were used. When cells had reached an OD_{600} of 0.6 (after approx. 3 h of growth), IPTG (c_{end}:1 mM) was added to the medium to induce effective protein expression. After 3 h at 37°C (200-220 rpm) the cells were pelletized by centrifugation (4°C, 4000 rpm, 15 min).

3.1.2 Cell growth on LB-agar-plates

For preparation of LB-agar-plates LB-medium was supplemented with 15 g/L Agar-Agar before autoclaving (Table 3. 3). For selection of cells with an antibiotic resistance the solution was supplemented with antibiotic (ampicillin,

100 µg/µL), when cooled down to ~50°C to prevent inactivation of thermo-labile antibiotics. The warm solution was cast into petri dishes and cooled down until it got solidified.

The LB-Agar-plates were stared upside down at 4°C for maximal 8 weeks.

Table 3. 3 Composition of lysogeny broth agar plates

LB agar-plates	1 L
Peptone	10 g
Yeast extract	5 g
NaCl	10 g
Agar-Agar	15 g

The pH was adjusted to 7.5 with NaOH before adding Agar-Agar to the solution

3.1.3 Preparation of competent cells

Competent cells are commonly used for recombinant DNA und protein expression (chapter 3.1.1.1. and 3.1.1.2). To give *E. coli* DH5α cells the capability to assimilate foreign DNA, they can be either treated with special buffers to induce chemical competence or with ice cold water for electro competence. For this study only chemically competent cells were used.

3.1.3.1 Preparation of chemical competent *E. coli* DH5α cells, $CaCl_2$ method

First, 3 mL LB-medium (Table 3. 1) was inoculated with *E. coli* DH5α cells from a glycerol stock and shaken overnight (37°C, 200-220 rpm). 500 mL LB-medium were inoculated with this ON-culture and incubated at 37°C (200-220 rpm), until it reached an OD_{600} of 0.5-0.7. The cells were transferred into two pre-chilled centrifuge tubes and pelletized at 4°C, 4000 rpm, 10 min. The supernatant was carefully removed and discarded. Afterwards the pellet was dissolved into 50 mL of ice cold 100 mM $CaCl_2$ solution. The mixture was incubated for 25 min on ice before the cells were again centrifuged at 4°C, 4000 rpm for 10 min. After discarding the supernatant the pellet was resuspended in 7 mL of a mixture of 75 mM $CaCl_2$ solution and

25% Glycerol (ice cold). The cells were aliquoted in portions of 100 µL each and snap frozen with liquid nitrogen. The aliquots were stored at -80°C. These competent cells are functional for several months.

3.1.3.2 DNA Transformation in chemical competent *E. coli* cells

The chemical competent *E. coli* DH5α cells (chapter 3.1.3.1) were slowly thawed on ice and 30 µL were transferred to a 1.5 mL reaction tube. Approximately 20 ng plasmid DNA (from a ligation, from a *DpnI* restriction reaction (chapter 3.3.6) or alternatively 1 µL of a 'Mini-prep' (chapter 3.1.1.1)) were added and the cells were incubated on ice for 20 min. To transform the foreign DNA into the cells, a heat-shock was performed for 30 s at 42°C. Subsequently, the cells were cooled on ice for 2 min before 600 µL fresh LB-medium (Table 3. 1) was added. To grow cells, the samples were shaken at 37°C and 800 rpm for 1 h. The grown cells were pelletized at room temperature with 4000 rpm for 3 min and the supernatant was discarded. The cells were resuspended in approx. 70 µL LB-medium, transferred to an LB_{Amp}-agar-plate (chapter 3.1.2) and struck out. The cells grew at 37°C overnight.

3.2 General nucleic acid techniques

3.2.1 Nucleic acid gel electrophoresis

The migration through a gel matrix of charged particles within an electric field is called gel electrophoresis. The efficiency of this separation correlates with differences in size and charge. The gel electrophoresis is a common technique used for separation of charged molecules as nucleic acids.

3.2.1.1 Agarose gel electrophoresis

Table 3. 4 Composition of fivefold TBE buffer

5x TBE buffer	c_{end}	5 L
Tris	445 mM	269.54 g
Boric acid	445 mM	137.57 g
EDTA	10 mM	18.61 g
ddH_2O	--	ad 5 L

Table 3. 5 Composition of fivefold DNA loading buffer

5x DNA loading buffer	c_{end}	10 mL
1% Bromophenol blue(BPB)	0.05% (w/v)	500 µL
1% Xylene cyanol blue(XCB)	0.05% (w/v)	500 µL
100% Glycerol	70% (w/v)	7 mL
1 M Tris/HCl, pH 7.5	100 mM	1 mL
0.5 M EDTA	50 mM (w/v)	1 mL
ddH_2O	--	ad 10 mL

Commonly, agarose gels are used to separate DNA fragments. Therefore the agarose, which is a polysaccharide composed of galactose and derivatives thereof, were solved in 1x TBE buffer (Table 3. 4) by heating in a microwave oven. Afterwards, for visualization of DNA, ethidium bromide is added to the solution to a final concentration of 40 µg/100 mL (chapter 3.2.1.3.1). The solution was shaken gently to avoid bubbles and poured into a clean gel tray with a comb to form sample pockets. The concentration of agarose affects the rate and separation efficiency of the particles and was chosen in dependency of the size of the analyzed fragments (Table 3. 6). After polymerization the gel tray was inserted in an electrophoresis chamber filled with 1x TBE buffer (running buffer; Table 3. 4). To load the DNA samples on the gel, 1 volume of the 5x DNA loading buffer (Table 3. 5) was mixed with 4 volumes of the sample. To determine the DNA fragments size, 3 µL of a 2kb ladder (Thermo Fisher Scientific; range: 100 bp to 10 kb) was also loaded on the gel. Gels ran at 120 V.

Table 3. 6 Separation range of DNA fragments in agarose gels of different concentration

% agarose (w/v)	DNA fragment size (kbp)
0.5	1.0-30
0.7	0.8-12
1.0	0.5-7
1.2	0.4-6
1.5	0.2-3
2.0	0.1-2

3.2.1.2 Polyacrylamide gel electrophoresis (PAGE)

For the separation of RNA (DNA is also possible) it is common practice to use polyacrylamide (PAA), which consist of cross-linked acrylamids. The crosslinks are initiated by bisacrylamide. By addition of APS (ammonium persulfate $(NH_4)_2S_2O_8$) and TEMED (N,N,N,N-tetramethylethylendiamin) the polymerization reaction is started, whereas TEMED serves as catalyst to stabilize the APS radical. The pore size of the gel is regulated by the density of the polymer chain as well as the yield of crosslinks which are formed by addition of bisacrylamide. Normally concentrations between 3.5% and 20% acrylamide/bisacrylamide, with a ratio of 48:2 acrylamide to bisacrylamide, are used. The RNA can be separated using two different types of PAA electrophoresis. The denaturing PAGE separates RNA exclusively by size, whereas the partition by native PAGE additionally depends on the three dimensional structure of the RNA.

3.2.1.2.1 Denaturing PAGE

Prior the RNA is able to be separated in dependence of its size its structure has to be denatured. Therefore, 1 volume 2x PPF loading buffer (Table 3. 7) is added. Optionally, the sample can be heated to 98°C for 5 min to denature all interactions. Usually, for nucleic acid structure denaturation, 8 M urea (Table 3. 9) is added to the PAA gel solution (Table 3. 8) before polymerization.

Table 3. 7 Composition of 2x PPF denaturing sample buffer

2x PPF denat. sample buffer	c_{end}	250 mL
1% BPB (w/v)	0.02%(w/v)	5 mL
1% XCB (w/v)	0.02%(w/v)	5 mL
Urea	2.6 M	39.04 g
Formamide	66% (v/v)	165 mL
10x TBE ~pH 8.3(3.2.1.1)	2x (pH 8.0)	50 mL
ddH_2O		ad 250 mL

Table 3. 8 Composition of PAA gel solution

PAA gel solution	20%
5x TBE	200 mL
Acrylamide/Bisacrylamid (48/2)	400 mL
Urea	480 g
ddH_2O	ad 1000 mL

Table 3. 9 Composition of 8 M urea solution

8 M urea	1 L
Urea	480 g
5x TBE	200 mL
ddH_2O	ad 1000 mL

The mixture was stirred at RT until urea is solved.

As indicated above, the percentage of PAA is in-between 3.5% and 20%. To dilute the 20% PAA solution (Table 3. 8) an appropriate amount of 8 M urea solution (Table 3. 9) is added. The co-migration of the single stranded RNA/DNA fragments with the BPB and XCB dye is shown in Table 3. 10

Table 3. 10 Fragment size of the single-stranded RNA/DNA (given in nucleotides) co-migrating with BPB/XCB dye from the denaturing sample buffer

% polyacrylamide	BPB	XCB
5	35	130
6	26	106
8	19	70-80
10	12	55
20	8	25

For analysis of the fragment size, different formats (10x11 cm, 16x24 cm, 16x40 cm, 20x30 cm) of glass plates are available in our lab, dependent on how much samples

should be separated and which kind of pattern is expected. E.g. for a control gel after a small scale *in vitro* T7 transcription (chapter 3.5.2), a gel format of 10x11 cm is used. For a gel separation subsequent to a structure probing reaction (chapter 3.5.6), 16x40 cm glass plates are used. To disenthrall the glass plates of contaminations they are cleaned with pure ethanol. To create space between the plates, spacers (0.5 or 1 mm) are attached and an appropriate volume of the gel solution (mixed with a 1/100 volume of APS and a 1/1000 volume of TEMED) is filled between the plates. To create pockets, a comb is integrated at the top of the glass plates. The polymerization of the gel takes approx. 30 min. To load the samples the comb has to be removed and the gel is vertically fixed into an electrophoresis chamber filled with 1x TBE buffer. The sample pockets have to be rinsed with 1x TBE buffer to remove urea that diffuses from the gel matrix and tends to accumulate in the pockets. Therefore a syringe has shown to be most suitable. The upper and the lower buffer reservoir are now connected to each other by the gel matrix. The electrophoresis is carried out at 8-40 mA (depending on gel size and PAA concentration).

3.2.1.2.2 Native PAGE

In contrast to the denaturing PAA gels native PAA gels do not contain urea, so that intermolecular and intramolecular interactions are not disrupted. The native PAA gel is commonly used for the analysis of nucleic acid structures, RNA/RNA, RNA/DNA and nucleic acids/protein interactions. Here it is not only the size of the molecule, but also the secondary and/or tertiary structure of the molecule that influences its electro-mobility. E.g. a mixture of two heterogeneous conformers of the same RNA shows different migration mobilities. As shown in Table 3.11 the size of the nucleic acid fragments co-migrates with BPB and XCB dye in the following range:

Table 3. 11 Estimated nucleic acid fragment size (bp) co-migrating with BPB and XCB in native PAA gels

% polyacrylamide	BPB	XCB
3.5	100	460
5	65	260
8	45	160
12	20	70
20	12	45

The preparation of the native gel solution is equivalent to the procedure explained for the denaturing PAA gels, but no urea is added. For dilution 1x TBE Buffer (Table 3. 4) is used. Priot to gel loading the samples were mixed with 2x native loading buffer.

Table 3. 12 Composition of twofold native loading buffer

2x native loading buffer	c_{end}	10 mL
100% Glycerol	30% (v/v)	3 mL
1% BPB (w/v)	0.02%	200 µL
1% XCB (w/v)	0.02%	200 µL

3.2.1.3 Detection of nucleic acids in a gel matrix

Dependent on the experimental context and further applications different methods are used for visualization of nucleic acid fragments within a gel. To qualitatively visualize nucleic acid within a gel ethidium bromide is commonly used. If the amount of the sample is low or small size nucleic acids should be visualized, other intercalating agents like SYBRgreen or SYBRgold were used. Especially for preparative purposes, the fragments can be visualized by UV-shadowing (254 nm) (chapter 3.2.1.3.2) or for quantitative detection ^{32}P-radiolabeled DNA/RNA can be visualized using a phosphor-imager.

3.2.1.3.1 Ethidium bromide (EtBr) staining

The aromatic molecule ethidium bromide intercalates between the stacked bases of DNA and RNA. Its core is composed of the planar, heterocyclic phenanthridine which is an isomer of the fluorescent dye acridine. Stimulation with UV light between 210 nm and 285 nm (absorption maxima of EtBr) leads to the emission of orange light at a wavelength of 605 nm. After intercalation to the nucleic acid the emission intensity is almost 20-fold higher, than in its free state.
For detection of nucleic acids 40 mg/100 mL EtBr are added to an agarose gel solution as described in chapter 3.2.1.1 to stain DNA fragments.
After PAA gel electrophoresis, the gel has to be carefully transferred into a plastic bag and 0.5 µg/mL EtBr in 1x TBE buffer are poured onto the gel. After sealing the bag, it was rotated for 5-10 min at RT. Gels were analyzed using an UV transilluminator after the EtBr solution had been removed with caution.

3.2.1.3.2 UV-shadowing

When DNA and RNA were purified via PAGE, UV-shadowing (254 nm) was used for the visualization of the nucleic acids. Subsequent to the electrophoresis the glass plates were removed, the gel was wrapped in clingfilm and was placed on a thinlayer chromatography plate with a fluorescence indicator (254 nm). An UV light source (254 nm) was focused on the surface of the gel. The absorption maxima of nucleic acids at 260 nm led to absorbance of the UV light by the RNA/DNA bands which prohibit the light passing through onto the thinlayer chromatography plate. The visualized dark band of the DNA/RNA was marked with an overhead marker, carefully excised. The nucleic acid was eluted from the gel slice by deffusion as described in chapter 3.2.4.

3.2.1.3.3 Radioluminography

Radioluminography is a commonly used method for detection and quantification of nucleic acids which are labeled with the radioactive isotope of phosphorus (^{32}P). To detect the nucleic acids after PAGE the PAA gel was wrapped into clingfilm and a phosphor-image-plate is exposed for a specific time frame dependent on the amount of radioactivity (e.g. a 1 min exposure for labeling reactions and overnight exposure for structure probing reactions). After exposition the image plate was readout by a phosphor-imager (BIO-imaging analyser BAS 1000 (Raytest, Fujifilm; Software: PC-BAS). Further evaluation was done with the software AIDA.

3.2.2 Photometric concentration determination of nucleic acids

For many reactions, e.g. after a plasmid purification, it is essential to know the concentration of the nucleic acids situated in a solution. Commonly, the concentration of nucleic acids is determined by measurement of the absorption of UV light (260 nm). Afterwards, according to the Lambert Beer law the concentration is calculated as follows:

$A = \varepsilon \cdot c \cdot d$

(A: Absorbance, c: molar concentration of the nucleic acid [mol/L], ε: molar extinction coefficient [L/(mol · cm)], d: path length of the cuvette [cm]).

The general formula for the concentration calculation of nucleic acids is:

$$c[\frac{\mu g}{\mu l}] = \frac{A_{260} \cdot c(1\ A_{260}) \cdot D_f}{1000}$$

(c: concentration in µg/µL, D_f: dilution factor)

When the expected absorbance outranges the range of 0.1 to 0.8 the sample was deluted with ddH_2O (commonly a dilution between 1:100 and 1:700 is appropriate). Deionized/double distilled water is used as blank value for the UV-spectrophotometer, before the absorbance of the samples is measured. Afterwards, the concentration is calculated using the known specific absorbance values c(1 A_{260}). This value represents the concentration corresponding to an absorbance of 1.0 at 260 nm (1 A_{260}) (cuvette-width=1 cm):

1 A_{260}: dsDNA	corresponds to a c(1 A_{260}) of ~50 µg/mL
1 A_{260}: ssDNA	corresponds to a c(1 A_{260}) of ~33 µg/mL
1 A_{260}: RNA	corresponds to a c(1 A_{260}) of ~40 µg/mL

3.2.3 Isolation of DNA from agarose gels

After agarose gel electrophoresis (chapter 3.2.1.1) the DNA was extracted from the gel using the Qiagen QIAquick Gel Extraction Kit. Therefore the DNA band was excised with a sterile, sharp scalpel and solved by heating the gel slice to 50°C for 10 min or until the gel slice has completely dissolved in 3 volumes of kit supplied high salt buffer. The mixture was then applied to a minispin silica membrane column and centrifuged at 13,000 rpm for 1 min for DNA binding. Thereby salts, nucleotides, agarose, enzymes, ethidium bromide and other impurities from the DNA sample were removed. After washing steps according to the manufacturer's recommendations the DNA was recovered from the columns using ddH_2O or a low salt buffer (Kit supplied). For detailed information on the procedure see the manufacturer protocol.

3.2.4 Isolation of RNA from PAA gels

RNA transcripts can be isolated after a PAA gel separation by diffusion elution in 0.3-1 M sodium-acetate solution (NaOAc). The RNA bands were visualized by UV-shadowing and excised with a sterile scalpel (see protocol 3.2.1.3.2). Afterwards the gel slice is transferred into 5-20 mL of 1 M NaOAc solution depending on the size of the gel slice and was shaken overnight at 4°C in a horizontal shaker at approx. 400 rpm (1 to 2 elution procedures; each overnight).

3.2.5 Alcohol precipitation

3.2.5.1 Ethanol precipitation

For removal of salt contaminations and for reduction of the sample volume nucleic acids were precipitated with ethanol. To visualize the DNA/RNA pellet especially for short nucleic acid fragments or small amounts of nucleic acids 20-40 µg of glycogen were added to the sample before precipitation. Precipitation of nucleic acids is achieved by addition of 2.5 volumes of ethanol p.a. and 0.1 volumes of 3 M NaOAc (c_{end} 0.3 M, pH 5.0) and mixed vigorously, followed by incubation at -20°C for at least 30 min or -80°C for 5 to 10 min, to increase precipitation efficiency. The precipitate was pelletized by centrifugation at 4°C for at least 30 min, the supernatant was discarded and the pellet was washed with 70% ethanol to remove salt contaminants. The reaction tube was incubated with an open lid at room temperature for 5 min to allow residual ethanol to evaporate. Subsequently, the pellet was resolved in an appropriate volume of double distilled water or TE buffer.

Table 3. 13 Composition of 10x TE buffer

10x TE buffer	c_{end}
Tris-HCl pH 8.0	100 mM
EDTA	10 mM

3.2.5.2 Isopropanol precipitation

A highly efficient method for alcohol precipitation of nucleic acids is the isopropanol precipitation. For precipitation of nucleic acids one volume of isopropanol was added to the samples at RT. The samples were centrifuged as described in chapter 3.2.5.1 and afterwards washed with 70% ethanol. Subsequently, the pellet was resolved in an appropriate volume of double distilled water or TE buffer.

3.2.6 Phenol/chloroform extraction

The separation of DNA or RNA from proteins e.g. restriction enzymes is usually conducted by a phenol/chloroform extraction. Deproteinisation is more efficient when two different organic solvents are used. For the extraction one volume of the nucleic acid sample solved in double distilled water is mixed rigorously with one volume of phenol/aqua phenol (depended on which nucleic acid should be purified (DNA/RNA)) on a vortex mixer and then centrifuged for 5 min with 13,000 rpm at RT, to achieve phase separation. The upper aqueous layer contains the DNA/RNA and is carefully transferred to a new tube. The sample is mixed with one volume of chloroform, vortexed for 1 min and centrifuged again for 5 min with 13,000 rpm at RT. Afterwards the DNA/RNA containing upper layer (water) is transferred into a new tube and the nucleic acid is precipitated with either isopropanol or ethanol as described in chapter 3.2.5.

3.2.7 Amicon Ultra gel filtration

To remove salts, single nucleotides or small fragments from DNA/RNA or protein samples 'Amicon Ultra centrifugal filter-units' were used. This device consists of a polypropylene tube and an ultracel regenerated cellulose membrane. Dependent on the size of the desired molecule and the sample volume, different filter units can be used. Filter units with a volume of 0.5 mL, 2 mL, 4 mL and 15 mL are available from Merck Millipore. To separate different molecule sizes membranes with a filter cut-off from 3K (kDa) up to 100K are accessible. E.g. the buffer exchange and removal of unbound pRNA after the *A. aeolicus* 6S RNA 132-nt (~44 kDa):pRNA hybridization, was operated with an Amicon ultra 0.5K filter unit with a cut-off of 30K. The procedure was performed according to the manufacturer's protocol.

3.3 DNA techniques

3.3.1 Preparation of plasmid DNA

Depending on the desired amount of plasmid DNA different column sizes of the Macharey-Nagel plasmid DNA preparation kit were used. For 'Mini-preps' the cells pelletized from a 3 mL *E. coli* bacterial culture were used for the preparation. 'Maxi-', 'Mega-' or 'Giga-preps' were performed from a 150 mL, a 250 mL or 1-4x 500 mL bacterial cultures dependent on the wet pellet weight. Giga-preps were performed for high yield DNA preparation (used as templetes for T7-Transkription of RNAs for NMR measurements (see chapter 3.5)). The plasmid preparation was

performed according to the protocol supplied by the manufacturer, briefly after a SDS/alkaline lysis step, the solution was neutralized and applied onto the provided AX silica-based anion exchange resin (hydrophilic, macro porous silica beads coupled to a methyl-ethylamine functional group) columns. The functional group provides a high overall positive charge density that permits binding of the negatively charged phosphate backbone of the plasmid DNA. Adjusted to a pH of 6.3 DNA was bound to the columns whereas salts, proteins and other molecules were washed off with the flowthrough. The elution was performed with an elution buffer with a pH of 8.5. After the elution the DNA was alcohol precipitated. For more details see the user manual provided by the manufacturer.

Table 3. 14 The classic anion exchanger for purification of transfection-grade plasmid DNA (according user manual provided by manufacturer).

	NucleoBond PC 20	NucleoBond PC 100	NucleoBond PC 500	NucleoBond PC 2 000	NucleoBond PC 10 000
Technology	Anion-exchange chromatography	Anion-exchange chromatography	Anion-exchange chromatography	Anion-exchange chromatography	Anion-exchange chromatography
Format	Mini -Gravity-flow columns	Midi-Gravity-flow columns	Maxi -Gravity-flow columns	Mega-Gravity-flow columns	Giga- Gravity-flow columns
Lysate clarification	Centrifugation	Folded filters	Folded filters	Folded filters	Folded filters
Sample material	1–5 mL (HC*) 3–10 mL (LC**)	5–30 mL (HC*) 10–100 mL (LC**)	30–150 mL (HC*) 100–500 mL (LC**)	150–500 mL (HC*)	500–2000 mL (HC*)
Vector size	< 300 kbp	< 300 kbp	< 300 kbp	< 300 kbp	< 300 kbp
Typical yield	3–20 µg	20–100 µg	400–500 µg	500–2000 µg	2000–10000 µg
$A_{260/280}$	1.80–1.95	1.80–1.95	1.80–1.95	1.80–1.95	1.80–1.95
Preparation time	60 min/ 4–6 preps	65 min/ 4–6 preps	80–90 min/ 4 preps	90–120 min/ 4–6 preps	120–150 min/ 2 preps
Binding capacity	20 µg	100 µg	500 µg	2000 µg	10000 µg

* High-copy plasmids; ** Low-copy plasmids

3.3.2 Restriction digestion of DNA

The linearization of plasmid DNA (e.g. for DNA analysis, *run-off* T7 transcription or double digestion for cloning reactions) normally restriction by specific endonucleases is performed. Double-stranded DNA is cleaved by these Type II nucleases at defined positions mostly within or close to palindromic recognition sequences. The DNA fragments have either 5'- or 3'-overhangs (sticky ends) or blunt ends with 3'-hydroxyl and 5'-phosphate termini after cleavage.

Table 3. 15 DNA digestion reaction

Digestion reaction	20 µL	1 mL
DNA (0.1 µg-1.5 mg)	x µL	x µL
10x buffer/FD buffer	2 µL	100 µL
Restriction enzyme	0.2-2 µL	40-100 µL
ddH_2O	Ad 20 µL	Ad 1000 µL

The used buffer conditions, the incubation temperature and the incubation time (3 h-ON) depended on the specific restriction enzyme and the amount of DNA that should be cleaved. The applied amount of enzyme was chosen in dependence of the amount of DNA and did not exceed more than 1/10 of the total reaction volume.
After digestion the cleaved DNA was analyzed on an agarose gel (see chapter 3.2.1.1). To separate the DNA from salts, enzymes etc. the digested DNA was extracted with phenol/chloroform (see chapter 3.2.6) followed by ethanol precipitation (chapter 3.2.5.1).

3.3.3 Dephosphorylation of DNA

To avoid self-ligation after a restriction digestion, it is important to dephosphorylate the 5'-ends of the digested DNA. Therefore the enzyme 'calf intestinal alkaline phosphatase (CIAP)' or 'thermosensitive alkaline phosphatase (Fast AP (Thermo Fisher))' were used. These enzymes catalyze the removal of terminal 5'-phosphates from DNA as well as from RNA, ribo- and deoxyribonucleotide triphosphates.

Table 3. 16 DNA dephosphorylation reaction with CIAP

Dephosphorylation reaction (CIAP)	20 µL	50 µL
DNA (1 -10 µg)	x µL	x µL
10x CIAP buffer	2 µL	5 µL
CIAP 1 U/µL	2 µL	5 µL
ddH_2O	Ad 20 µL	Ad 50 µL

The mixture was incubated for 30 min at 37°C.

Table 3. 17 DNA dephosphorylation reaction with Fast AP

Dephosphorylation reaction (Fast AP)	20 µL	50 µL
DNA	x µL (1 -10 µg)	x µL (90-175 µg)
10x Fast AP buffer	2 µL	5 µL
Fast AP 1 U/µL	2 µL	10 µL
ddH_2O	Ad 20 µL	Ad 50 µL

The sample was incubated for 15 min to 3 h at 37°C dependent on the amount of DNA.

The linearized plasmid DNA was either mixed with the reaction buffer and was incubated with the enzyme at 37°C or the dephosphorylation was performed in parallel with the digestion as a one-pot reaction in case of the Fast AP.

Table 3. 18 DNA dephosphorylation and digestion reaction with Fast AP

Dephosphorylation reaction (Fast AP) with parallel digestion	21 µL
DNA (1 µg)	x µL
10x Fast AP buffer	2.1 µL
Fast AP 1 U/µL	2 µL
Fast restriction enzyme 1	1 µL
Fast restriction enzyme 2	1 µL
ddH_2O	Ad 21 µL

The mixture was incubated for 15 min at 37°C.

To inactivate the enzyme it is possible to heat it to 65°C for 15 min, to perform a phenol/chloroform extraction (chapter 3.2.6) or to purify the linearized DNA by gel extraction (chapters 3.2.1.1 and 3.2.3)

3.3.4 5’-phosphorylation of DNA

An insert for ligation of linear DNA into a linearized plasmid (chapter 3.3.5) were e.g. generated by PCR amplification (chapter 3.3.6). The primers used for the PCR need to be phosphorylated on their 5'-end in advance. Therefore, T4 Polynucleotide Kinase (T4 PNK) is commonly used, which is able to transfer the gamma phosphate of a nucleoside triphosphate (here ATP) to the 5'-OH group of DNA.

Table 3. 19 DNA phosphorylation reaction with T4 PNK

Phosphorylation reaction	50 µL
DNA (100 pmol/µL)	x µL
10x T4 PNK buffer A (forward)	5 µL
10 mM ATP	5 µL
T4 PNK (10 U/µL)	2 µL
ddH_2O	Ad 50 µL

The sample was incubated for 1 h at 37°C.

T4 PNK can be inactivated by incubation at 75 °C for 10 min. Purification of the phosphorylated primers is possible by phenol/chloroform extraction (chapter 3.2.6), but normally not necessary as primers can be added to the PCR directly from the inactivated phosphorylation reaction mixture.

3.3.5 Ligation of DNA fragments

For the mutation of DNA sequences usually dsDNA fragments, so called inserts, whose sequence is carriing a mutation or a mutated region in comparison to the wild type, were used. These inserts be produced either by annealing of chemically synthesized ssDNAs or by PCR reaction (chapter 3.3.6). Afterwards, the insert is ligated into linearized vector DNA, which has been linearized with the respective restriction enzyme. The T4 DNA Ligase catalyses the formation of a phosphodiester bond between the 5’-phosphate of the insert and the dephosphorylated 3’-OH-group of the plasmid DNA.

Table 3. 20 DNA ligation reaction

Ligation reaction	control (0:1)	control (10:1) without T4 ligase	10:1
Linearized DNA (50 ng)	1 µL	1 µL	1 µL
Insert DNA (8 pmol/µL)	--	1.5 µL	1.5 µL
10x T4 DNA ligase buffer	2 µL	2 µL	2 µL
T4 DNA ligase	0.5 µL	--	0.5 µL
ddH_2O	Ad 20 µL	Ad 20 µL	Ad 20 µL

The mixture was incubated for 1 h or overnight at 22°C.

The negative controls without insert DNA or without T4 DNA ligase were performed to gain insight of the amount of uncut or religated plasmid DNA.

10 µL of the ligation mixture was directly used for transformation (30 µL of chemical competent cells (chapter 3.1.3)).

3.3.6 Polymerase chain reaction (PCR)

To amplify a small amount of DNA, the polymerase chain reaction (PCR) is commonly used. For a standard PCR the dsDNA template, a pair of short ssDNA primers (oligonucleotides) (forward and reverse direction), dNTPs (N= A, T, G, C) and a thermostable DNA polymerase (*Pfu* (*pyrococcus furiosus*;; 0.5 kb/min; exhibits a proofreading activity (3'-→5'-exonuclease activity); does not produce 3'-overhangs), *Taq* (*Thermus aquaticus*; 1 kb/min; error rate of 1/10,000 (8x less accurate than *Pfu* polymerase); produces adenine overhangs) or *Phusion* polymerase (4kb/min, error rate > 50-fold lower than *Taq* and 6-fold lower than *Pfu*, proofreading activity (5´-→ 3´-polymerase activity, 3´- → 5´-exonuclease activity), generates blunt-ended products) are mixed. The reaction mixture is then exposed to a circular succession of different temperature steps using a thermal cycler with a heated lid (to avoid condensation). The first step is the denaturing of the dsDNA by heating to 95°C for 30 sec. Afterwards, 30 cycles are performed as follows: 1) 98°C – 20'', 2) x°C – 30'', 3) 72°C – y''. Step 1 denatures the dsDNA in the beginning of each cycle. Step 2 gives the primers 30 sec to hybridize to the ssDNA. Therefore, an annealing temperature (x) usually between 45 and 65°C is chosen (calculated according to the T_m of the

primers minus 3-5°C). The third step of each cycle (72°C) allows the added polymerase to elongate the primer. The elongation time (y) is dependend on the length of the desired DNA fragment and the used polymerase.

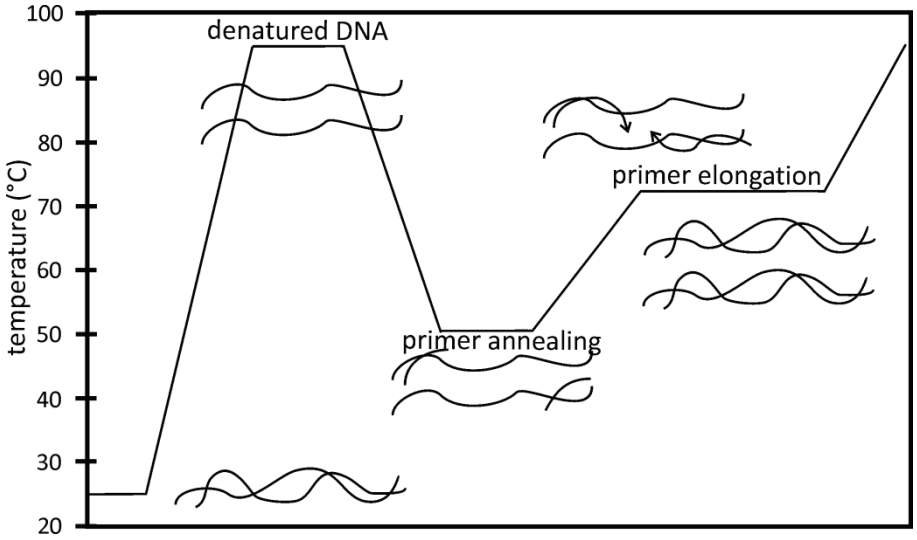

Figure 3. 1 Schematic illustration of a PCR reaction profile.

Table 3. 21 Polymerase chain reaction with Pfu or Taq polymerase

PCR program (*Pfu*/*Taq*)

Initial denaturation	95°C	30''
Denaturation	95°C	20''
Annealing	45-65°C	30''
Elongation	72°C	30''-7' (30 cycles)
Final elongation	72°C	3'

Table 3. 22 Polymerase chain reaction with Phusion polymerase

PCR program (*Phusion*)

Initial denaturation	98°C	30''
Denaturation	98°C	5-10''
Annealing	45-72°C	10-30''
Elongation	72°C	15''-2' (30 cycles)
Final elongation	72°C	5-10'

After the PCR 1-10 µL of each sample was checked on an agarose gel ideally one clear product band should be visible. For removal of the template DNA e.g. prior transformation a digestion with 1-3 µL *Dpn* I for 1-4 h at 37°C was performed. *Dpn* I is a restriction enzyme degrading only methylated DNA (plasmid DNA isolated from recombinant DNA preparation) containing the recognition sequence GATC, whereas the newly amplified unmethylated DNA is not affected.

3.3.7 DNA sequencing

3.3.7.1 Sanger sequencing

Sanger sequencing is a method to investigate the sequence of DNA based on the selective incorporation of didesoxynucleotides by DNA polymerase during DNA replication *in vitro*, which leads to a chain-termination [Sanger and Coulson, 1975; Sanger *et al.*, 1977].

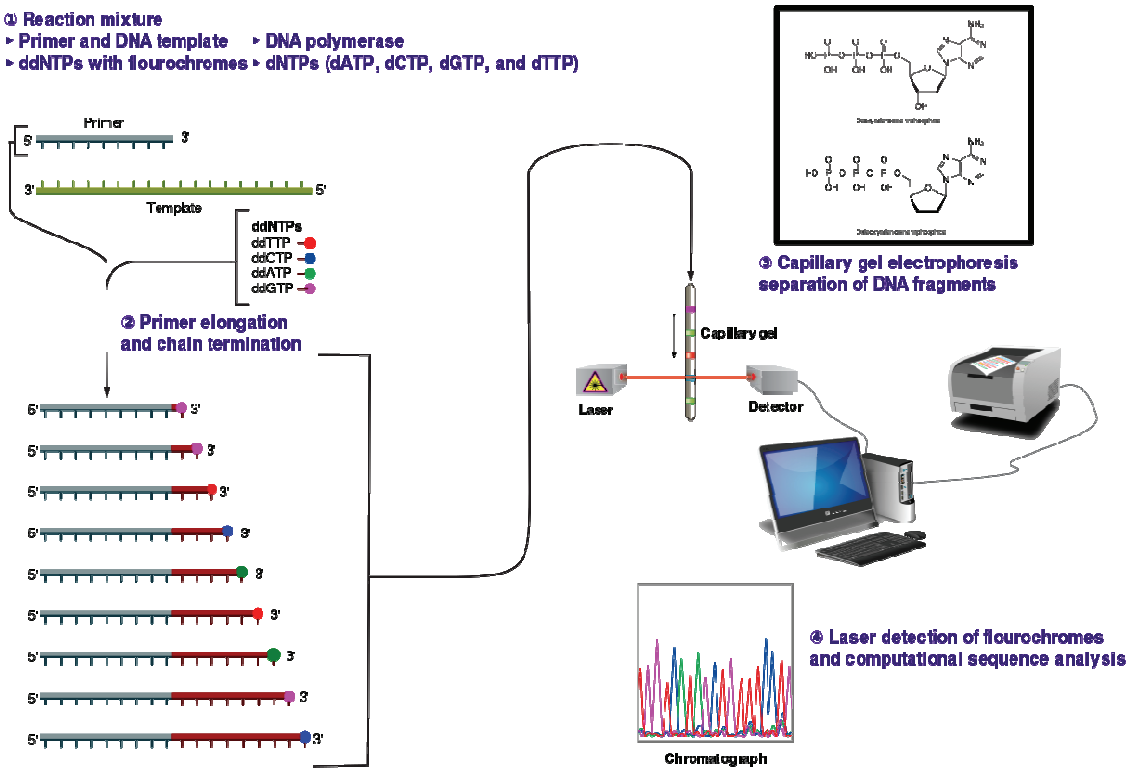

Figure 3. 2 The Sanger method for DNA sequencing. (1) A sequence specific primer is annealed to a sequence. (2) DNA polymerase, dNTPs, and a small amount of all four dideoxynucleotides (ddNTPs) labeled with fluorophores are added to the primer and template. The random insertion of a ddNTP instead of a dNTP during primer elongation leads to chain termination. All possible lengths of fragments are produced. (3) The products are separated on a single lane capillary gel and viualized by radioluminography. (4) This produces are detected by laser and evaluated *in silico*. (Figure according to http://commons.wikimedia.org/wiki/File:Sanger-sequencing.svg)

SsDNA templates were supplemented with a sequence-specific DNA primer which hybridized to the template. The primer was elongated by DNA polymerase using dNTPs and modified ddNTPs. The incorporation of the ddNTPs terminates the DNA elongation which produces DNA fragments of all possible length according to the ssDNA sequence. The ddNTPs are labeled either radioactive of fluorescently and thereby the length of the different fragments can be detected in automated sequencing machines (Figure 3. 3)

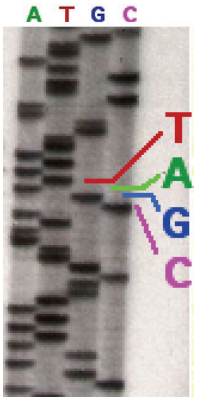

Figure 3. 3 DNA sequencing gel. Sequence visualized by autoradiography. (Figure taken from en:Image:Sequencing.jpg)

3.3.7.2 Deep sequencing

The so called "Next-Gen" sequencing methods displaced the Sanger sequencing after decades of application, especially for large-scale, automated genome analyses.

To investigate the exact order of nucleotides within DNA molecules DNA sequencing is a frequently used method. E.g. the 454 sequencing (Figure 3. 4), where dsDNA fragments between 100 and 400 bp can be analyzed.

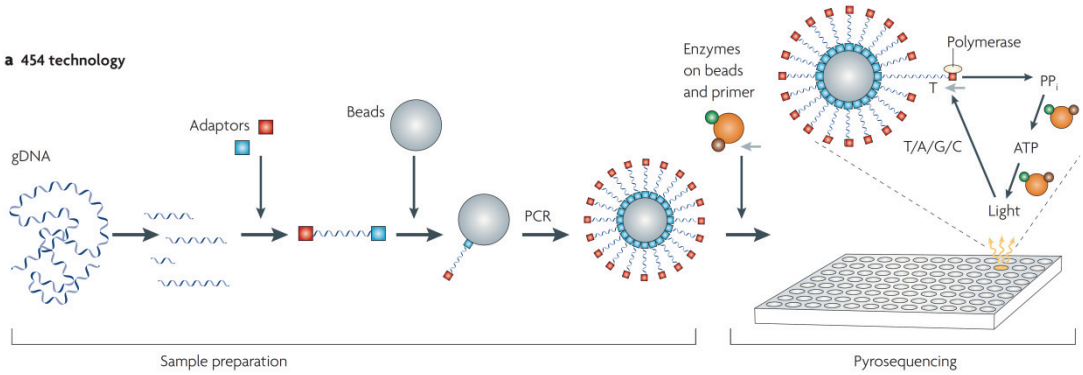

Figure 3. 4 454 sequencing is a highly parallel, two-step method. After the desired DNA is sheared, oligonucleotide adaptors are attached and further each fragment is fixed to a bead. The beads are located in an oil-water emulsion droplet. Within this droplet the fragments are amplified by PCR which generates multiple copies of the same DNA sequence an each bead. Afterwards the beads are transferred in picolitre-sized wells and pyrophosphate-based sequencing is performed in parallel on each DNA fragment. Pyrophosphate (PPi) arises during nucleotide incorporation and is detected. The PPi is released and converted to ATP. Luciferase uses the ATP to generate light. This is performed for each of the four bases (according to Medini *et al.*, 2008).

These fragments were sorted by size and mixed with two different oligonucleotide adapters. These adapters served as starting point for the elongation. One of these adapters carried a biotin label, so ssDNA fragments could be excluded. To amplify the fragments the selected fragments were linked on beads in a water-oil emulsion

droplet. In these droplets the PCR reaction takes place and during the nucleotide integration pyrophosphate (PPi) is released. This PPi is converted to ATP and this ATP is used by luciferaseto generate a light signal, which is proportional to the amount of integrated nucleotides. This circle is performed for each of the four bases. Also other DNA sequencing methods like Sanger sequencing, Ion torrent sequencing, SOLiD or Illumina/Solexa sequencing are nowadays commonly used [Medini *et al.*, 2008].

3.4 RNA techniques

3.4.1 Preparation of total RNA/ hot phenol method

For preparation of the *A. aeolicus* total RNA cell pellets were prepared by M. Thomm and R Huber from the University of Regensburg. The total RNA was extracted using the hot phenol extraction method. Therefore, the dry pellets were resolved in 4 mL of pre-chilled extraction buffer (4°C).

Table 3. 23 Composition of Extraction buffer

Extraction buffer	c_{end}	100 mL
3 M NaOAc pH 6.5	10 mM	333 µL
Sucrose	150 mM	5.1 g
ddH_2O	--	Ad 80 mL
The sample was addjucted to pH 4.8 with HOAc		
ddH_2O	--	Ad 100 mL

For sterilization a sterile-filter with the pore size of 0.2 µm was used.

For lysis of gram-positive bacteria it is essential to add lysozyme to a final concentration of 1.8 mg/mL and incubate them for 10 min at room temperature. Afterwards, 200 µL of 20% SDS solution was added and the aqueous phase was mixed with 4 mL pre-heated aqua phenol (65°C) followed by rigorous vortexing. The solution was incubated for 5 min at 65°C and then 5 min on ice. For phase separation the mixture was centrifuged at 10,000 rpm, 4°C for 20 min. The supernatant was transferred to a fresh tube and again 4 mL aqua phenol were added to the aqueous phase and thoroughly mixed. After an identical centrifugation step the supernatant

was transferred to a new tube and 4 mL chloroform were added and mixed to remove remaining phenol. Another centrifugation step was performed at room temperature and the supernatant was transferred to a clean tube. 0.1 volumes of 3 M NaOAc and 1 volume of isopropanol were added to precipitate the RNA. Centrifugation was carried out at 10,000 rpm at 4°C for 45 min to pelletize the RNA. After discarding the supernatant the pellet was washed with 200 µL 70% ethanol, centrifuged for 15 min (10,000 rpm, 4°C) and dried for 5 min at room temperature. At last the pellet was resuspended in 100 µL ddH_2O.

3.4.2 dRNA-seq

Differential RNA sequencing (sRNA-seq) is a method to use the deep-sequencing technologies to transcriptome analysis for the selective analysis of primary transcripts in the cell. Based on the treatment of the total RNA sample with a differential exonuclease (5'-TEX: terminator^{TM} 5'-phosphate-dependent exonuclease), which leads to depletion of processed RNAs, the primary transcripts get enriched in relative terms. Afterwards, cDNA libraries are generated from untreated RNA and TEX treated RNA sample. Comparison of both leads to a global mapping of transcriptional start sites, relieves the determination of new promoter regions and can be used to identify small regulatory RNAs and antisense transcripts (Figure 3. 5) [Harbers and Kahl, 2012].

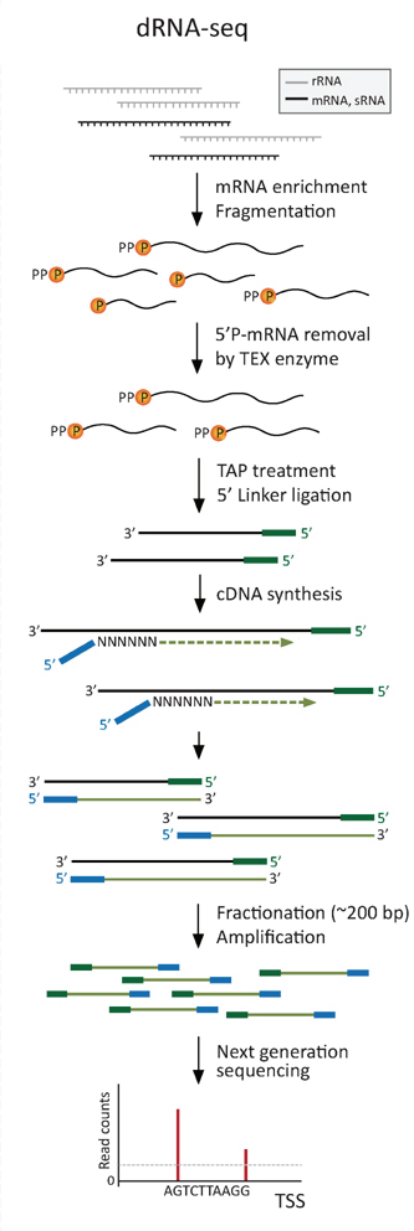

Figure 3. 5 Differential RNA sequencing- Method for strand-specific RNA-sequencing (according to Cho *et al.*, 2013).

The total RNA from *A. aeolicus* cells were extracted by hot phenol extraction (chapter 3.4.1) and used for the differential deep sequencing (dRNA-seq) approach [Sittka *et al.*, 2008, Sharma *et al.*, 2010]. The total RNA was treated with TEX to enrich primary transcripts which afterwards were separated by gel electrophoreses to yield transcript lower 50 bp. The data analysis was performed by Dr. Marcus Lechner from our lab.

3.5 T7 transcription

3.5.1 *in vitro* T7 *run off* transcription

In our lab the transcription of RNA were commonly performed by a standard protocol with a reaction volume of 500 or 1000 µL with an Mg^{2+} endconcentration of 33 mM.

Table 3. 24 Composition used for the standard transcription protocol

Standard transcription protocol	c_{end}	500 µL
Linearized plasmid DNA/ PCR product	40 µg	x µL
3 M $MgCl_2$	33 mM	5.5 µL
1 M Hepes pH 7.5	50 mM	40 µL
1 M DTT	50 mM	25 µL
100 mM Spermidine	1 mM	5 µL
2 mg/mL BSA	60 µg	30 µL
200 µg/mL Pyrophosphatase	0.5 µg	2.5 µL
100 mM NTP (25 mM each)	15 mM	75 µL
ddH_2O	--	Ad 490 µL
T7-RNA Polymerase	--	10 µL

The mixture, descript in Table 3. 24, was incubated at 37°C for 2 h before an additional 10 µL of T7-RNA Polymerase were supplemented. Further incubation at 37°C for 2 h was performed. The reaction process was monitored afterwards by gel electrophoresis of 2 µL sample mixted with 3 µL ddH_2O and 5 µL 2x PPF loading buffer on an 8% denaturing PAA gel. Subsequently, the remaining sample was mixed with one volume 2x PPF loading buffer and separated by a preparative gel electrophoresis (8% denaturing PAA gel). In place of a comp, a spacer was used to generate a large pocked to load the whole sample volume (maximal 2.5 mL). As size marker, an RNA with a similar size as the desired transcription product was loaded in a second smaller pocket. Afterwards, the RNA was eluted as descriped in chapter 3.2.4

3.5.2 Large-scale *in vitro* T7 *run off* transcription

For large scale production of RNAs, which are used in downstream applications (e.g. structure probing, functional assays) *in vitro* transcription utilizing the T7 phage RNA polymerase and the corresponding promoter was carried out. The T7 phage RNA polymerase recognizes the specific T7 phage promoter sequence 5'-TAA TAC GAC TCA CTA TA-3' (sense strand) and the polymerization is processed in 5'- → 3'-direction. To terminate the transcription process on a defined position, the template plasmid was linearized downstream of the desired sequence, by a restriction endonuclease. The polymerase then runs off the template after transcription. Disadvantages of this technique are a) the polymerase reads through the restriction site of the template and b) T7 phage polymerase adds nonspecific adenosine residues. This leads to non homogenous 3'-ends of the transcript and to addition of non desired bases on the 3' end of the transcript.

For production of homogenous 5'- and/or 3'-ends of RNA, either a hammerhead (HH) or a HDV (hepatitis delta virus) ribozyme (small autocatalytic RNA motifs that catalyzes phosphodiester bond hydrolysis at a single defined position) (chapter 3.5.2.1, 3.5.2.2) was used. Autocatalytic cleavage of a 5'-end HH ribozyme leads to a terminal 5'-OH group which can be directly labeled radioactive using γ-^{32}P ATP (chapter 3.5.3). 3'-HH- and 3'-HDV-cleavage leads to a 2'-, 3'-cyclo phosphate end which has to be hydrolyzed before 3'-labeling with 5'-^{32}P pCp (chapter 3.5.4). RNA substrates without 5'-HH sequence need to be 5'-dephosphorylated (chapter 3.3.3) prior to labeling to provide the terminal 5'-OH group.

The efficiency of the transcription reaction is remarkably dependent on the magnesium concentration during the transcription. Therefore, for every RNA substrate a small 50 µL pre-transcription was performed for validation of the optimal Mg^{2+}-concentration.

Table 3. 25 Composition of the analytically pre transcription reaction

Pre transcription reaction	c_{end}	50 µL
Linearized plasmid DNA/ PCR product	5 µg	x µL
150-400 mM $Mg(OAc)_2$	15-40 mM	5 µL
1 M Tris-HCl pH 7.9	200 mM	10 µL
1 M DTT	20 mM	1 µL
100 mM Spermidine	2 mM	1 µL
100 mM NTP (25 mM each)	16 mM	8 µL
ddH_2O	--	Ad 49 µL
T7-RNA Polymerase	--	1 µL

The incubation of the pre transcription was done at 37°C for 3 h. Afterwards the samples together with a size control were loaded on a 10% denat. PAA gel to determine the optimal Mg^{2+} concentration. Therefore, the gel was stained with EtBr and the RNA was then visualized withy UV-light (254 nm). The following preparative T7 transcription was performed with the validated concentration of Mg^{2+} and dependent on the desired RNA amount in a volume between 2-15 mL. For pecial purposes the used NTPs can be varied, by using e.g. ^{15}N-isotope marked GTP and UTP or all four ^{15}N-isotope marked-NTPs, which were important for following NMR analyses (^{1}H,^{15}N-HSQC). Owing the fact that the ^{15}N-isotope marked NTPs in some cases have lithium as counterion the mixed NTPs had to be ethanol precipitated in the presence of NaOAc prior to use. Therefore, the concentration of the mixed NTPs was first checked photometric, than 3 M NaOAc pH 5.3 (c_{end}: 0.3 M; sterile and RNase free) was added and the NTPs were precipitated by addition of 5.5 volume of 100% ethanol followed by incubation at -20°C overnight. The NTPs were pelletized by centrifugation at 13,000 rpm, 4°C for 30 min, dried at room temperature for approx. 10 min and resolved in 90% of the initial volume to consider the volume of pellet. Finally, the mixture was filled up to the whole initial volume.

Table 3. 26 Composition of the preparative transcription reaction

Transcription reaction	c_{end}	5 mL	10 mL	15 mL
Linearized plasmid DNA/ PCR product	0.2 mg-1.5 mg	x µL	x µL	x µL
150-400 mM $Mg(OAc)_2$	15-40 mM	0.5 mL	1 mL	1.5 mL
1 M Tris-HCl pH 7.9	200 mM	1 mL	2 mL	3 mL
1 M DTT	20 mM	100 µL	200 µL	300 µL
100 mM Spermidine	2 mM	100 µL	200 µL	300 µL
100 mM ATP	4 mM	200 µL	400 µL	600 µL
100 mM UTP	4 mM	200 µL	400 µL	600 µL
100 mM CTP	4 mM	200 µL	400 µL	600 µL
100 mM GTP	4 mM	200 µL	400 µL	600 µL
ddH_2O	--	Ad 4.95 mL	Ad 9.9 mL	Ad 14.85 µL
T7-RNA Polymerase	--	50 µL	100 µL	150 µL

The transcription reaction was carried out at 37°C overnight. During reaction, pyrophosphate is generated which forms complexes with Mg^{2+} ions. This weighs in a white precipitate. To solve these complexes 0.5 M EDTA solution pH 8.0 was added dropwise until all precipitate has solved, before the solution was mixed with 2.5 volumes of 100% ethanol for precipitation of the nucleic acids. Afterwards the precipitate was pelletized by centrifugation (8,500 rpm, 4°C, 30 min), the pellet was dried at room temperature for 10 min and the dry pellet was resolved in 1-4 mL ddH_2O and supplemented with 1-4 mL twofold denaturing gel loading buffer. Up to 2.5 mL were transferred to 1-5 preparative denaturing PAA gel(s) (together with a size marker on each gel). The desired band was excised and eluted as described in chapters 3.2.1.2.1, 3.2.1.3.2 and 3.2.4. Following to the elution step(s) the RNA was ethanol precipitated and resolved in ddH_2O (chapter 3.2.5.1)

3.5.2.1 Homogeneous 3'- or 5'-ends of RNA transcripts

For some experiments it is necessary to produce homogeneous 3'- and/or 5'-ends. For production of homogeneous 5'-ends of the RNA a hammerhead ribozyme sequence was added (e.g. pKK4). hammerhead ribozymes are small autocatalytic RNA motifs. They catalyze the hydrolysis of phosphodiester bonds at a single defined position. Immediately after synthesis the hammerhead ribozyme folds into its active conformation and the cleavage occurs already during transcription. For the cleavage reaction Mg^{2+}-ions have to be available in an adequate concentration. The reaction leads to a 5'-terminal OH group. A prerequisite for the application of HH-ribozymes at 5'-ends of RNA transcripts, is the presence of a nucleotide-triad (preferentially a GUC) upstream of the cleavage side. For a homogeneous 3'-end of an RNA transcript, two different autocatalytic RNA motifs can be used. A hammerhead ribozyme sequence can be added downstream of the RNA transcript sequence or a hepatitis delta virus ribozyme (HDV) sequence can be used. Both ribozames produce a 2'-, 3'-cyclic phosphate end. To generate an accessible end for 3'-end labeling, the 2'-, 3'-cyclic phosphate has to be hydrolyzed prior to the labeling reaction.

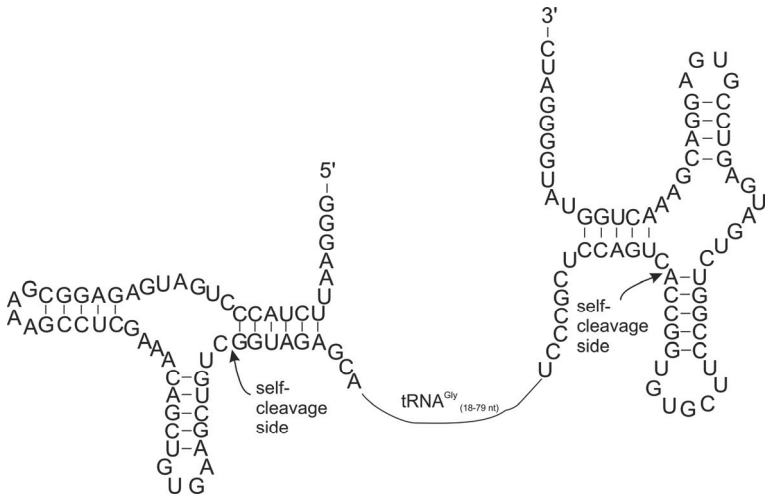

Figure 3. 6 Example of a primary transcript with self-cleaving hammerhead ribozyme structures at the 5'- and 3'-termini of the RNA of interest ($tRNA^{Gly}$; nucleotides 18-79).

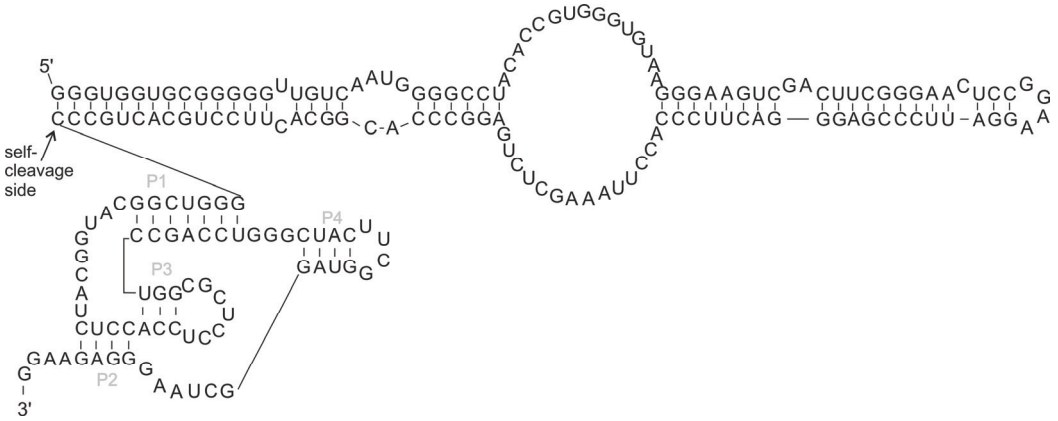

Figure 3. 7 Example of a primary transcript with self-cleaving hepatitis delta virus (HDV) structures at the 3'-termini of the *A. aeolicus* 6S RNA 132-nt variant.

3.5.2.2 Hydrolysis of 2'-, 3'-cyclic phosphate

To generate a terminal 3'-OH group the RNA transcript was incubated with T4 PNK for 4 h at 37°C (Figure 3. 8).

Table 3. 27 2',3'-cyclic phosphate hydrolysis reaction

Hydrolysis reaction	100 µL
Purified RNA-transcript	76 µL
5x buffer P	20 µL
T4 PNK (10 U/µl)	4 µL

Incubation of the reaction mixture for 4 h at 37°C

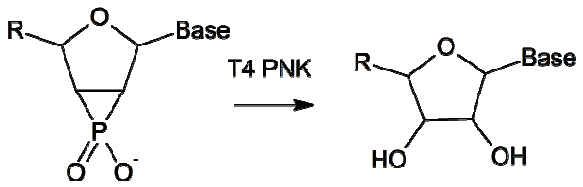

Figure 3. 8 Hydrolysis reaction catalyzed by T4 PNK.

Table 3. 28 Composition of fivefold buffer P

5x buffer P	c_{end}	5 mL
1 M MES pH 6.5	250 mM	1.25 mL
2 M $MgCl_2$	500 mM	1.25 mL
ddH_2O		Ad 5 mL

3.5.3 5'-end labeling of RNA

For visualization of RNA the radioactive isotope ^{32}P was used. 5'-end labeling of RNA is catalyzed by T4 polynucleotide kinase (T4 PNK) from the *E. coli* phage T4. A 5'-OH group at the terminus of the desired RNA is necessary, to be able to add a radiolabeled phosphate-group (chapter 3.5.2.1). Different methods can be used to produce RNAs with 5'-OH groups. If there is no hammerhead ribozyme sequence in front of the RNA transcript, i) guanosine or ii) ApG was added to the transcription which then were incorporated as first nucleotide of the RNA transcript. iii) the RNA can be dephosphorylated (chapter 3.3.3) prior the labeling reaction.

Table 3. 29 5'-end labeling reaction conditions

5'-end labeling reaction	15 µL
10x T4 PNK buffer A	1.5 µL
25 mM DTT	1.5 µL
Purified 5'OH-RNA	x µL(30-75 µM)
ddH_2O	ad 10.5 µL
γ-^{32}P ATP (0.38 MBq/µL)	2 µL
T4 PNK (10 U/µL)	2.5 µL

The ingredients were mixed in a reaction tube and incubated for 1 h at 37°C. Following to this, one volume of 2x PPF loading buffer was supplemented to the reaction mixture and loaded on an 8-10% denaturing PAA gel (0.5-1 mm). After electrophoresis for 2-3 h, the requested band should be extracted as described in chapter 3.2.4. Therefore, to be able to locate the radioactive band, the gel was wrapped into clingfilm and three location marks (radioactive symbols) were applied

before an image-plate was exposed for 1 min. Afterwards, the image plate was scanned by a phosphor-imager and the print was placed below the PAA gel, for location of the radioactive band, followed by excision with a scalpel. The elution was done by diffusion with 1 M NaOAc overnight. Afterwards, the supernatant was transferred into a fresh 2 mL reaction tube and 2 µL 20 mg/mL glycogen was added to the sample. Two volumes of isopropanol were added to precipitad the labeled RNA. After incubation at -20°C for 1 h and centrifugation with 13,000 rpm at 4°C for 1 h the pellet was washed with 70% ethanol, centrifuged (13,000 rpm at 4°C for 15 min) and dried for 5 min at room temperature. Dependent on the radioactivity in the pellet, it was resolved in 10-40 µL ddH_2O. The efficiency of the reaction was determined by measurement of 1 µL labeled RNA using the scintillation counter for 1 min.

3.5.4 3'-end labeling of RNA

The structure of longer RNAs can not be solved completely by secondary structure probing experiments when only 5'-end labeled RNA is used. Therefore, the 3'-terminal OH group cn be labeled. Instead of γ-^{32}P ATP, in this case [5'-^{32}P] pCp (cytidine 3'-, 5'- bis [α-^{32}P] phosphate) is used. The T4 RNA ligase is able to ligate this single nucleotide to the 3'-OH end of the RNA.

Table 3. 30 3'-end labeling reaction conditions

3'-end labeling reaction	15 µL
10x T4 RNA ligase buffer	1.5 µL
2 mM ATP	2.25 µL
Purified 3'OH-RNA	x µL(10-70 µM)
ddH_2O	ad 10.5 µL
[5'-^{32}P] pCp (0.38 MBq/µL)	2.5 µL
T4 RNA ligase (10 U/µL)	2 µL

After the components were mixed in the indicated order, the sample was incubated at 4°C overnight. One volume of 2x PPF loading buffer was added and the sample was loaded on an 8-12% denaturing PAA gel. The RNA band was visualized and extracted as described above for the 5'-end labeling (chapter 3.5.3).

3.5.5 *In vitro* pRNA transcription

A mixture of 1 µL *A. aeolicus* 6S RNA (132 nt, 10 µM) and 1 µL 2x TE (Table 3. 13) was heated at 80°C and stepwise cooled down to 50°C (10°C steps; each for 2 min) followed by a final incubation step of 37°C for 2 min. Afterwards, a master mix including transcription buffer and *B. subtilis* σ^A-RNAP holoenzyme was added and adjusted to 1x buffer and 1 µM enzyme as final reaction concentration. This mix was incubated at 37°C for 10 min. The reaction was started by adding 200 µM of each NTP as well as trace amounts of α-^{32}P-UTP, α-^{32}P-CTP or γ-^{32}P-GTP. GTP is the initial nucleotide for pRNA transcription in *A. aeolicus* 6S RNA. Thus, γ-^{32}P-labeled GTP was used to be sure that incorporation only takes place at position one. After incubation at 37°C for 1 h, 5 µL were taken from the reaction mixture and stopped with 15 µL of 2x PPF loading buffer. The samples were heated at 98°C for 3 min, afterwards incubated on ice for 20 min and loaded onto a 25% denaturing PAA gel. Two 5'-labeled synthetic pRNAs (8 nt and 15 nt) of *A. aeolicus* were used as size marker.

For deep sequencing analysis we perform *in vitro* pRNA transcription six times as described above. Instead of labeled RNA water was used. The six samples were combined and extracted with phenol/chloroform. RNA precipitation was performed with ethanol (chapter 3.2.5.1). The precipitate was resuspended in 5 µL ddH_2O. The experiments were performed in cooperation with Katrin Damm (AG Hartmann).

3.5.6 Secondary structure probing

To perform secondary structure experiments *A. aeolicus* 6S RNA 132-nt variant as well as 6S RNA 85-nt variant were prepared by *in vitro* T7 transcription (chapter 3.5), purified by denaturing PAGE (chapter 3.2.1.2.1) and labeled with radioactive phosphorus on their 5'- or 3'-end as described in chapter 3.5.3 and 3.5.4. Trace amounts of labeled RNA (5'- or 3'-end labeled) were mixed with unlabeled 6S RNA to a final concentration of 9 µM in 1x TN-buffer pH 7.5 (20 mM Tris-acetate, 100 mM NaCl). The samples used for the rearrangement determination were additionally mixed with an approx. 5-fold higher concentration of pRNA 15-mer (c_{end}=50 µM). All samples were incubated for 1 min at 95°C to denature unstable secondary structures, followed by immediate cooling to 2°C for 2 min and given time to refold by slow temperature increase up to 22°C for 5 min. Afterwards the samples were mixed either with RNase T1, V1 or lead and incubated for different time frames for determination of different secondary structure regions. One negative control with the same conditions but without RNase or lead was performed for the RNase T1 and

lead as well as for RNase V1 reaction. The cleavage reaction with 1U RNase T1 at room temperature took 1 min in case of the 6S RNA 132-nt variant. In case of the 6S RNA 85-nt variant, 0.1 U RNase T1 cleaves the sample within 4 min at room temperature. To generate an RNase T1 ladder, one sample of each variant (6S RNA 132-nt/85-nt) was preheated to 55°C for 5 min and cleaved in 1x TN-buffer with 1 U/0.1 U RNase T1 for 1 min/2 min at 55°C, respectively, to allow cleavage independent of secondary structure elements after every guanosine residue. For lead cleavage the different samples were incubated with 0.4 µM $Pb(OAc)_2$. The cleavage reaction was performed for 6 min (6S RNA 132-nt) and 4 min (6S RNA 85-nt) respectively at room temperature. For the 6S RNA 132-nt variant the cleavage reaction was additopnally performed at higher temperatures (37°C, 55°C and 75°C), but with decreased incubation time. At 37°C and 55°C 2 mM $Pb(OAc)_2$ reacts with the sample within 4 min and 1 min, respectively. At 75°C 0.5 mM $Pb(OAc)_2$ was used for a time frame of 1 min. To perform RNase V1 cleavage 0.01/0.001 U RNase V1 were added to the 6S RNA 132-nt/85-nt variant and incubated for 1 min/ 30 sec at room temperature, accordingly. Directly prior cleavage reaction by RNase V1, $MgCl_2$ (c_{end}= 5 µM; because of Mg^{2+} dependent RNase V1 activity) was added to the negative control, the free 6S RNA sample and the 6S RNA:pRNA hybrid sample. To generate an alkaline ladder, unlabeled and the labeled RNA were mixed in alkaline buffer (0.1 M Na_2CO_3/0.1 M $NaHCO_3$ pH 9.0) and heated to 95°C for 1 min. After the cleavage reaction one volume of 2x PPF loading buffer was added to all samples to stop the reaction. The samples were separated on a 15% or 20% denaturing PAA gel. After electrophoresis the gel was transferred to a 2 mm whatman paper, covered with clingfilm and dried in a vacuum gel drier at 60°C for 1 h. The gel was covered by an image plate and exposed overnight. For data collection the plate was transferred into a phospho imager.

3.5.7 Folding analysis on native PAA gels

3.5.7.1 Homogeneity analysis of *E. coli* RNase P RNA and its shortened variant (Ecat)

Table 3. 31 Composition of Buffer KN4.5

Buffer KN4.5	c_{end}
Hepes-KOH pH 7.4	20 mM
$Mg(OAc)_2$	4.5 mM
NH_4OAc	150 mM
Spermidine	2 mM
Spermine	0.05 mM
β-mercaptoethanol	4 mM

The analysis of the folded state of the RNA in case of the full length *E. coli* RNase P RNA (M1 RNA) and its reduced variant Ecat (Figure 3. 9) were done as follows.

Table 3. 32 Folding analysis reaction condition

Folding analysis		c_{end}
M1 RNA or Ecat RNA	x µL	10 nM
5x KN4.5 buffer	1 µL	1x
ddH_2O	Ad 5 µL	
Preincubation:	a) No preincubation (4°C)	
	b) 55°C for 5 min, 37°C for 50 min	

After preincubation the different samples were supplemented with one volume of 2x native loading buffer (chapter 3.2.1.2.2) and loaded on an 11.25% native PAA gel with a size of 16x24 cm and run at 10 mA for 5-7 h. The gel temperature was

controlled not to exceed 15°C (surrounding temperature 8°C (chill room)). The RNA was visualized by EtBr staining.

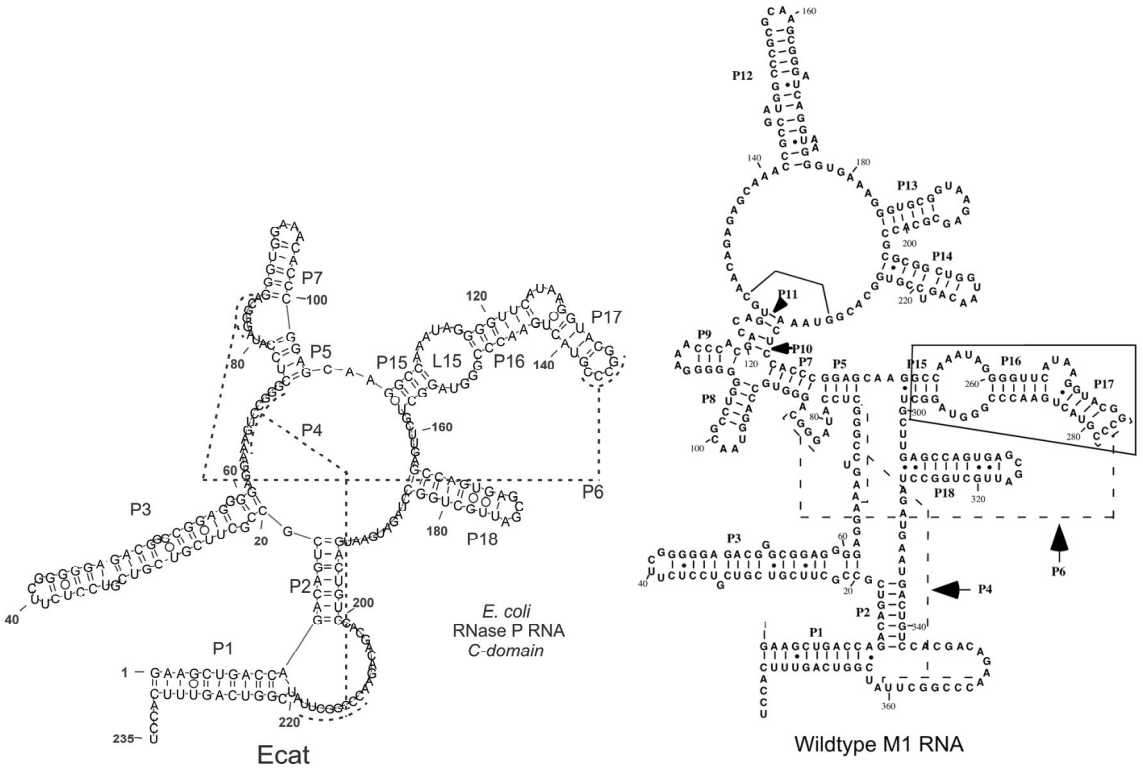

Figure 3. 9 Two dimensional structures of the *E. coli* RNase P RNA C-domain, termed Ecat (left) and the wildtype P RNA of *E. coli* RNase P (right; according to Kikovska *et al.*, 2007). In Ecat the S-domain is replaced by a tetra loop at the end of the P7 helix which is a part of the S-domain.

3.5.7.2 Gel retardation experiments (EMSA)

The electro mobility shift assay (EMSA) was used for analysis of the complex formation of RNA with other RNA molecules, proteins or both *in vitro*. After complex formation the RNA migrates slower on a native PAA gel as if it migrates as free RNA. For visualization trace amounts of radiolabeled RNA were added to the reaction mixture.

3.5.7.2.1 RNA-RNA gel shifts

For the determination of the shift occurrence after complex formation *A. aeolicus* 6S RNA or *B. subtilis* 6S-1 RNA were mixed with their respective pRNA oligomer. For the *A. aeolicus* 6S RNA 85-nt variant, the invasion of the pRNA into the 6S RNA secondary structure worked autonomous. For the longer variants the reaction

mixture was heated to 95°C for 5-10 min to denature the secondary structure followed by stepwise cooling (5°C steps for 5 min each) to 37°C.

Table 3. 33 Consistence of RNA hybridization reaction sample

RNA hybridization mixture		c_{end}
1 µM 6S RNA	2 µL	360 nM
5x Annealing buffer	1.05 µL	1x
10-50 µM pRNA	2 µL	3.6-18 mM
5'-labeled 6S RNA	0.5 µL	Up to 30,000 cpm

Table 3. 34 Consistence of hybridization buffer

Hybridization buffer	c_{end}
$KHPO_4$ buffer pH 6.2	25 mM
KCl	50 mM
NH_4Cl	100 mM

Table 3. 35 Hybridization program

	Time	Temperature
Initial denaturation	5-10 min	95°C
Stepwise cool down	5 min	90°C
	5 min	85°C
	5 min	80°C
	5 min	75°C
	5 min	70°C
	5 min	65°C
	5 min	60°C
	5 min	55°C
	5 min	50°C
	5 min	45°C
	5 min-∞	37°C

For the thermostable *A. aeolicus* 6S RNA the initial denaturation step was prolonged to 10 min.

The components were mixed as described above. As negative control ddH_2O was added instead of pRNA. After the hybridization procedure the samples were either mixed with 2x native loading buffer (Table 3. 12) and loaded on a native 7.5% PAA gel or a further complex formation with RNA polymerase was done (chapter 3.5.7.2.2).

3.5.7.2.2 RNA-protein gel shifts

For the investigation of the complex formation of *B. subtilis* RNA polymerase with *A. aeolicus* 6S RNA, *A. aeolicus* 6S RNA:pRNA hybrids, *B. subtilis* 6S-1 RNA or *B. subtilis* 6S-1 RNA:pRNA hybrids, the samples (processed as described in chapter 3.5.7.2.1) were mixed with 1-10fold excess of *B. sub* RNA polymerase in RNA-protein complexation buffer. The complex formation was done at 37°C for 30 min. To avoid unspecific RNA-protein binding heparin, with a final concentration of 8 ng/µL was added to the reaction mixture.

Table 3. 36 Consistence of the RNA-protein complexation buffer

RNA-protein complexation buffer	c_{end}
Tris-HCl pH 8.0	40 mM
$MgCl_2$	5 mM
KCl	160 mM
DTT	1 mM

3.6 Protein methods

3.6.1 Preparation of recombinant *E. coli* RNase P protein

E. coli DH5α cells carrying the plasmid encoding the RNase P protein (lab stock; *E. coli* C5 protein) were cultured for approx. 3 h (OD_{578}=~0.6) at 37°C with 200-220 rpm in 500 mL LB medium containing 100 µg/mL ampicillin. The OD_{578} was determined frequently until it reached 0.6. For induction of the protein expression, IPTG was added to the reaction mixture to a final concentration of 1 mM. Three hours after induction of protein expression the cells were harvested by centrifugation (4,000 rpm, 4°C for 15 min). The following steps were performed at 4°C (on ice) and all buffers contained 40 µg/mL PMSF (phenylmethylsulfonylfluoride) for inhibition of RNases. The cell pellet was resuspended in 10 mL sonication buffer (SB).

Table 3. 37 Consistence of Sonication buffer (SB)

SB	c_{end}
Tris-HCl pH 8.0	50 mM
NaCl	300 mM
Triton X-100	0.1% (w/v)
NH_4Cl	1 M

Afterwards, the sample was sonicated (Branson Sonifier 250, output 20, duty cycle 50%, 15 min on ice) and then centrifugated, to clear the crude lysate from

cell debris (13,000 rpm, 4°C, 30 min). The supernatant contained the RNase P protein with an N-terminal His-tag (His-tagged peptide leader: MRGSHHHHHHGS). For purification a Ni-nitrilotriacetic acid (Ni-NTA) agarose matrix (binding poly His stretched) was used. Therefore, the supernatant was mixed with the matrix (400 µL Ni-NTA for lysate prepared from 2 L of cell culture) which has been prewashed twice with 10 mL SB. By gentle rotation at 4°C the matrix was incubated with the sample for 1 h. To detach other proteins etc. of the cell lysate the matrix was washed with pre chilled washing buffer (WB) (3x: centrifugation with 8,500 at 4°C for 15 min, afterwards resuspension with 10 mL WB).

Table 3. 38 Consistence of Washing buffer (WB)

WB	c_{end}
Tris-HCl pH 8.0	50 mM
Imidazol	30 mM
Triton X-100	0.1% (w/v)
Urea	8 M

The supernatant was removed carefully after each washing step to avoid release of protein from the matrix. Then, the protein was eluted with 500 µL elution buffer by gentle shaking at 4°C for 45 min.

Table 3. 39 Consistence of Elution buffer (EB)

EB	c_{end}
Tris-HCl pH 7.0	50 mM
Imidazol	300 mM
Glycerol	10% (v/v)
EDTA	20 mM
Urea	7 M

The sample was transferred into a dialysis bag with a molecular-weight-cut-off of 12-14 kDa and dialyzed twice for 1 h against 500 mL dialysis buffer.

Table 3. 40 Consistence of Dialysis buffer (DB)

DB	c_{end}
Tris-HCl pH 7.0	50 mM
NaCl	100 mM
Glycerol	10% (v/v)

Last the sample was dialyzed against 500 mL fresh DB overnight. The dialyzed sample was transferred from the dialysis bag into a 2 mL reaction tube. By centrifugation (13,000 rpm, 4°C, 20 min) the RNase P protein, solved in the supernatant, was separated from traces of RNase P RNA contamination, which were fixed in a precipitation formed during dialysis. All steps were examined by SDS-PAGE.

3.6.2 Laemmli SDS-PAGE

The separation of proteins of different sizes is commonly performed via SDS-PAGE (sodium dodecylsulphate-polyacrylamine gel electrophoresis). The anionic detergent SDS denatures the proteins by binding to hydrophobic amino acid side chains. The proteins own charge is masked by the negative charge of the phosphate group in the SDS so that the proteins can be separated by mass independently of their side chain composition.

Table 3. 41 Consistence of the fourfold separation gel buffer

4x Separation gel buffer	c_{end}
Tris-HCl pH 8.8	1.5 M

Table 3. 42 Consistence of the eightfold stacking gel buffer

8x Stacking gel buffer	c_{end}
Tris-HCl pH 6.8	1 M

Table 3. 43 Consistence of the fivefold gel running buffer

5x Gel running buffer	c_{end}
Tris-HCl pH 8.3	20 mM
Glycine	250 mM
SDS	0.1% (w/v)

Gels are run in 1x running buffer (25 mA/180 V)

Table 3. 44 Consistence of fourfold loading buffer

4x Loading buffer	c_{end}
Tris-HCl pH 6.8	250 mM
Glycerol	20% (v/v)
β-mercaptoethanol	5%
Bromophenol blue	0.001%
SDS	4% (w/v)

Table 3. 45 Consistence of SDS-PAGE gel solutions with different acrylamide concentration

SDS-PAGE gels

Separation gel (5 mL)	10%	13%	15%	17%
Acrylamide (48 %)/bisacrylamide (2 %)	1 mL	1.3 mL	1.5 mL	1.7 mL
4x Separation gel buffer	1.25 mL	1.25 mL	1.25 mL	1.25 mL
20 % (w/v) SDS	25 µL	25 µL	25 µL	25 µL
ddH_2O	2.73 mL	2.45 mL	2.23 mL	2.03 mL
10 % (w/v) APS	50 µL	50 µL	50 µL	50 µL
TEMED	5 µL	5 µL	5 µL	5 µL

Stacking gel (5 mL)	4%
Acrylamide (48%)/bisacrylamide (2%)	400 µL
8x Stacking gel buffer	625 µL
20% (w/v) SDS	25 µL
ddH_2O	3.95 mL
10% (w/v) APS	50 µL
TEMED	5 µL

For gel preparation, the glass plates were cleaned with ethanol and fixed in the Mini Protean® 3 cell chamber system (Biorad). After polymerization was started by addition of TEMED and APS to the gel solution (Table 3.45), the gel solution was poured between the glass plates. To ensure a straight gel surface and prevent air inclusions, the gel solution was overlaid with isopropanol during polymerization procedure (for approx. 30 min). After the isopropanol was washed away with water, the polymerization of the stacking gel solution was started and the solution was poured onto the polymerized separation gel. At last a comb was inserted to form sample loading pockets. After complete polymerization the gel assembly was placed into the electrophoresis chamber and the buffer basin was filled with 1x gel running buffer. For protein denaturation three volumes of the protein sample were mixed with one volume of the 4x SDS-PAGE sample buffer and were than additionally denatured by heating to 95°C for 2 min. A protein size marker (PageRuler prestained protein ladder (Figure 3. 10)) was loaded onto the gel for size estimation.

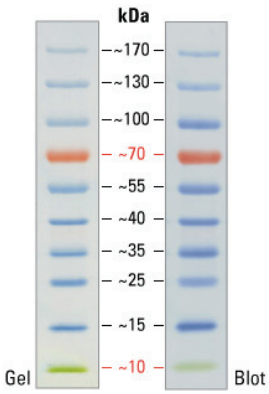

Figure 3. 10 Protein ladder image from a 4-20% Tris-glycine gel (SDS-PAGE) and subsequent transfer to membrane (according to Thermo Fisher Scientific; PageRuler Prestained Protein Ladder Description).

After electrophoresis the protein bands were stained by coomassie staining (chapter 3.6.3).

3.6.3 Coomassie staining

To visualize protein bands after SDS-PAGE (chapter 3.6.2), the gel was released from the glass plates and covered with coomassie staining solution and incubated for 30 min at room temperature while gently shaking.

Table 3. 46 Composition of the coomassie staining solution

Coomassie staining solution	c_{end}
Methanol	40% (v/v)
Acetic acid	10% (v/v)
Coomassie Brilliant Blue R-250	0.5%

To remove unspecific coloration the coomassie staining solution was exchanged with ddH_2O and shaken gently for another 30 min. The results were recorded by photographic imaging with the Biostep Gerix 1000 (Dark Hood DH-50, Transiluminator Bio View UV light UST-30M-8E).

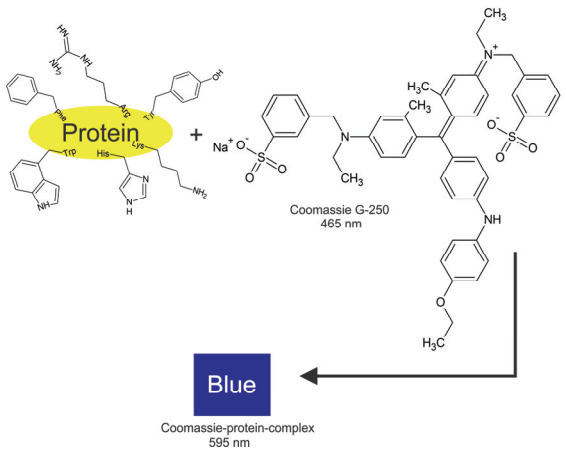

Figure 3. 11 Schematic illustration of the coloring of a protein by coomassie dye.

3.6.4 Bradford protein concentration determination

The Bradford protein assay is a simple procedure for the determination of the protein concentration in a solution. The procedure is based on the formation of a complex between proteins and the Brilliant Blue G dye (BioRad protein assay, München). The complex formation causes a shift on the light absorption maximum, from 465 to 595 nm. To start the reaction the protein samples are mixed with the dye reagent and incubated for 5 min at room temperature, followed by absorption measurement at a wavelength of 595 nm. To determine the concentration of the protein solution, a calibration line is established with protein solutions containing BSA in a known concentration.

3.7 Kinetic analysis

The kinetic analyses of the RNase P holoenzyme, the RNase P RNA and the RNase P variant Ecat were all performed under single turnover conditions. Thus, one enzyme molecule can cleave one substrate molecule during the reaction. Because of the fact, that only the cleavability of the different substrates was tested, no rate-determination was performed.

Table 3. 47 Composition of the modified Buffer KN4.5

Buffer mKN4.5	c_{end}
Hepes-KOH pH 7.4	20 mM
$Mg(OAc)_2$	4.5 mM
NH_4OAc	100 mM

3.7.1 Kinetic analysis of *in vitro* reconstituted RNase P holoenzyme

The analysis of the RNase P catalyzed cleavage was performed in KN4.5 (Table 3. 31) and mKN4.5 buffer (Table 3. 47), respectively. The conditions were changed to the mKN4.5 buffer because of the reduced disturbance during NMR measurement due to less detergent derived background signals. For reconstitution of the RNase P holoenzyme the P RNA was incubated for 5 min at 55°C and further 25 min at 37°C. Afterwards the P RNA was mixed with the P protein and incubated for further 30 min at 37°C in the KN4.5/mKN4.5 buffer. The Ecat RNA variant is folded

properly even without any preincubation steps (chapter 3.5.7.1), so that the RNA was either directly used for the kinetic reaction in KN4.5/mKN4.5 buffer or preincubated for 30 min at 37°C with the *E. coli* RNase P protein. For the kinetic measurement an equimolar amount of substrate RNA together with trace amounts of 5'-^{32}P labeled substrate RNA was added to the RNase P and the mixture was incubated at 37°C. After different time points (0', 5', 15', 30', 60', 120') 5 µL of the reaction mixture were removed and immediately mixed with 5 µL 2x PPF loading buffer. The probes were then transferred to a 20% denaturing PAA gel and ran at 30 mA for 2-3 h, until the BPB band reached the bottom of the gel. Afterwards an imaging plate was exposed to the gel overnight as described in chapter 3.2.1.3.3.

3.8 Cloning experiments

3.8.1 Plasmids for recombinant DNA preparation

The plasmids used for this study were either pUC18 or pUC19 derivetives (Figure 3. 12).

Figure 3. 12 Schematic illustration of pUC18/19 plasmid with a closer view at the multiple cloning sites.

The T7 promoter sequence directly upstream of the desired RNA genes allowed efficient *in vitro* transcription by T7 RNA polymerase. To generate DNA inserts

carrying the T7 promoter sequence, the desired RNA sequence and potentially a HH or HDV sequence, primers were designed dependend on the kind of mutation which should be included. Before the amplification of the desired RNA, the primers were phosphorylated (chapter 3.3.4) to be able to ligate e.g. the digested and dephosphorylated pUC vector with the amplified sequence.
The template plasmids for preparation of the RNase P RNA variant Ecat (pUCT7_Ecat), of *E. coli* RNase P RNA (pDW98) and of the *A. aeolicus* 6S RNA (pUCT7_ssrS) as well as mutants thereof with different lengths (pUCT7_Aae_6Slong-HDV, pUCT7_Aae_6Sshort-HDV), were already stored in our lab. Also the plasmid containing the sequence of the pATSerUG hairpin substrate was already in stock. The circular permuted mutant of *B.sub* 6S-1 RNA (pBB-T7-bsrA-82_shortened_circular_permuted) was cloned by Philipp Gustav Hoch (AK Hartmann).

3.8.1.1 Cloning of minimal substrates

Dependent on the used NMR method the RNA sequence has to be composed of isotope marked nucleotides. Therefore, it was important to transcribe the RNA sequence by *in vitro* transcription with ^{15}N-NTPs.

The cloned plasmids pKK1 and pKK2 were designed to produce 5'-N9-MiniGly minimal substrates (pKK1; substrate for RNase P RNA and its variant Ecat) or a hairpin structure formed by the *A. aeolicus* 6S RNA pRNA 15-mer (pKK2), respectively.

In general for all performed cloning experiments it was preceded as follows: The plasmid and the insert were ligated (chapter 3.3.5) and subsequently transformed into *E. coli* DH5α cells (chapter 3.1.3.2). To select the cells carrying the desired plasmids, the cell suspension was plated on ampicillin agar plates. The next day 16 single colonies were picked, inoculated first into a 3 mL LB_{Amp}-medium culture, secondly streaked on fresh ampicillin agar plates and finally transferred to 50 µL of a PCR mastermix solution for colony PCR, to select the clones which carrying the coding sequence by amplification with the sequencing primer (Seq8 and Seq9/ Table 3. 49). The PCR products, which have different length, after an effective ligation reaction as the original plasmid used for ligation, were tested by agarose gel electrophoresis. Also a sample of an untreated pUC19 plasmid was amplified by PCR and tested as negative control. The next day the 3 mL cultures of 2-4 chosen clones were used for further DNA preparation. On the one hand, 500 µL of each culture were mixed with 1 volume glycerol for long term storage (chapter 3.1.1.1) and immediately frozen in liquid nitrogen. The remaining 2.5 mL were used for 'Mini-preps' (chapter 3.3.1). The purified plasmid DNA was sent to eurofins, Ebersberg for DNA sequencing using primers M13 uni (-43) and M13 rev (-49) (eurofins genomics), respectively.

3.8.1.1.1 pKK1 (pUC19_T7_N9-MiniGly (x*Nco*I))

To introduce the desired coding sequence into the pUC19 vector two chemically synthesized 5'-phosphorylated (chapter 3.3.4) ssDNA oligonucleotides carrying the *Eco*RI restriction site, the T7 promoter sequence, the N9-MiniGly sequence and the *Nco*I restriction site were annealed to each other by heating to 95°C and stepwise cooling to 37°C (primer 1 (Nr.5:N9-MiniGly_forw) and primer 2 (Nr.6:N9-MiniGly_rev) (Table 3. 49).

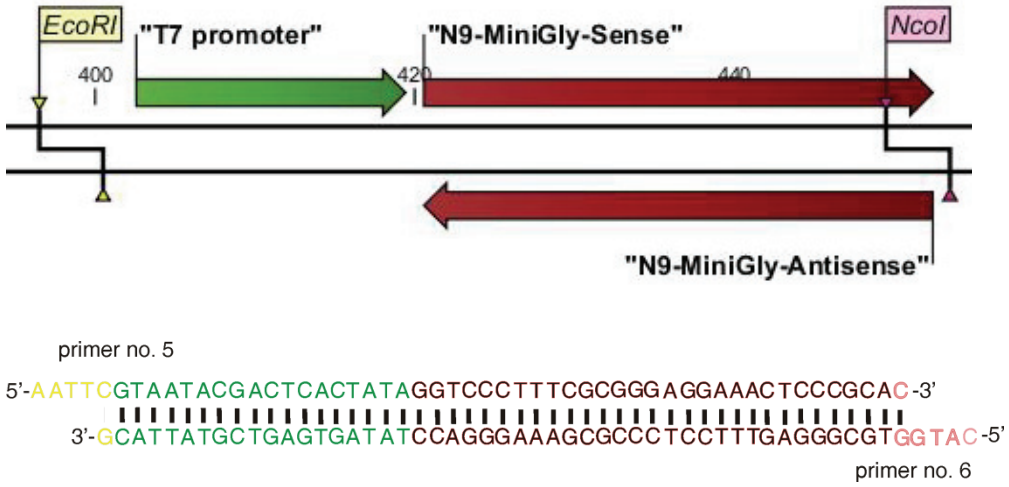

Figure 3. 13 Illustrations of the insert formed by primers no.5 and 6.

The pUC19 vector DNA was linearized by restriction digestion using *Eco*RI and *Nco*I according to manufacturer's recommendations. At the same time dephosphorylation of the 5' ends was performed using Fast AP, to prevent religation of the vector (chapter 3.3.3). The efficiency of linearization of the plasmid DNA was tested by agarose gel electrophoresis (chapter 3.2.1.1). After ligation, transformation, DNA purification and a successful verification by DNA sequencing as described above the plasmid DNA (Figure 3. 14) was used for *in vitro* transcription (chapter 3.5).

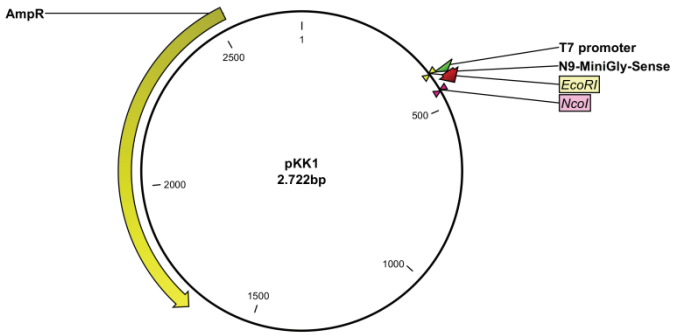

Figure 3. 14 pKK1: pUC19_T7_N9-MiniGly (x*Nco*I), a pUC19 derivate containing the coding sequence for the N9-MiniGly substrate under control of a T7 promoter, selectable via the *bla* gen (AmpR).

3.8.1.1.2 pKK2 (pUC19_T7_*Aae*_6S-pRNA-pATSerCA (x*Mca*I))

To introduce the coding sequence into the pUC19 vector an insert carrying the *EcoR*I restriction site, the T7 promoter sequence, the pRNA-pATSerCA sequence and the *Mva*I restriction site was designed. The annotation CA within the pATSerCA indicates the identity of the base at position +1 and the discriminator base at position "+73". The dsDNA insert was produced according to the procedure for pKK1.

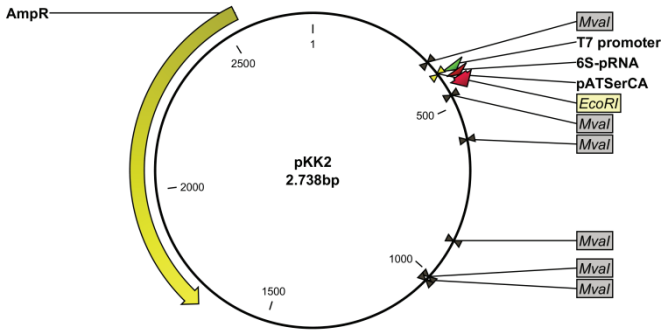

Figure 3. 15 pKK2: pUC19_T7_*Aae*_6S-pRNA-pATSerCA (x*Mva*I), a pUC19 derivate containing the coding sequence for the *Aae*_6S-pRNA-pATSerCA substrate under control of a T7 promoter, selectable via the *bla* gen (AmpR).

After the sequence identity of the plasmid (Figure 3. 15) was verified as described above, it was used for transcription of the sequence shown in Figure 3. 16. The RNA was purified and afterwards processed by *E. coli* RNase P RNA to obtain homogeneous pRNA 15mer oligonucleotide (6S RNA) (Figure 3. 16, 5'-pRNA leader).

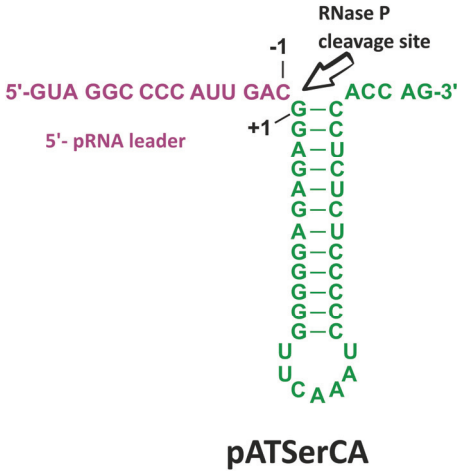

Figure 3. 16 *Aae*_6S-pRNA-pATSerCA substrate hairpin structure with the RNase P cleavage site as indicated by the arrow. The sequence marked in purple shows the 5'-leader and is simultaneously the sequence of the pRNA 15-mer. The sequence in green is the pATSerCA sequence which is well known as substrate for bacterial RNase P.

3.8.1.2 Cloning of 6S RNA genes

The gene for the *A.aeolicus* 6S RNA (ssrS) was cloned into the pUC19 vector whereas the gene for 6S-1 RNA of *B.sub* (bsrA) was cloned into the pUC18 vector. After the PCR amplification steps the PCR products were treated with *Dpn*I to get rid of recombinant DNA template contamination.

3.8.1.2.1 pKK3 (pUC19_T7_(5'-)HH_6S-(short)112nt_HDV (x*BamH*I))

Upstream of the coding sequence for the *A. aeolicus* 6S-(short)112-nt (cloned by Dagmar K. Willkomm) a hammerhead ribozyme was cloned. To amplify the whole sequence by PCR (chapter 3.3.6) the phosphorylated primer 5, 6 and 7, 8 (Table 3. 49) were used and the plasmid carrying the pUCT7-6S-short_HDV sequence. Therefore at first the primer 5 and 6 was amplified by PCR whereas primer 5 carrying the *EcoR*I restriction site, the T7 promoter and the first 22 nt of the hammerhead sequence. Primer 6 overlapped this sequence with a length of 16 nt and provides further 31 nt for the hammerhead sequence. Primer 7 and 8 generated an amplified DNA fragment which contains a 5'-overhang overlapping the hammerhead sequence, the 6S short sequence with the HDV and the *BamH*I restriction side. The 5'-ends of primers 6 and 7 overlap and were used for the third PCR amplification step. After the three steps the PCR product was analyzed and cloned between the *EcoR*I/*BamH*I sites of the pUC19 plasmid as described above. The final plasmid (Figure 3. 17) was controlled by DNA sequencing.

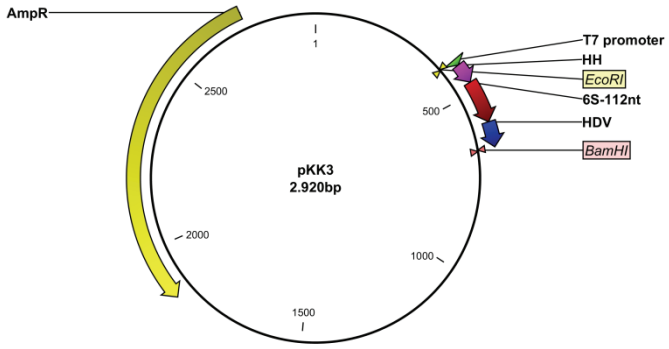

Figure 3. 17 pKK3: pUC19_T7_(5'-)HH_6S-(short)112nt_HDV (x*BamH*I), a pUC19 derivate containing the coding sequence for the HH_6S-(short)112-nt_HDV under control of a T7 promoter, selectable via the *bla* gen (AmpR).

3.8.1.2.2 pKK4 (pUC19_T7_(5'-)HH_6S-85nt_HDV (x*BamH*I))

The coding sequence of the shortened *A. aeolicus* 6S 85-nt was amplified by PCR (chapter 3.3.6). Therefore the phosphorylated primers 9 and 10 (Table 3. 49) and the plasmid pKK3 were used. The PCR product was analyzed and ligated as described above. The final plasmid (Figure 3. 18) was controlled by DNA sequencing.

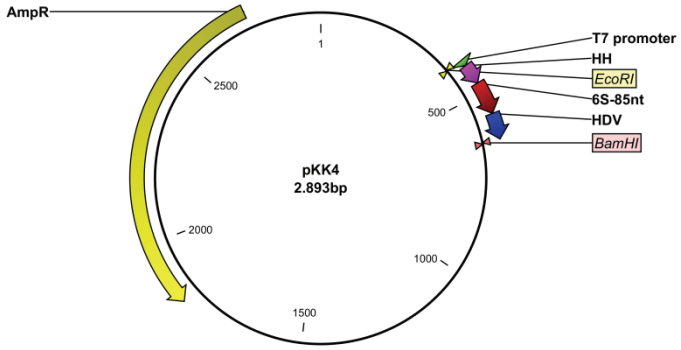

Figure 3. 18 pKK4: pUC19_T7_(5'-)HH_6S-85nt_HDV (x*BamH*I), a pUC19 derivate containing the coding sequence for the HH_6S-85-nt_HDV under control of a T7 promoter, selectable via the *bla* gen (AmpR).

3.8.1.2.3 pKK5 (pUC19_T7_(5'-)HH_6S-132nt_HDV (x*BamH*I))

The coding sequence of the *A. aeolicus* 6S-132-nt-HDV variant with an additional 5'-hammerhead ribozyme sequence was amplified by PCR (chapter 3.3.6). Therefore the phosphorylated primers 11 and 12 (Table 3. 49) and the plasmid pUCT7_*Aae*_6Slong-HDV cloned by Dagmar K. Willkomm were used. The PCR product

was analyzed and ligated as described above. The final plasmid (Figure 3. 19) was controlled by DNA sequencing.

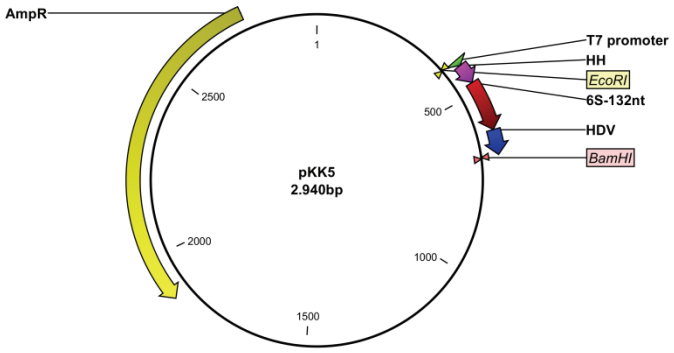

Figure 3. 19 pKK5: pUC19_T7_(5'-)HH_6S-132nt_HDV (x*BamH*I), a pUC19 derivate containing the coding sequence for the HH_6S-132-nt_HDV under control of a T7 promoter, selectable via the *bla* gen (AmpR).

3.8.1.2.4 pKK6 (pUC19_T7_(5'-)HH_6S-159nt_HDV (x*BamH*I))

The coding sequence of the *A. aeolicus* 5'-HH_6S-159-nt-HDV was amplified by PCR (chapter 3.3.6). Therefore, the phosphorylated primers 13 and 14 (Table 3. 49) and the plasmid pUCT7_Aae_6S-163nt-HDV cloned by Dagmar K. Willkomm were used. The PCR product was analyzed and ligated as described above. The final plasmid (Figure 3. 20) was controlled by DNA sequencing.

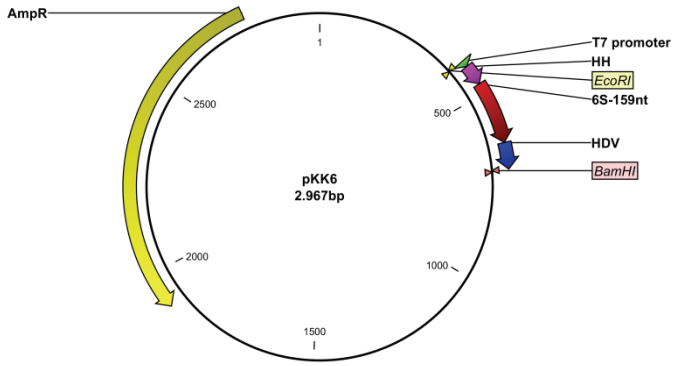

Figure 3. 20 pKK6: pUC19_T7_(5'-)HH_6S-159nt_HDV (x*BamH*I), a pUC19 derivate containing the coding sequence for the HH_6S-159-nt_HDV under control of a T7 promoter, selectable via the *bla* gen (AmpR).

3.8.1.2.5 pKK7 (pBB(pUC18)_T7_6S-1-82ntcp (x*Sma*I))

The coding sequence of the *B. subtilis* 6S-1-82-nt-cp digestible by *Sma*I was amplified by PCR (chapter 3.3.6). Therefore, the phosphorylated primers 15 and 16 (Table 3. 49) and the plasmid pBB(pUC18)_T7_6S-1-82ntcp cloned by Philipp Gustav Hoch were used to introduce a point mutation. The PCR product was analyzed and ligated as described above. The final plasmid (Figure 3. 21) was controlled by DNA sequencing.

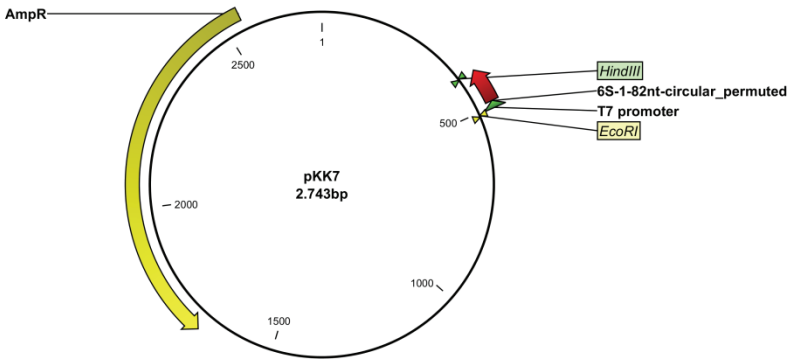

Figure 3. 21 pKK7: pBB(pUC18)_T7_6S-1-82ntcp (x*Sma*I), a pUC18 derivate containing the coding sequence for the 6S-1-82-nt-cp under control of a T7 promoter, selectable via the *bla* gen (AmpR).

3.8.1.2.6 pKK8 (pUC19_T7_6S-132nt(CCA)_HDV (x*BamH*I))

The coding sequence of the *A. aeolicus* 6S-132-nt(CCA)_HDV with one missmatch within the last three nucleotides of the *A. aeolicus* 6S-132-nt_HDV sequence was amplified by PCR (chapter 3.3.6). Therefore the phosphorylated primers 17 and 18 (Table 3. 49) and the plasmid pUCT7_*Aae*_6Slong-HDV cloned by Dagmar K. Willkomm were used to introduce a point mutation. The PCR product was analyzed and ligated as described above. The final plasmid (Figure 3. 22) was adjusted by DNA sequencing.

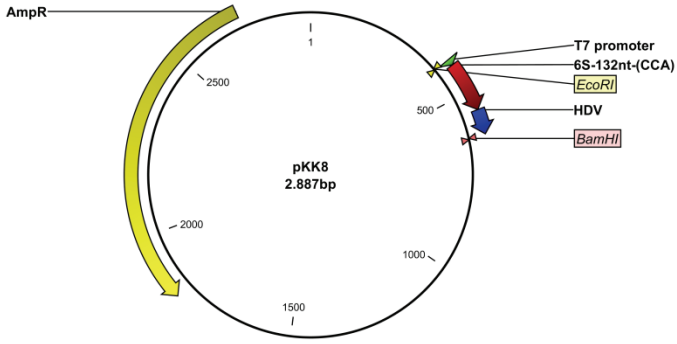

Figure 3. 22 pKK8: pUC19_T7_6S-132nt(CCA)_HDV (x*BamH*I), a pUC19 derivate containing the coding sequence for the 6S-132-nt(CCA)_HDV under control of a T7 promoter, selectable via the *bla* gen (AmpR).

3.8.1.2.7 pKK9 (pUC19_T7_6S-132nt(CAA)_HDV (x*BamH*I))

The coding sequence of the *A. aeolicus* 6S-132-nt(CAA)_HDV with two mismatches within the last three nucleotides of the *A. aeolicus* 6S-132-nt_HDV sequence was amplified by PCR (chapter 3.3.6). Therefore the phosphorylated primers 17 and 19 (Table 3. 49) and the plasmid pUCT7_*Aae*_6Slong-HDV cloned by Dagmar K. Willkomm were used to introduce a point mutation. The PCR product was analyzed and ligated as described above. The final plasmid (Figure 3. 23) was controlled by DNA sequencing.

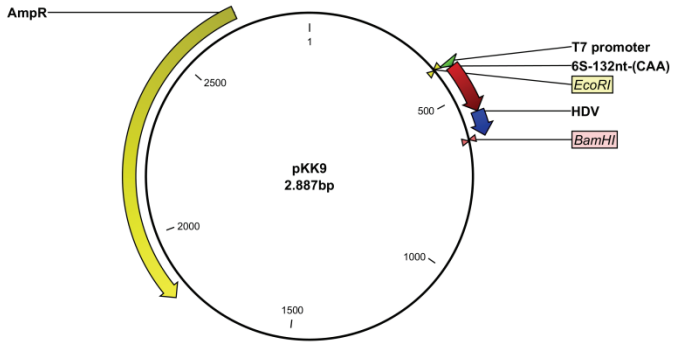

Figure 3. 23 pKK9: pUC19_T7_6S-132nt(CAA)_HDV (x*BamH*I), a pUC19 derivate containing the coding sequence for the 6S-132-nt(CAA)_HDV under control of a T7 promoter, selectable via the *bla* gen (AmpR).

3.9 *In silico* methods

3.9.1 CLC Sequence Viewer 6.5.1 (www.clcbio.com)

CLC Sequence Viewer is a tool which gives the opportunity to make a large number of bioinformatic analyses. These options are combined with smooth data management and excellent graphical viewing and output variants e.g. creating and editing alignments, interactive restriction site analysis, phylogenetics, intergrated GenBank searches or advanced DNA to Protein translation. Here, the CLC sequence viewer was used for the illustration of the different plasmid sequences, the vector cards, for selection of putative restriction sites and to generate graphics with high resolution.

3.9.2 RNAfold (rna.tbi.univie.ac.at/cgi-bin/RNAfold.cgi)

The RNAfold web server is a tool for prediction of the secondary structure of single stranded RNA or DNA sequences. It predicts minimal free energy structures and base pair probabilities. The tool was in this work mainly used for prediction of the 6S RNA structure at different temperatures but also to predict hammerhead or HDV ribozyme structures. An alternative method to predict secondary structures is mfold.

3.9.3 PyMOL (www.pymol.org)

PyMOL is a molecular visualization program for rendering and animating three-dimensional molecular structures with more than 600 settings and representation options like spheres, surface and mesh, lines and sticks or ribbon and cartoon. Here it was used for the visualization of RNA or RNA/protein interactions, to highlight the important regions with colors and generate graphics with high resolution.

3.10 NMR methods

All NMR experiments were performed in collaboration with our Cooperation-partners from the Wöhnert group, Goethe University Frankfurt especially by Dr. Elke Duchardt-Ferner, Dr. Sina Schmidtke and Prof. Dr. Jens Wöhnert.

Nuclear magnetic resonance (NMR) is a physical phenomenon. The isotopes of different elements containing an odd number of protons or protons and neutrons show a magnetic moment (nonzero spin) and can be used for NMR. An even number

of protons and neutrons of an isotope have a total spin of zero. When nuclei are placed in the magnetic field they absorb and re-emit electromagnetic radiation (Figure 3. 24, Figure 3. 25). The specific resonance frequency of this energy depends on the strength of the magnetic field and differs depending on the specific atom properties. Different isotopes of the elements show different specific quantum mechanical magnetic properties also depending on the structural environment. NMR measurements can be done with liquid, crystals and non-crystalline samples and are also used in medical image techniques like magnetic resonance imaging (MRI) [Veeman, 1997].

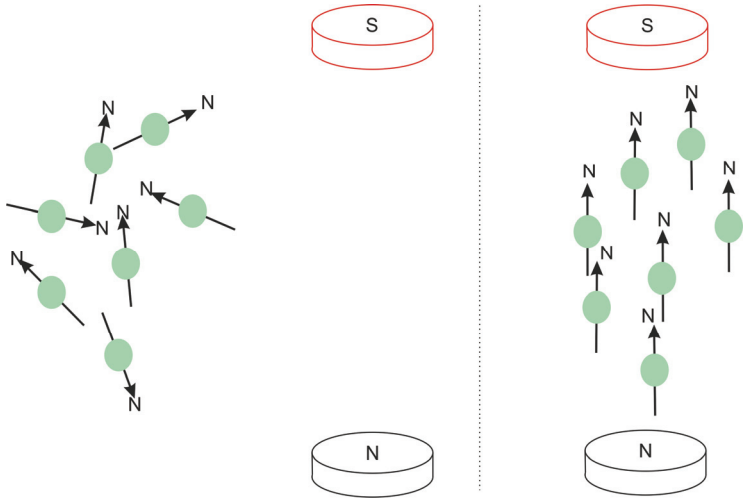

Figure 3. 24 Orientation of proton spins outside (left) and inside a magnetic field (right).

In the magnetic field the spin states of a nucleus differ in their energy and can be seperated in the parallel state (α) with a lower energy but slightly more populate and the antiparallel state (β) (for spin ½ nuclei) (Figure 3. 25) [Veeman, 1997].

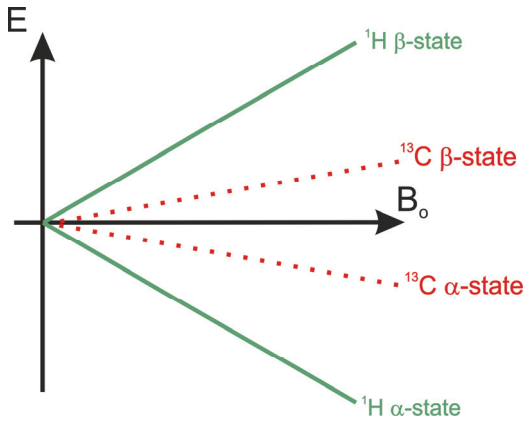

Figure 3. 25 Energy Separation of the different spin states of the isotopes of ^{1}H and ^{13}C depending on the external magnetic field.

3.10.1 General method

^{1}H and ^{13}C are the usually used isotopes. But further magnetic nuclear isotope, such as deuterium (^{2}H), fluorine 19 (^{19}F), nitrogen 15 (^{15}N), phosphorus 31 (^{31}P), sodium 23 (^{23}Na) or tritium (^{3}H) are used for high-field NMR spectroscopy as well. The re-emitted resonance of the sample can be detected and due to the different frequencies structural information can be determined (Table 3. 48) [Veeman, 1997].

Table 3. 48 Different NMR active isotopes

Isotope	Abundance	Spin I	Possible spin states (2*I+1)	Magnetquantum-number
^{1}H	100%	½	2	+½,- ½
^{2}H	0.015%	1	3	+1, 0, -1
^{13}C	1%	½		
^{15}N	0.4%	½		
^{19}F	100%	½		
^{31}P	100%	½		

Therefore a high power radiofrequency pulse (ca. 10 µs) is used to excite all frequencies at ones and the nuclei start precession with their resonance frequency and a free induction decay (FID) is recorded. From this FID a NMR spectrum is calculated via Fourier Transformation (FT) (Figure 3. 26) [Veeman, 1997].

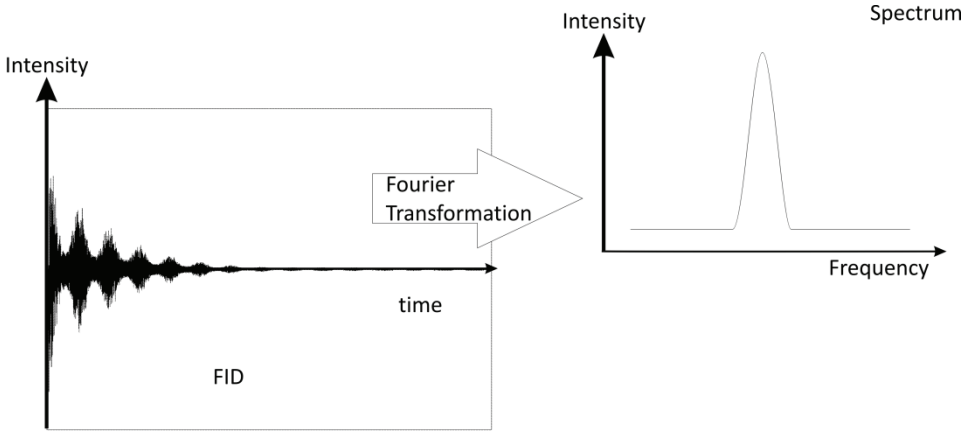

Figure 3. 26 Transformation of the FID in a NMR spectrum via Fourier Transformation.

3.10.2 One dimensional ^{1}H-spectrum

For the most commonly used NMR method, the one dimensional proton spectrum, the spin ½ of the ^{1}H nucleus is exploited. Hydrogen is highly abundant in most chemical compounds as well as in biological systems. It is not hazardous, does not have to be especially incorporate in the sample and is beside Tritium the most sensitive nucleus to NMR signal. Hence, the ^{1}H-spectrum shows destinct chemical shift with sharp signals and leads to quantitative results due to short relaxation time (Figure 3. 27). To avoid signal interference from the hydrogen-containing solvents usually deuterated solvents (spin 1) are used [Veeman, 1997].

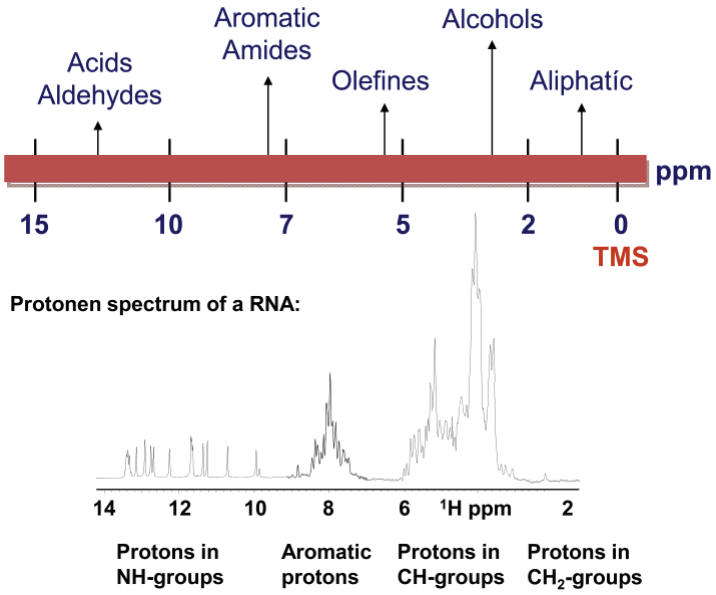

Figure 3. 27 Chemical shift of a ^{1}H spectrum.

The chemical environment of a nucleus affects the resonance frequency and thus leads to resolution in the NMR spectra (Figure 3. 27, Figure 3. 28). The magnetization transfer that occurs between nuclei of the same type is called scalar spin-spin coupling or J-coupling (J= coupling constants (Hz)) and takes place between nuclei connected by up to five bonds whereas they are independent of the magnetic field B_0.

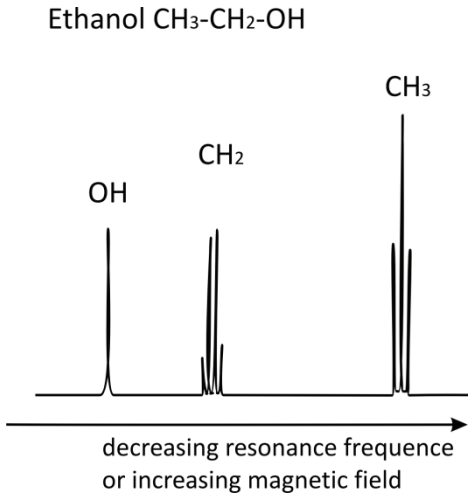

Figure 3. 28 Schematic ^{1}H-NMR spectrum of ethanol. The chemically different protons show different chemical shifts. Due to the J-coupling between the proton spins splitting of the CH_2 and the CH_3 signals into a triplet (CH_3) and into a quartet (CH_2) appears.

In a NMR spectrum the scalar coupling effect manifest by a splitting of the signals of the coupling nuclei. With the structural information occurred from the scalar coupling it is possible to correlate the nuclei in multi-dimensional NMR experiments [Veeman, 1997].

3.10.3 Homonuclear two-dimensional spectroscopy

To detect a homonuclear two dimensional spectrum two RF pulses (P1 and P2) separated by a specific evaluation time (t1) were sent on the sample followed by a time frame (t2) to detect the FID signals (Figure 3. 29).

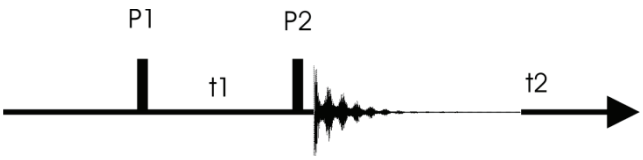

Figure 3. 29 Pulse and detection event performed for two-dimensional spectroscopy.

The frequencies resulting for the two nuclei are illustrated along both axes whereas the peaks on the diagonal have the same frequency on both axes which correspond to the peaks in a 1D NMR spectrum. The cross peaks appearing off the diagonal indicate the coupling between nuclei like a signal splitting in a 1D-NMR spectrum. The cross peaks appear symmetrical on both sides of the diagonal (Figure 3. 30). With this information it is possible to determine coupling partners (COSY-correlation spectroscopy) [Veeman, 1997].

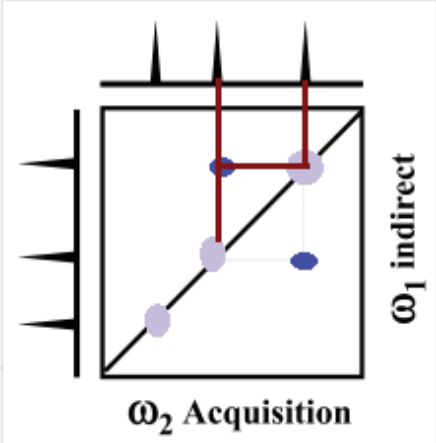

Figure 3. 30 Illustration of diagonal and cross peaks in a 2D spectrum.

Further magnetization transfer can occur via through bond-scalar coupling (J) which gives information about the connectivities, but also via through-space dipolar couplings (D) which provides information on conformation. With the 2D through-space correlation methods physically close nuclei which are not connected though bonds can be investigated. These methods use the nuclear Overhauser effect (NOE). Atoms in a distance within ~ 5.5 Å show cross relaxation. For the Nuclear Overhauser effect spectroscopy (NOESY) this NOE during the second pulse (P2) is used to establish the correlation between nuclear spins. Here again peaks on and off the diagonal appear. In contrast the COSY the cross peaks indicates spatial correlation (Figure 3. 30, Figure 3. 31) [Fürtig *et al.*, 2003].

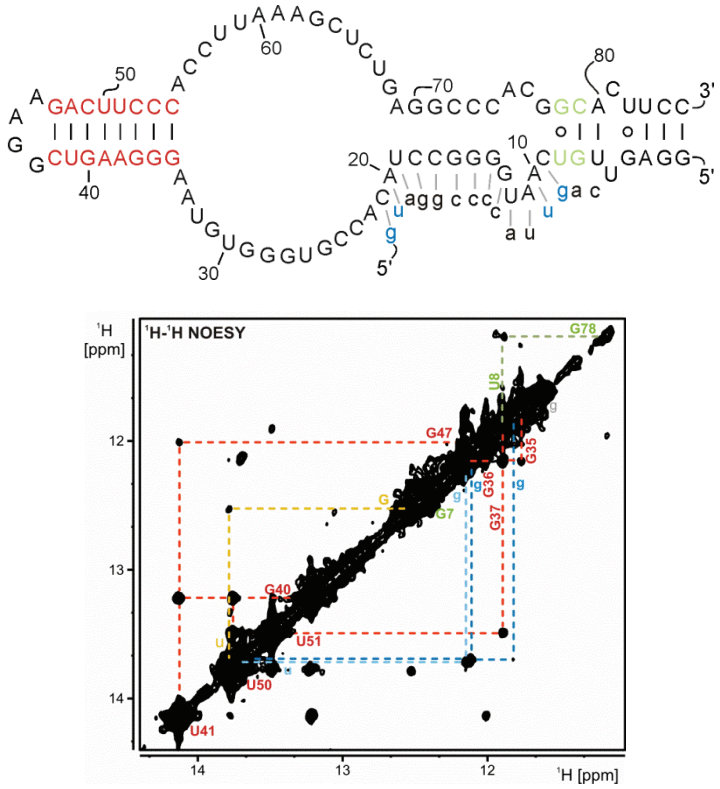

Figure 3. 31 Secondary structure of *A. aeolicus* 6S RNA (85 nt):pRNA hybrid (top). Example for a ^{1}H,^{1}H-NOESY spectrum of *A. aeolicus* 6S RNA (85 nt) at 950 MHz recorded at 283K (bottom). Assignment colored according to the secondary structure. pRNA is shown in small letters.

3.10.4 Two dimensional ^{1}H,^{15}N-HSQC

The Heteronuclear Single Quantum Correlation method, routinely used for protein- and nucleic acid-NMR, utilizes the different chemical shifts of nitrogen ^{14}N (spin-1/ wide chemical shift) and ^{15}N (spin-½/sharp signals). ^{15}N is commonly used to label biomolecules such as proteins or nucleic acid, to discriminate between amino acids backbone amide groups and nucleobase imino groups, respectively. In the 2D spectrum one axis is attributed to ^{1}H and the other to ^{15}N. So, each proton attached to a ^{15}N is represented by a peak and thereby can usually be correlated to the diagonal peaks of the corresponding ^{1}H,^{1}H-NOESY and further in combination with the cross peaks of the NOESY to the secondary structure of the protein or the nucleic acid, respectively. Here the transfer of the magnetization from the proton to the directly attached ^{15}N via Insensitive nuclei enhanced by polarization transfer (INEPT) is the basis of this method. The chemical shift of the proton is detected directly in each experiment, whereas the ^{15}N signal has to be collected in the indirect dimension. This is achieved by recording a series of 1D experiments with varying delay t. The HSQC method is also used to determine protein-protein, protein-ligand as well as RNA-RNA binding (Figure 3. 32). E.g the comparison of free RNA sample with

one sample, where the RNA is bound to a RNA ligand, leads to a chemical shift or a depletion of some peaks which indicates an interaction between the ligand and the RNA nucleotide. For this method also carbon ^{13}C is applicable as nucleus [Griffey *et al.*, 1983; Veeman, 1997; Fürtig *et al.*, 2003].

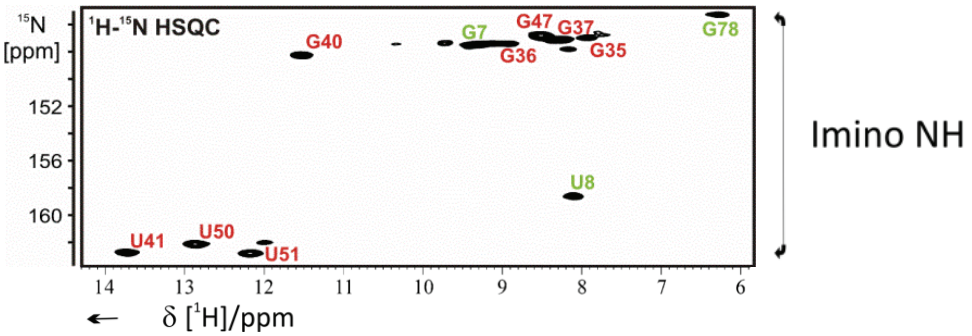

Figure 3. 32 ^{1}H, ^{15}N-HSQC spectrum of *A. aeolicus* 6S RNA (85 nt) at 950 MHz recorded at 283K. Assignment as indicated. Structure shows in Figure 3. 31.

The possibly discrimination between imino protons of a guanosine or a uridine due to their separated chemical shifts illustrated by the ^{1}H,^{15}N-HSQC spectrum (Figure 3. 32) is used to distinguish between the nucleic acids of the structure.

3.11 Material

3.11.1 Chemicals

All chemicals not listed below were commonly ordered at Roth, Karlsruhe.

γ^{32}P-ATP:	Hartmann Analytic, Braunschweig
β-Mercaptoethanol:	Roth, Karlsruhe
Acetic acid:	Roth, Karlsruhe
Acetone:	Roth, Karlsruhe
Acryl amid/Bis acryl amid solution (24/1):	GERBU, Heidelberg
Agar-Agar:	Roth, Karlsruhe
Agarose:	Roth, Karlsruhe
Ammonium acetate:	Roth, Karlsruhe
Ammonium persulfate (APS):	Roth, Karlsruhe

Ampicillin:	Roth, Karlsruhe
Bovine serum albumin (BSA):	Sigma Aldrich, Seelze
Bromophenol blue (BPB):	Merck, Darmstadt
Calcium chloride:	Roth, Karlsruhe
Chloroform:	Merck, Darmstadt
Coomassie Brilliant Blue R-250:	Serva, Heidelberg
Desoxynucleosidtriphosphate (dNTPs):	Boehringer, Mannheim
1,4-Dithiothreitol (DTT):	Roth, Karlsruhe
Dimethyl sulfoxide (DMSO):	Roth, Karlsruhe
Dipotassium phosphate (K_2HPO_4):	Roth, Karlsruhe
Ethylenediamintetraacetic acid (EDTA):	GERBU, Heidelberg
Ethanol, p.a.:	Roth, Karlsruhe
Ethidium bromide:	Roth, Karlsruhe
Formaldehyde:	Sigma Aldrich, Seelze
Formamide:	Roth, Karlsruhe
Glucose:	Roth, Karlsruhe
Glycerin:	GERBU, Heidelberg
HEPES:	GERBU, Heidelberg
Isopropyl β-D-thiogalactopyranoside (IPTG):	Roth, Karlsruhe
Isopropanol:	Roth, Karlsruhe
Lead acetate:	Roth, Karlsruhe
Magnesium acetate:	Sigma Aldrich, Seelze
Monopotassium phosphate (KH_2PO_4):	Roth, Karlsruhe
Peptone:	Roth, Karlsruhe
Phenol:	Roth, Karlsruhe
Potassium chloride (KCl):	Roth, Karlsruhe

Rotiphorese 30 (Acrylamid-/Bisacrylamid-Lsg.):	Roth, Karlsruhe
Size standard (proteins and DNA):	Thermo Fisher Scientific, Schwerte
Sodium acetate:	Grüssing, Filsum
Sodium chloride (NaCl):	Roth, Karlsruhe
Sodium dodecyl sulfate (SDS):	Roth, Karlsruhe
Sodium hydroxide (NaOH):	Roth, Karlsruhe
Tetramethylethylenediamine (TEMED):	Roth, Karlsruhe
Tris-(hydroxymethyl)aminomethane (Tris):	Roth, Karlsruhe
Triton X-100:	Roth, Karlsruhe
Urea:	Roth, Karlsruhe
Xylencyanol blue (XCB):	Roth, Karlsruhe
Yeast Extract:	GERBU, Heidelberg

3.11.2 Equipment

Agarose gel chamber	Biorad, Mini Sub Cell
Autoclave	Systec V_{95}
Centrifuges	Eppendorf 5810R, Heraeus Biofuge Fresco, Sigma 112
Dewar vessel	KGW Isotherm, Karlsruhe
Gel documentation	Cybertech CS1
Gel dryer	Membran Vakuum-Pumpe (Vacuubrand GmbH, Wertheim); Phero-Temp (Biotech-Fischer, Reiskirchen)
Hand counter	Berthold LB 1210 B
Heating block	Biometra TB1

Ice maker	Typ 125-75 (Ziegra, Isernhagen)
Incubator	Memmert BE400
Imager cassettes	Fuji Film Bas cassette 4043
Magnetic stirrers	Heidolph MR 2002
Power supply	Biorad 160/1.6
PAA-gel chamber	Custom-made, University of Lübeck
PCR cycler	Biometra TGradient Thermocycler
pH-Meter	WTW pH Level 1
Phosphoimager Raytest Bio-Imaging Analyser	BAS 1000 (Fujifilm), FLA 3000 (Fujifilm)
Pipets	Eppendorf Research (0.1–2.5 µl, 2–20 µl, 20–200 µl, 100–1000 µl)
Mixer	Eppendorf Thermomixer 5436
SDS gel chamber	BioRad Mini-PROTEAN Tetra System, Hercules, California
Shaking incubator	Typ 3033 (GFL, Burgwedel)
Spectrophotometer	Thermo Spectronic Biomate 3
Scintillation counter	Perkin Elmer Wallac WINSPECTRAL a/b 1414
Ultrapure water purification system	Milli-Q® biocell (Millipore, Schwalbach
Ultrasonic installation	Sonicator Sonoplus GM70 mit UW70/SH70G (Bandelin; Berlin)
UV-transilluminator	Chromato-VUE TS-15 (Ultra Violet Products Inc., Upland, CA, USA)

3.11.3 Other laboratory tools

Quartz cuvette	Hellma 104-QS, 105.202, 115B-QS, 105
Filter device	Sarstedt, Nürnbrecht
Half-micro cuvette	Sarstedt, Nürnbrecht
Nucleic acid preparation coulums	Macherey-Nagel, Düren; Qiagen, Hilden
Reaction device 0.5 mL;	PP Sarstedt, Nürnbrecht
Reaction device 1.5 mL safety caps,	PP Sarstedt, Nürnbrecht
Reaction device 2.0 mL safe-seal,	PP Sarstedt, Nürnbrecht
Reaction device 5.0 mL	Eppendorf Research, Hamburg
Reaction device 15 mL 120 X 17 mm,	PP Sarstedt, Nürnbrecht
Reaction device 50 mL 114 X 28 mm,	PP Sarstedt, Nürnbrecht
RiboRuler low Range RNA ladder (100-1000 bp)	Thermo Fisher scientific, Schwerte
Phosphoimager Raytest Bio-Imaging plates	Fuji, Tokyo, Japan
PageRuler prestained protein ladder,	Thermo Fisher scientific, Schwerte

3.11.4 Enzymes

DNase I	Thermo Fisher scientific, Schwerte
FD *BamH* I	Thermo Fisher scientific, Schwerte
FD *EcoR* I	Thermo Fisher scientific, Schwerte
FD *Hind* III	Thermo Fisher scientific, Schwerte
Mva I	Thermo Fisher scientific, Schwerte
Nco I	Thermo Fisher scientific, Schwerte
Pfu-polymerase	Thermo Fisher scientific, Schwerte
Phusion-polymerase	Thermo Fisher scientific, Schwerte

RNA polymerase (*B. sub*)	Margarita Salas lab, Spain; Hartmann lab, Marburg
RNase A	Macherey-Nagel, Düren
RNase T1	Thermo Fisher scientific, Schwerte
RNase V1	Ambion (Thermo Fisher scientific, Schwerte)
Sma I	Thermo Fisher scientific, Schwerte
T4 DNA-ligase	Thermo Fisher scientific, Schwerte
T4 RNA-ligase	Thermo Fisher scientific, Schwerte
T4-Polynucleotide-kinase (PNK)	Thermo Fisher scientific, Schwerte
T7 RNA polymerase	Hartmann lab, Marburg; Thermo Fisher scientific, Schwerte

3.11.5 Synthetic DNA oligonucleotides

Table 3. 49 Primer sequences used for cloning experiments (primer concentration 100 pmol/µL)

No	Primer name	Sequence
1	*Nr.5:*N9-MiniGly-forw	5'-AAT TCG TAA TAC GAC TCA CTA TAG GTC CCT TTC GCG GGA GGA AAC TCC CGC ACC ATG-3'
2	*Nr.6:*N9-MiniGly-rev	5'-GAT CCA TGG TGC GGG AGT TTC CTC CCG CGA AAG GGA CCT ATA GTG AGT CGT ATT ACG-3'
3	*Nr.11T7-6SlpRNA_pAT_s*	5'-AAT TCT AAT ACG ACT CAC TAT AGT AGG CCC CAT TGA CGG AGA GAG GGG GTT CAA ATC CCC CTC TCT CCA CCA G-3'
4	*Nr.12T7-6SlpRNApA_as*	5'-GAT CCT GGT GGA GAG AGG GGG ATT TGA ACC CCC TCT CTC CGT CAA TGG GGC CTA CTA TAG TGA GTC GTA TTA G-3'
5	*Nr.13_HH-sense+EcoRI*	5'-CGG AAT TCG TAA TAC GAC TCA CTA TAG GGA GAC AAC TCC CTG ATG AGT-3'
6	*Nr.14_HH-Antisense*	5'-GAC GGT ACC GGG TAC CGT TTC GTC CTC ACG GAC TCA TCA GGG AGT TG-3'
7	*Nr.15_6Sshort5'extHHsen*	5'-GTA CCC GGT ACC GTC GGA GTT GTC AAT GGG-3'
8	*Nr.16_6Sshort+BamHIantI*	5'-CGC GGA TCC TTCTCC CTT-3'
9	*Nr.17_6Sshort85nt_sen*	5'-GGA AGA CTT CCC ACC TTA AAG-3'

10	*Nr.18_6Sshort85nt_ant*	5’-GAC TTC CCT TAC ACC-3’
11	*Nr.25. HH6Slong_Sense*	5’-GAG GAC GAA ACG GTA CCC GGT ACC GTC GGG TGG TGC GGG GGT TG-3’
12	*Nr.26. HH6Slong Antis*	5’-ACG GAC TCA TCA GGC CAC CCT CTC CCT ATA GTG AGT CGT ATT ACG AAT TCA CTG GCC GTC GTT TTA-3’
13	*Nr.27 HH_6S159nt_sens*	5’-GAG GAC GAA ACG GTA CCC GGT ACC GTC AAG GTC TGC CCT GTT CG-3’
14	*Nr.28 HH_6S159nt_antis*	5’-ACG GAC TCA TCA GAA GGG TCT CTC CCT ATA GTG AGT CGT ATT ACG AAT TCA CTG-3’
15	*Nr.29. Bsub6S1xSmaIsen*	5’-GGG CTC CCA AAT CAA AAA AAT GTT CGG T-3’
16	*Nr.30. Bsub6S1xSmaI_AS*	5’-GGG AAG CTT GGC ACT GGC CGT-3’
17	*Nr.31. Aq6Slmiss1/2sen*	5’-GGG TCG GCA TGG CAT CTC-3’
18	*Nr.32. Aq6Sl_miss1_as*	5’-TGG CAG TGC AGG AAG TGC-3’
19	*Nr.33. Aq6Sl_miss2_as*	5’-TTG CAG TGC AGG AAG TGC C-3’
20	*M13 uni (-43)*	5’-AGG GTT TTC CCA GTC ACG ACG TT-3’
21	*M13 rev (-49)*	5’-GAG CGG ATA ACA ATT TCA CAC AGG-3’
22	*Seq8*	5’-GTA AAA CGA CGG CCA G-3’
23	*Seq9*	5’-CAG GAA ACA GCT ATG AC-3’

3.11.6 Synthetic RNA oligonucleotides

No	Oligonucleotide name	Sequence
1	*pMini3bpUG*	5’-rGrArU rCrUrG rArArU rGrCrG rGrArA rArCrG rCrGrC rCrArC-3’
2	*pMini7bpUG*	5’-rGrArU rCrUrG rArArU rGrCrG rGrGrA rGrGrA rArArC rUrCrC rCrGrC rGrCrC rArC-3’
3	6S-1 p_14; *B. sub.*6S-1 pRNA-14; *B. sub.*6S-1 pRNA-14_nr2	5’-rGrUrU rCrGrG rUrCrA rArArA rCrU-3’
4	*Aq* 6Sp_15; *Aae* pRNA 15mer; *Aae* pRNA 15mer_1; *Aae* pRNA 15mer_2	5’-rGrUrA rGrGrC rCrCrC rArUrU rGrArU-3’
5	*LNA-15mer*	5’-lGlUlA lGlGlC lClClC lAlUlU lGlAlU-3’
6	*Aae* pRNA 8mer	5’-rGrUrA rGrGrC rCrC-3’
7	*Aae* pRNA 9mer	5’-rGrUrA rGrGrC rCrCrC-3’

8	*Aae* pRNA 10mer	5’-rGrUrA rGrGrC rCrCrC rA-3’
9	*Aae* pRNA 11mer	5’-rGrUrA rGrGrC rCrCrC rArU-3’
10	*Aae* pRNA 12mer	5’-rGrUrA rGrGrC rCrCrC rArUrU-3’
11	*Aae* pRNA 13mer	5’-rGrUrA rGrGrC rCrCrC rArUrU rG-3’
12	*Aae* pRNA 14mer	5’-rGrUrA rGrGrC rCrCrC rArUrU rGrA-3’
13	6S 132 aspRNA 15mer(rev)	5’-rArCrU rCrCrG rGrGrU rGrCrC rGrUrG-3’
14	6S 132 aspRNA 15mer 5’-3’	5’-rGrUrG rCrCrG rUrGrG rGrCrC rUrCrA-3’
15	*Bsub*6S-1_3’pRNA16nt	5’-rGrCrU rUrUrC rCrUrU rUrGrU rUrUrU rG-3’

3.11.7 Bacterial strains

E. coli DH5σ

4. Results and Discussion

In the first part, a series of experiments were conducted that aimed at studying the cleavage mechanism of RNase P by NMR. The second part is dedicated to the structural and functional characterization of primarily *A. aeolicus* 6S RNA.

4.1.1. RNase P

To identify specific RNA-RNA and RNA-metal ion interactions that are involved in the cleavage mechanism catalyzed by bacterial RNase P, we pursued an NMR approach that has the additional potential to uncover the dynamics of the catalytic process. Towards this goal, a shortened RNase P RNA, minimized substrates and the RNase P protein were prepared and subjected to NMR measurements. The protein subunit itself did not yield additional signals that could hamper structure determination. The results are described in the following chapters.

4.1.2. Homogeneous *E. coli* C-domain (Ecat)

To gain insight into the cleavage mechanism of the 5'-end maturation of precursor tRNAs by RNase P, we aimed to determine the RNA-RNA as well as RNA-metal ion interactions before, during and after the cleavage reaction. The efforts of several groups to solve a crystal structure of RNase P in combination with (pre-)tRNA or another cleavable substrate were not successful at that time, which contributed to our motivation to use NMR apart from its advantage to permit analyses of the dynamics of the process. Therefore, a variant of the *E. coli* RNase P RNA (M1 RNA; 377 nt) was prepared which is lacking nearly the entire S-domain (termed Ecat, 235 nt), to minimize the number of signals in NMR spectra. Since P RNA is not accurately folded after preparation (shown in Figure 4. 1 (right) lane 3), the RNA has to be pre-incubated. Therefore, the P RNA was incubated at 55°C for 5 min and at 37°C for 50 min (shown in Figure 4. 1 (right) lane 4). To determine the folding state of Ecat after preparation a sample was treated in the same manner as P RNA (Figure 4. 1 (left) lane 2) and compared with an untreated sample (Figure 4. 1 (left) lane 1).

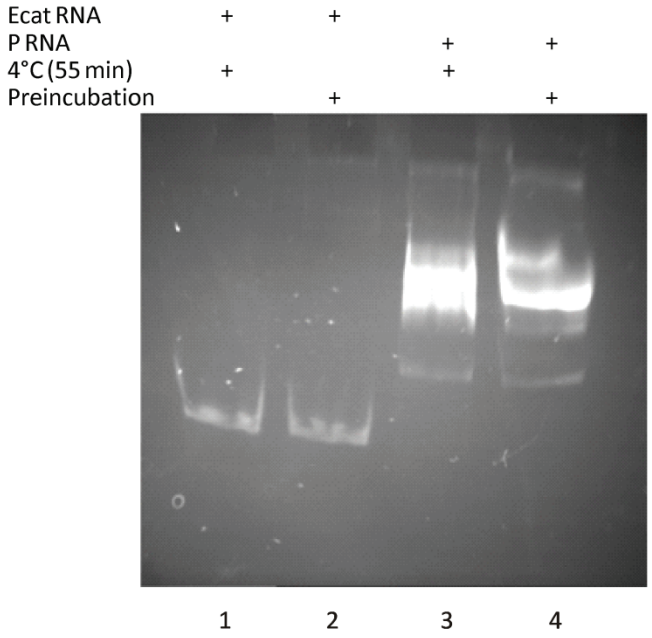

Figure 4. 1 Electrophoretic mobility shift assay (EMSA; 11% native PAGE in 1 x TBE buffer) of the catalytic domain of *E. coli* RNase P RNA (Ecat; lanes 1 and 2) next to the full-length RNA (P RNA; lanes 3 and 4). In lanes 1 and 3, the sample was stored at 4°C for 55 min before gel loading. In lanes 2 and 4, samples were preincubated for 5 min at 55°C and 50 min at 37°C before gel loading.

The EMSA experiment (Figure 4. 1) demonstrated that Ecat adopts a homogeneous secondary structure. Due to the fact that Ecat is not catalytically active on its own (in contrast to full-length P RNA), the RNA had to be preincubated with the *E. coli* RNase P protein (P protein) to assemble a functional holoenzyme before measuring cleavage activity.

4.1.3. RNA transcription in *large-scale*

In vitro T7 *run off* transcription were performed as described in chapter 3.5. The standard procedure usually yields in an RNA amount around 50- 100 µg. The required amount of RNA for NMR measurements is in a range of 5-7 mg (500 to 800 mM) which posed a challenge due to the limits of the standard protocol. Additionally, some produced and purified RNAs could not be resolved in ddH_2O or mKN4.5 buffer in concentrations exceeding approx. 1 mg. This problems demand a change of the transcription protocol.

I could determine that a key role for high yields of RNA played the Mg^{2+}-concentration during transcription. The commonly (in our lab) used 33 mM Mg^{2+}-concentration had shown to be suboptimal for most of the transcribed

RNA during this work. Therefore, prior to the preparative transcription, for each RNA (produced during this work) several small pre-transcription reactions (chapter 3.5.2) with a total volume of 50 µL were performed. Thereby, the Mg^{2+}-concentration was altered in the range of 10-40 mM. Subsequently, the samples were analysed on a 10 to 12% denaturing PAA gel. Dependent on the size of the RNA bands, visualized by EtBr in combination with UV-light, the optimal Mg^{2+}-concentration was determined. Afterwards several attempts to optimize the transcription reaction (Table 3. 26), *large-scale* transcription (3.5.2) with a reaction volume between 2 to 15 mL were performed which yielded in RNA amounts of 4-5.5 mg. I could show that the NaOAc concentration (0.3 M versus 1 M) of the gel elution buffer, used after preparative gel electrophoresis, had a strong influence on the solvability of the transcribed RNA. Finally, Ecat RNA is solvable after elution in 0.3 M NaOAc up to 8 mg/125 mL whereas after usage of 1 M NaOAc Ecat RNA remained as precipitate regardless of which solvent volume and consistency.

4.1.4. Substrate kinetics

Similar to the size reduction of P RNA, resulting in Ecat, minimal RNase P substrates with good-quality NMR spectral properties were explored. Several of such minimal substrates were designed (Figure 4. 2) and tested in reactions catalyzed by the Ecat:P protein holoenzyme(Figure 4. 3).

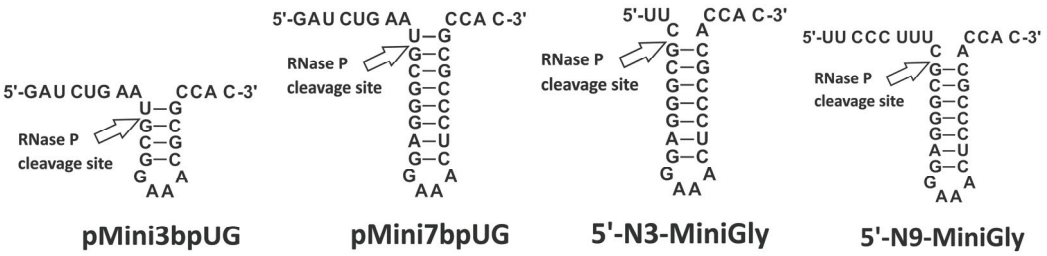

Figure 4. 2 Different minimal substrates designed for cleavage analysis.

Reactions with Ecat alone, i.e. in the abesence of P protein, were performed as negative controls in cleavage reactions of the different minimal substrates. As shown in Figure 4. 3. substrates pMini3bpUG and pMini7bpUG could be cleaved by the Ecat-holoenzyme and were thus considered as suitable substrates for further investigation by NMR.

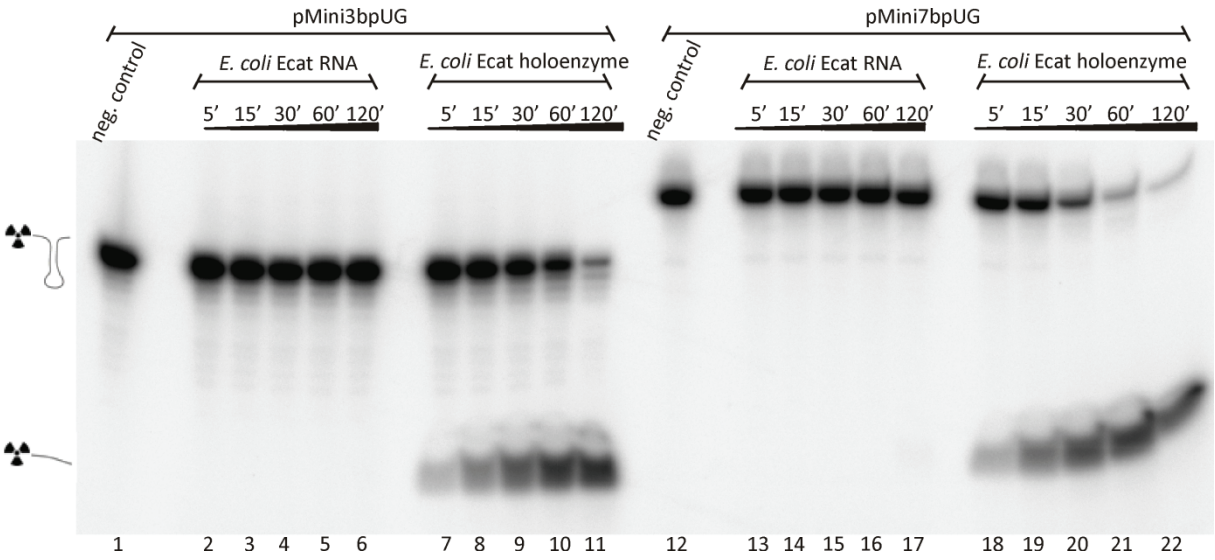

Figure 4. 3 Cleavage analysis of substrates pMini3bpUG (left) and pMini7bpUG (right) (end concentraton 100 µM) in samples containing Ecat, either in the absence or presence of *E. coli* P protein. The concentration of Ecat and P protein were 20 µM each. Corresponding ^{32}P-radiolabeled substrates were present in trace amounts (< 1 nM) and reactions were conducted in KN4.5 buffer, followed by 20% denaturing PAGE; for further details, see Materials and Methods.

The cleavable pMini3/7bpUG substrates failed to give interpretable NMR spectra. Hence, we analyzed two other minimal substrates whose design was based on substrates that have been approved for NMR measurements (5'-N3-MiniGly and 5'-N9-MiniGly; (Figure 4. 3)). These substrates were found to be detectable by NMR. As we could generate an acceptable NMR spectrum of the 5'-N9-MiniGly substrate, this substrate was incubated with Ecat holoenzyme in buffers with two different Mg^{2+}-concentrations (Figure 4. **4**; $MgCl_2$ endconcentration: 4.5 mM or 9 mM) to find favorable low salt conditions for the desired processing reaction to be performed during NMR measurements.

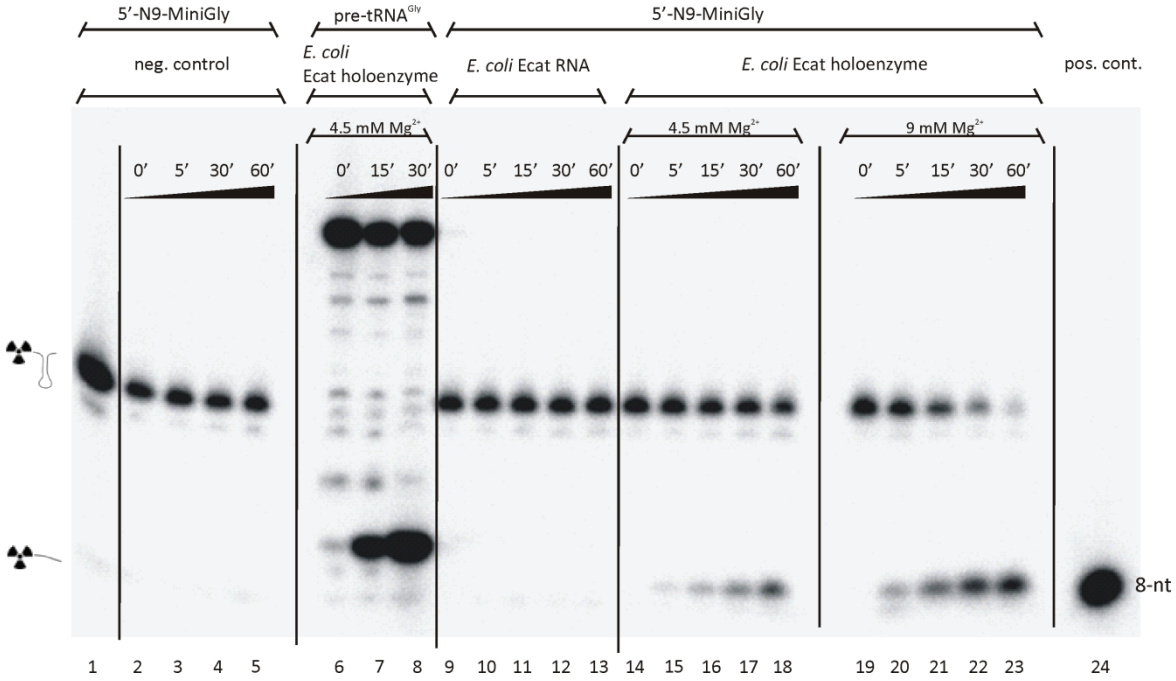

Figure 4. 4 Cleavage analysis of the substrate 5'-N9-MiniGly in reaction catalyzed by Ecat holoenzyme at Mg^{2+} concentration of 4.5 mM (lane 14-18) and 9 mM (lane 19-23), respectively. As positive control, the standard substrate pre-tRNA^{Gly} (Mg^{2+}-concentration of 4.5 mM) was used (lane 6-8). Samples of 5'-N9-MiniGly which were incubated with or without Ecat, but in the absence of P protein, were loaded as negative controls (lane 1-5, 9-13). For experimental details, see legend to Figure 4. 3 and Materials and Methods.

This experiment clearly showed that 5'-N9-MiniGly can be efficiently cleaved by Ecat holoenzyme and that the cleavage reaction has a lower reaction rate at lower Mg^{2+} concentration (4.5 mM versus 9 mM, (Figure 4. **4**)) which could be an important adjustable parameter during investigations of the reaction mechanism.

4.1.5. Analysis of *E. coli* P-protein stability

Most NMR investigations within this work have been performed for several hours at 37°C, where the Ecat holoenzyme cleavage reaction occurs with high efficiency. Therefore, it is important that all reaction partners are stable throughout the whole period of time. To determine the stability of the RNase P protein, it was kept at room temperature (RT) for up to 96 h and afterwards its function was analyzed in Ecat-catalyzed cleavage reaction using the pMini7bpUG substrate (Figure 4. 5). As no activity losses were observed after incubation at RT for 96 h, the P protein was stored for months at RT in the following. P protein handled in this manner was consistently used for activity assays (e.g. Figure 4. **4**) without any obvious activity losses.

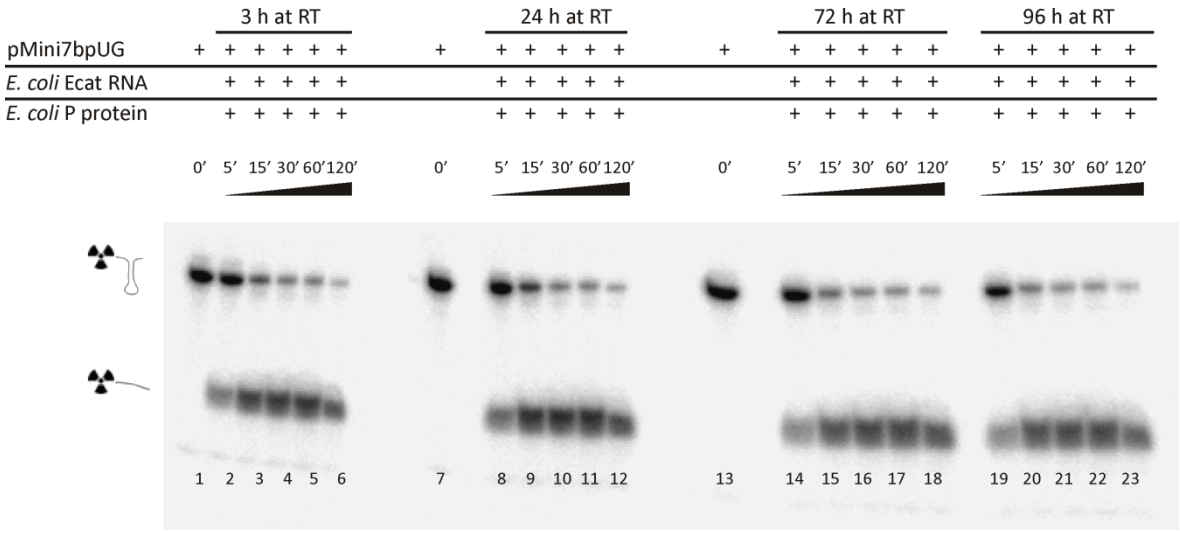

Figure 4. 5 Capacity of the P protein to activate Ecat RNA after protein storage at room temperature for 3, 24, 72 or 96 h. The substrate was 5'-^{32}P-labeled pMini7bpUG; for details, see legend to Figure 4. 3 and Materials and Methods.

These results underline the high structural stability of the *E. coli* P protein and prove its suitability for the usage under conditions of NMR experiments.

4.1.6. NMR spectrum of the 5'-N9-MiniGly substrate

The chemically synthethized 5'-N9-MiniGly RNA was used to collect an $^{1}H,^{13}C$-HSQC spectrum at 600 MHz and 283 K. Within the C_2H_2 area of the spectrum, six signals representing the six adenosine residues of the RNA could be detected (Figure 4. 6), including one strong signal, four weaker ones and one very weak signal.

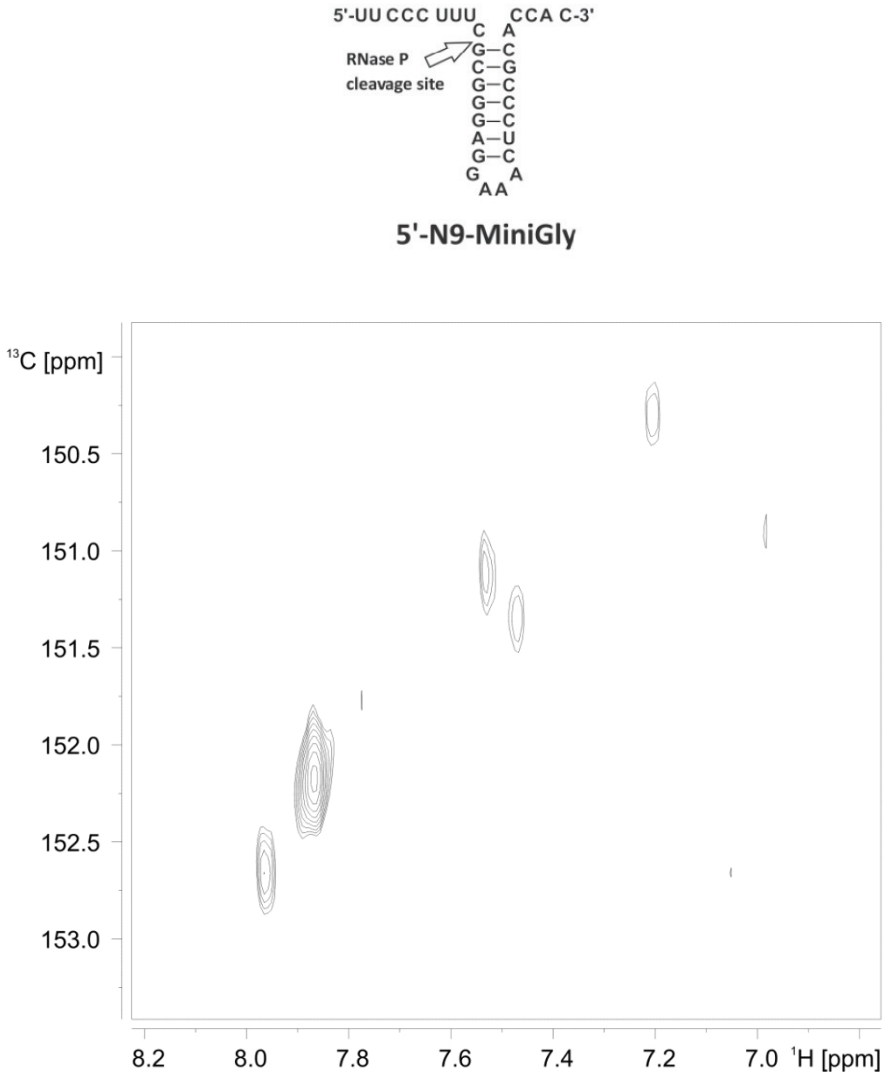

Figure 4. 6 $^{1}H,^{13}C$-HSQC spectrum of the 5'-N9-MiniGly substrate. The spectrum was recorded at 600 MHz and 283 K (10°C). The six signals represent the six adenosines in the sequence shown at the top.

In summary, several conditions for NMR investigations of the bacterial RNase P reaction mechanism could be fulfilled. I was able to demonstrate that the shortened *E. coli* RNase P C-domain (Ecat) adopts a homogenous conformation as inferred from native PAGE analysis, even without applying a specific folding (preincubation) protocol. The *E. coli* RNase P protein was catalytically active, even after storage at room temperature for up to 3 months. Further, I could identify several minimal substrates that were good substrates for the Ecat holoenzyme. Unfortunately, only one of the four substrates yielded interpretable NMR spectra. However, attempts to record NMR spectra of the 5'-N9-MiniGly substrate with higher signal intensities failed thus, the method were insufficient for further mechanistic analyses of RNA-RNA or RNA-metal ion interactions. As a consequence, the project was given up at this point.

4.1.7. 6S RNA

4.1.8. *A. aeolicus* 6S RNA

The 6S RNA of *A. aeolicus*, representing the most thermostable 6S RNA known to date, was identified by an RNomics approach before the coming of high-throughput sequencing techniques [Willkomm *et al.*, 2005]. During this work, we performed a follow-up transcriptome analysis of *A. aeolicus* using 454 high-throughput sequencing of cDNA using the differential RNA-seq (dRNA-seq) approach [Sharma *et al.*, 2010]. In dRNA-seq, the total RNA (in this case from *A. aeolicus*) is split in two fractions of which one is additionally treated with with Terminator™ 5'-Phosphate-Dependent Exonuclease (5'-TEX), an enzyme that degrades RNAs with 5'-monophosphate ends but not primary transcripts with 5'-triphosphate ends. This procedure indirectly enriches primary RNA transcripts. A quantitative comparison of cDNA read patterns obtained for 5'-TEX-treated and untreated RNA fractions allows to identify primary transcripts and thus bacterial transcription start sites. In this work, particularly reads corresponding to pRNAs transcribed from *A. aeolicus* 6S RNA *in vivo* were of interest (chapter 4.1.9).

Additionally, we analyzed the secondary structure of *A. aeolicus* 6S RNA by two different methods, solution structure probing (chapter 4.1.10) and NMR (chapter 4.1.11). Based on a previous bioinformatic analysis [Beckmann, Hoch *et al*., 2012], it was proposed that a pRNA-induced rearrangement of *A. aeolicus* 6S RNA may involve formation of a stable hairpin in the 3'-CB as well as a central bulge collapse (CBC) helix (Figure 4. **7**).

For the purpose of 6S RNA crystallization attempts and owing to a RNA size limit of approx. 80 nt for high resolution NMR measurements, we prepared shortened *A. aeolicus* 6S RNA variants (85 nt and 132 nt/ Figure 4. **7**). Further, we used a synthetic pRNA (15 nt; sequence: 5'-GUA GGC CCC AUU GAC; chapter 3.11.6) to investigate the secondary structure of the structure after the pRNA-induced rearrangement in comparison with the free 6S RNA.

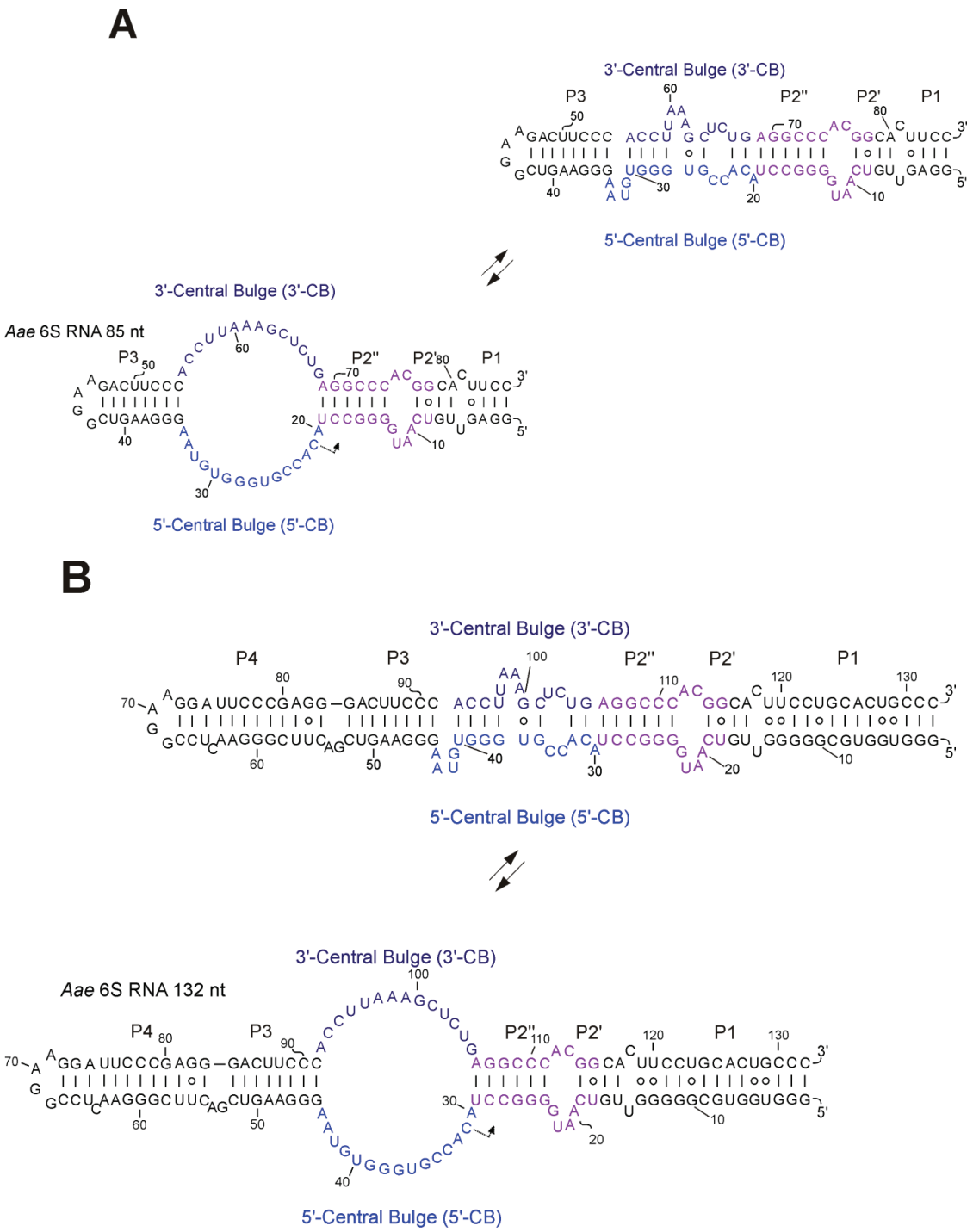

Figure 4. 7 Structures of shortened *A. aeolicus* 6S RNA variants, 85 and 132 nt in length (the native RNA is shown in Figure 1. 19). (A) The 85-nt variant shown in its predicted minimal free energy (MFE; `RNAfold`) structure (top) or its open bulge structure (centroid secondary structure; `RNAfold`). The 5'-central bulge (5'-CB) and the 3'-central bulge (3'-CB) are marked in blue and dark blue, respectively. The helix P2'' marked in purple unwinds during pRNA transcription. (B) Corresponding illustration for the 132-nt variant.

Likewise, we were interested to determine if *A. aeolicus* 6S RNA shows the same effect on RNAP as described for *E. coli* and *B. subtilis* 6S RNA. Therefore, we investigated gel migration of free 6S RNA structure, 6S RNA:pRNA hybrid structure

using native PAGE. The capacity of *A. aeolicus* 6S RNA to bind to σ-RNAP and to serve as a template for pRNA transcription was analyzed with *B. subtilis* σ^A-RNAP, as *A. aeolicus* RNAP was not available (chapters: 4.1.12, 4.1.13, 4.1.14, 4.1.15).

4.1.9. Identification of pRNA synthesized from *A. aeolicus* 6S RNA *in vivo* using dRNA-seq

After the *A. aeolicus* 6S RNA had been found (by an RNomics approach), the question arose if the RNA can serve as template for pRNA synthesis by RNA polymerase, which is a hallmark feature of bacterial 6S RNAs. To elucidate if *A*. aeolicus pRNAs are produced *in vivo* we performed a deep sequencing experiment with total cellular RNA isolated from *A. aeolicus* cell pellets by the hot phenol method (chapter 3.4.1); The RNA was further fractionated to fragments ≤ 50 nt by denaturing PAGE. Library preparation and 454 sequencing were carried out together with Jörg Vogel's group (Univ. Würzburg) and vertis Biotechnologie AG, Freising-Weihenstephan (Germany). One half of the RNA samples was additionally treated with 5'-TEX to enrich for primary transcripts. Poly(A) tails were then added to RNA 3'-ends using poly(A) polymerase, followed by ligation of an adapter/linker to the 5'-ends. cDNA libraries were synthesized according to the method described in chapter 3.4.2. Bioinformatic analysis of the cDNA sequencing reads indeed identified pRNAs transcribed by *A. aeolicus* RNAP *in vivo* (Figure 4. 8). Such pRNA reads were only detected in the 5'-TEX-treated library, indicating that they are primary transcripts carrying a 5'-triphosphate which had to be enriched to enter the cDNA library in sufficient amounts. All pRNA reads had the same 5'-terminus (Figure 4. 9), supporting the notion that they are bona fide pRNAs and not fortuitously matching reads orignating from other locations in the genome. The transcription initiation site could be assigned to nucleotide C48 located in the 5'-CB of *A. aeolicus* 6S RNA (cf. Figure 1. 19 and Figure 4. 9). Based on the read alignment shown in Figure 4. 9, pRNAs have a length spectrum of 7 to 15 nt. This does not exclude the possibility that smaller pRNAs are also synthesized *in vivo*, but those are likely to be underrepresented in the library (for technical reasons) apart from the difficulty of their unequivocal assignment to the 6S RNA locus. Single mismatches within the read sequence are indicated by parentheses and lowercase letters in Figure 4. 9. We have nevertheless classified such reads as genuine pRNAs reads, as they had the same 5'-terminus as the other pRNA reads and based on our general observation of considerable sequencing errors in various 454 sequencing data sets. Regarding the relative abundance of pRNA length variants, 9 to 14-mers dominated, raising the question if hybrids of *A. aeolicus* 6S RNA and pRNA 9 to 14-mers form sufficiently stable duplexes at growth temperatures of ≥ 85°C to be able to persistently rearrange the 6S RNA structure as a prerequisite for RNAP release under the native growth conditions of *A. aeolicus*.

Nevertheless, the findings described here verifiy that this unique regulatory mechanism involving RNA-dependent RNA transcription also takes place in a bacterium that thrives at a temperature of 85°C or higher.

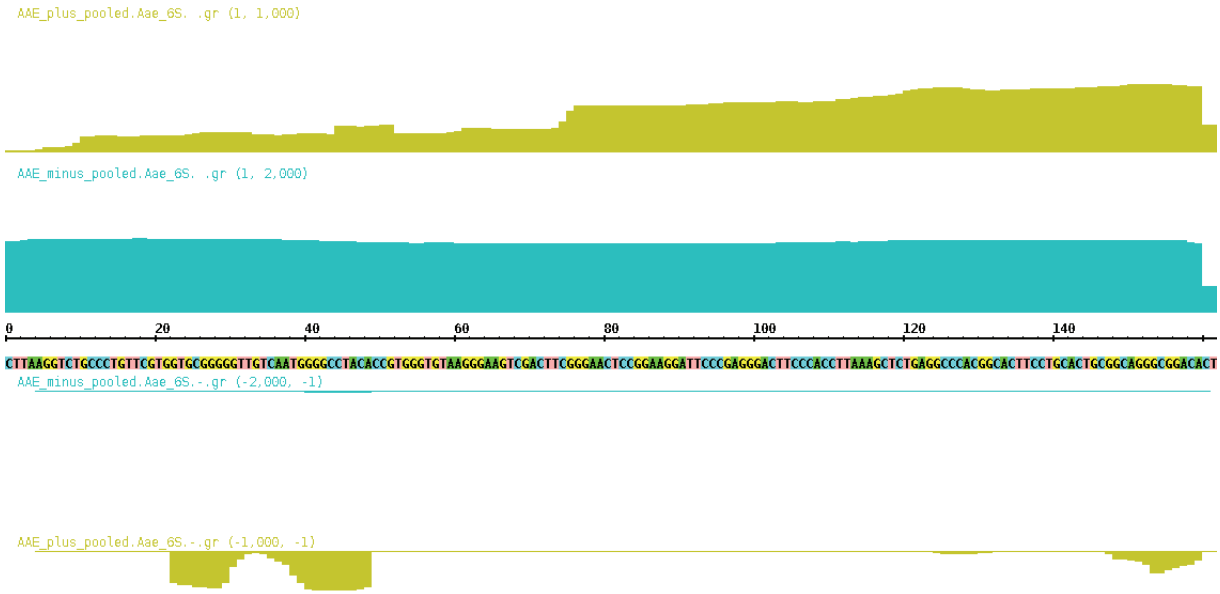

Figure 4. 8 cDNA read profile screenshot of the *A. aeolicus* 6S RNA gene locus based on 454 sequencing data obtained with total RNA isolated from *A. aeolicus* cells harvested in late exponential growth phase. The read data are displayed using the Integrated Genome Browser software [Nicol *et al.*, 2009]. The DNA sequence is shown in the center and reads corresponding to the (+) and (-) strand are shown at the top and bottom, respectively. Reads from the RNA fraction additionally treated with 5'-TEX to enrich for primary transcripts are shown in yellow, those for the untreated RNA fraction are depicted in cyan. The 6S RNA sequence corresponds to the (+) strand and pRNA reads to the (-) strand. The number of reads ranges between 1-1000 (yellow) and 1-2000 (cyan).

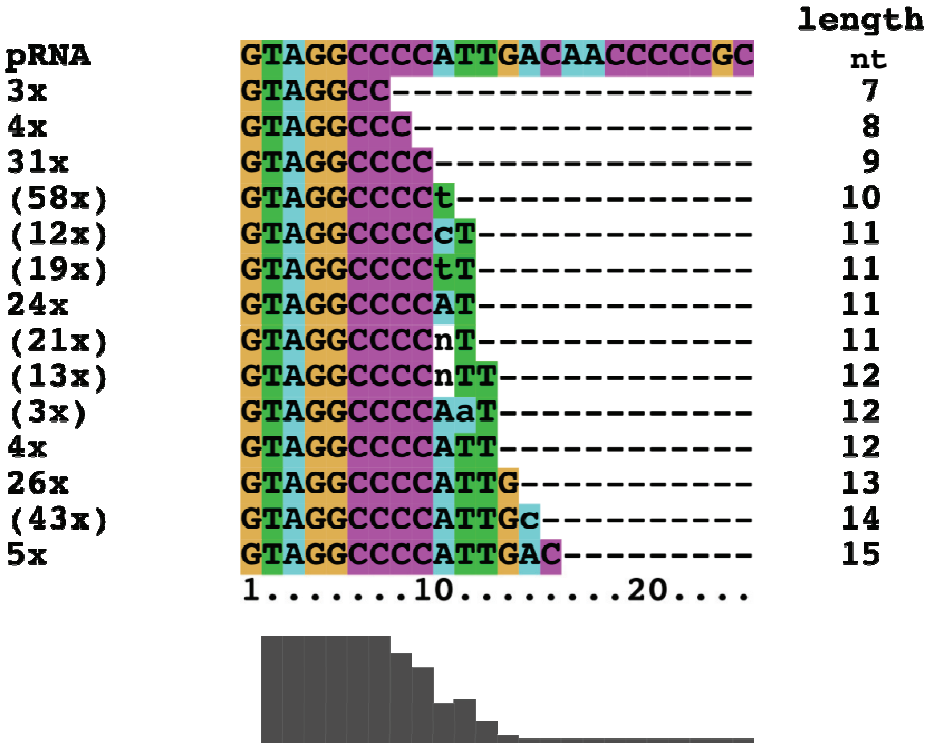

Figure 4. 9 Alignment of *A. aeolicus* 6S RNA-derived pRNAs reads identified in 5'-TEX treated libraries enriched for primary transcripts. A 24-nt reference sequence is shown at the top. The number and length of reads are indicated on the left and right, respectively. Mismatches owing to sequencing errors are marked by lowercase letters. Reads including mismatches are indicated by parentheses.

4.1.10. Secondary structure analysis via enzymatic and chemical probing

To address the question if pRNA binding to *A. aeolicus* 6S RNA leads to a structural rearrangement as described for *E. coli* and *B. subtilis* 6S RNA, enzymatic and chemical probing experiments with both variants of the *A. aeolicus* 6S RNA (85 nt and 132 nt) were performed. By incubating the samples with one of the three probing agents Pb^{2+} ions, RNase T1 or RNase V1, we were able to identify structural differences between 6S RNA in its free state and as part of a 6S RNA:pRNA duplex structure, especially in the region forming the central bulge. Pb^{2+} ions preferentially cleave unpaired nucleotides (leaving 2'-,3'-cyclic phosphate and 5'-OH ends) that are present in bulges and internal loops of structured RNAs. RNase T1 cleaves 3' of unpaired guanosine residues (also generating 2'-,3'-cyclic phosphate and 5'-OH ends), whereas RNase V1 cleaves base-paired as well as single-stranded stacked regions. Thus, cleavage fragments of identical length generated by RNase V1 have slightly different gel mobilities than those generated by Pb^{2+} ions and RNase T1, migrating faster (3'-labeled RNA) or slower (5'-labeled RNA) than fragments generated by alkaline, RNase T1 or Pb^{2+} cleavage.

As references for the probing experiments, we predicted the minimal free energy (MFE) structures of the 85-nt and 132-nt 6S RNA variants using `RNAfold`. This was done at different temperatures used for the probing experiments, as well as at 87°C to consider the growth temperature of *A. aeolicus* where the central bulge is predicted to be entirely single-stranded. We also predicted the structures under conditions where the target region of the pRNA 15-mer in the 6S RNA variants was constrained to be excluded from any intramolecular base-pairing interactions (Figure 4. 10).

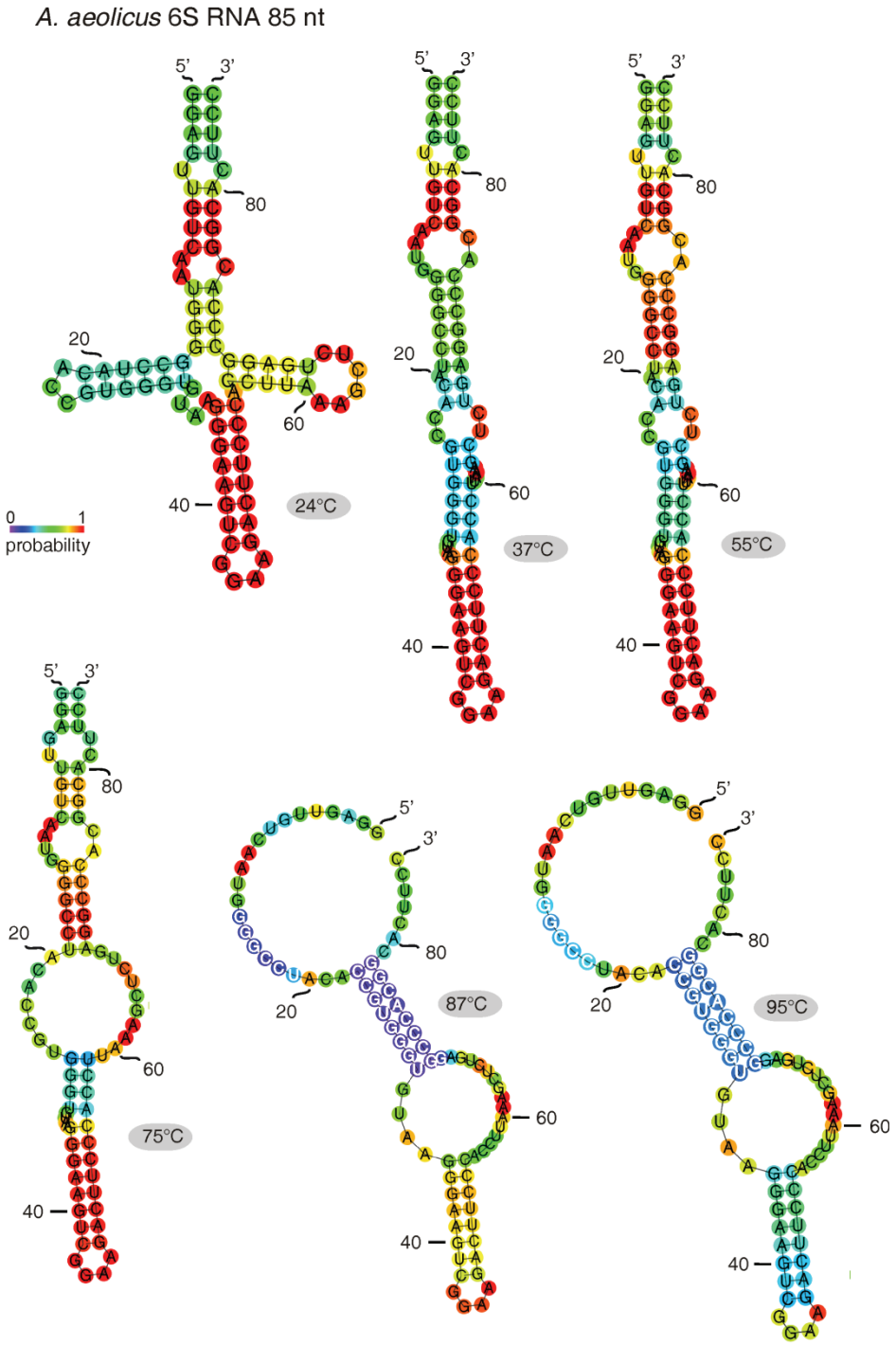

Figure 4. 9 A

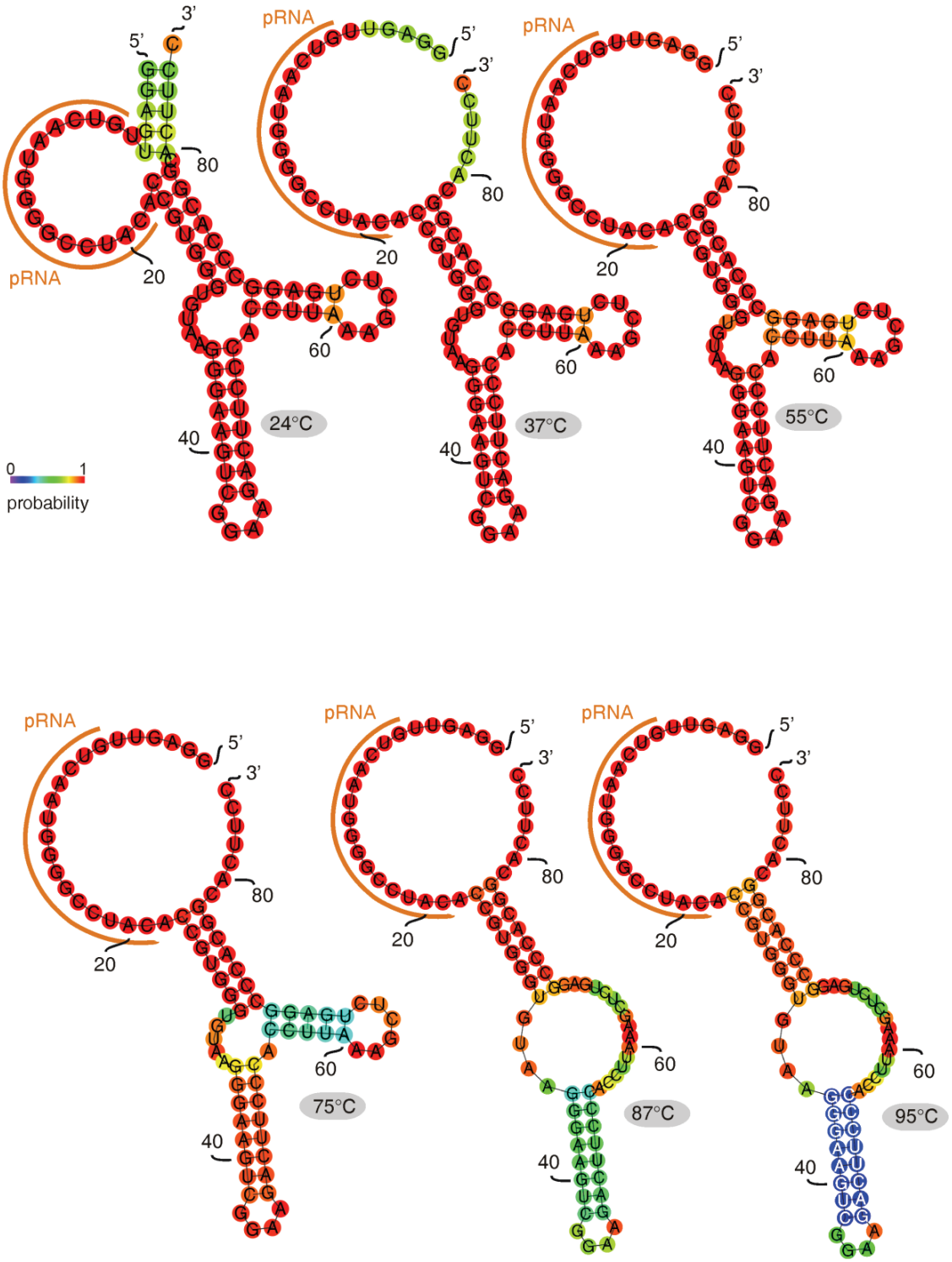
A. aeolicus 6S RNA 85 nt:pRNA hybrids
pRNA
5'
3'
20
60
80
40
24°C
37°C
55°C
75°C
87°C
95°C
0
1
probability

Figure 4. 9 B

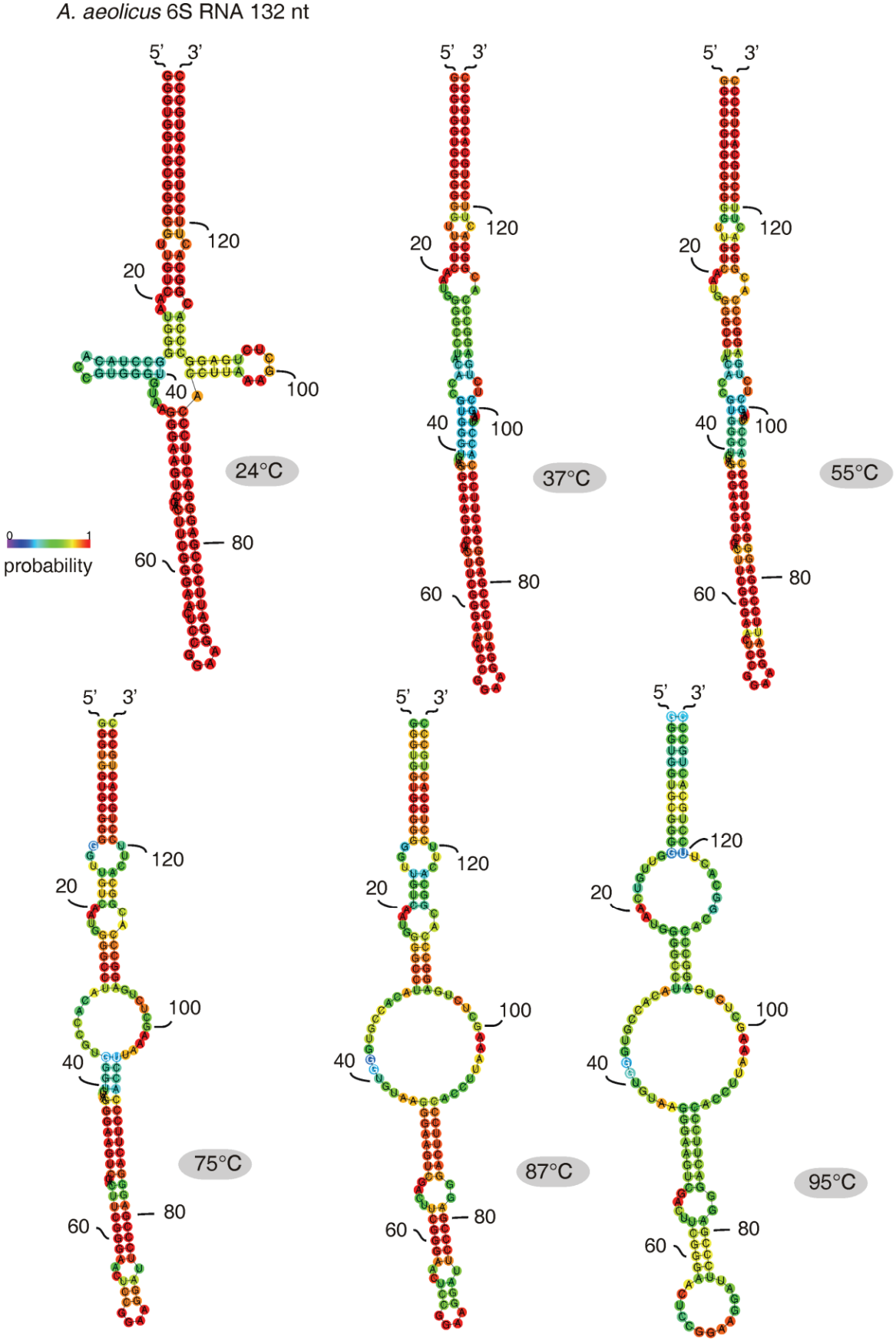
A. aeolicus 6S RNA 132 nt
5'
3'
120
20
100
40
24°C
probability
0
1
80
60
37°C
55°C
75°C
87°C
95°C

Figure 4. 9 C

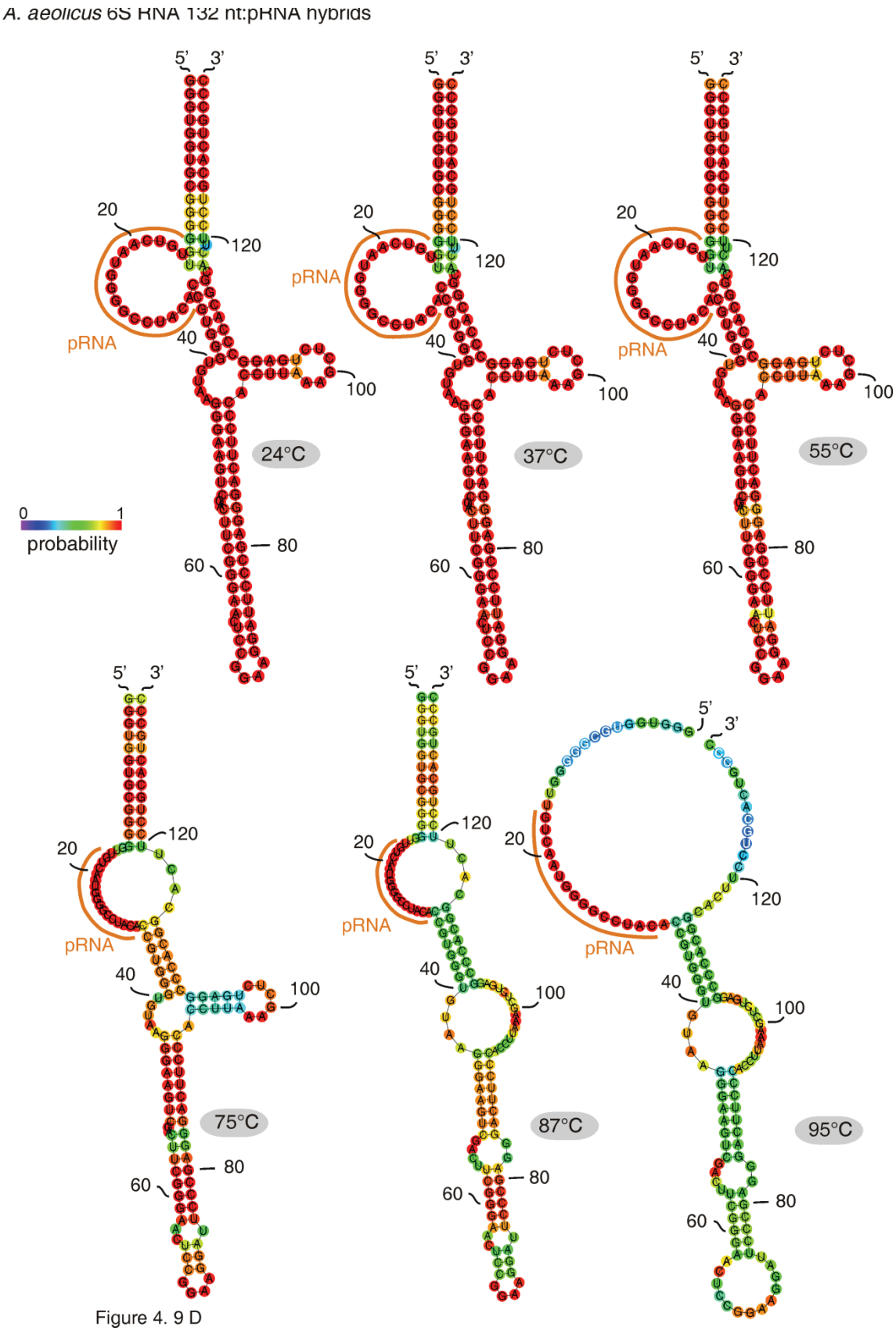

Figure 4. 9 D

Figure 4. 10 *A. aeolicus* 6S RNA (85-nt and 132-nt variants) secondary structures predictions by RNAfold. (A) 6S RNA 85-nt variant structure prediction at different temperatures (24°, 37°, 55°, 75°, 87° and 95°C) according to the used temperatures for secondary structure probing. (B) 6S RNA 85-nt:pRNA (15-mer) hybrid structure prediction at different temperatures (24°, 37°, 55°, 75°, 87° and 95°C) according to the used temperatures for secondary structure probing. The pRNA

binding site is indicated by an orange line. (C) 6S RNA 132-nt variant structure prediction at different temperatures (24°, 37°, 55°, 75°, 87° and 95°C) according to the used temperatures for secondary structure probing. (D) 6S RNA 132-nt:pRNA (15-mer) hybrid structure prediction at different temperatures (24°, 37°, 55°, 75°, 87° and 95°C) according to the used temperatures for secondary structure probing. The pRNA binding site is indicated by an orange line.

Pb^{2+} probing of the 132-nt variant was performed at room temperature, 37°, 55° and 75°C to get information about the temperature dependent structural dynamics of the central bulge region of this thermostable 6S RNA. Probing experiments were conducted with 5'- and 3'-^{32}P-labeled RNAs to achieve high resolution cleavage patterns over the entire molecule length. Alkaline hydrolysis and RNase T1 cleavage under partially denaturing conditions served as ladders for cleavage site assignment.

At room temperature (~24°C), probing of the 85-nt variant revealed pronounced accessibility to Pb^{2+}-induced hydrolysis at positions 9-12, ~19-26, to a minor extent at nt 27, and 30-34 (Figure 4. 11 A, lane 2), as well as at positions 55-61, 64-68 and, to a minor extent, at nt 76 and 79-81 (Figure 4. 11 B, lane 2). Cleavage by RNase T1 under native conditions (Figure 4. 11, panel A, lane 6, and panel B, lane 5) revealed accessibility of G25, G31, G43/44, G63, and G68, in line with the Pb^{2+} hydrolysis data. RNase V1 cleavage of the 3'-^{32}P-labeled 85-nt variant (Figure 4. 11, B, lane 8) suggested helical structures in the region of approx. nt 36-40, 48-51, 55-58, 69-75 and 79/80, in accordance with the MFE and the open bulge structure (except for the stretch of nt 55-58; Figure 4. 12 A and B). In conclusion, hydrolysis patterns for the 85-nt variant are consistent with the MFE structure (Figure 4. 10 A) being in equilibrium with an open central bulge structure at room temperature, as illustrated in Figure 4. 12. It is thus expected that the open central bulge structure will dominate at temperatures closer to the natural growth temperature of *A. aeolicus*.

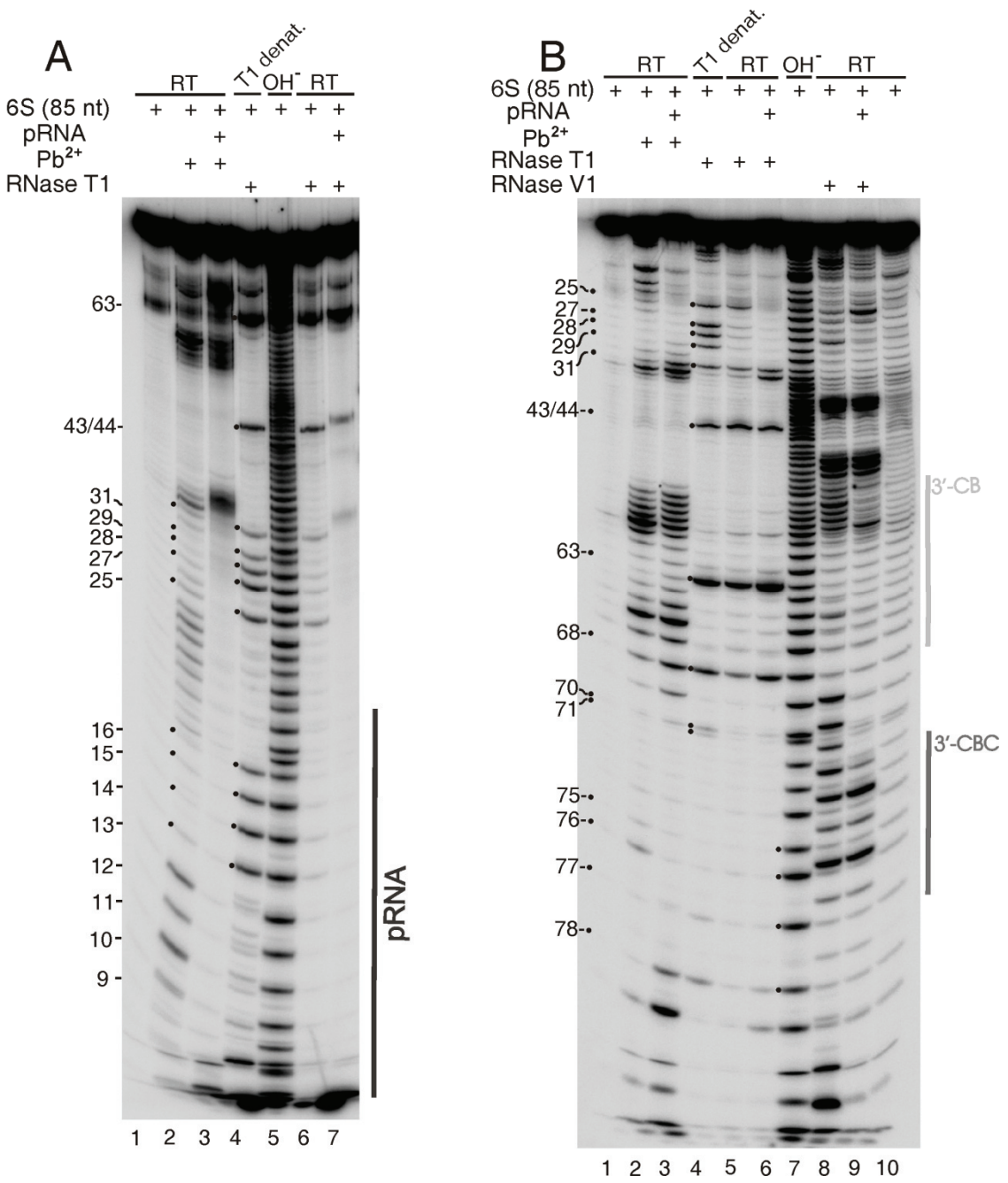

Figure 4. 11 Secondary structure probing of *A. aeolicus* 6S RNA (85 nt). (A) Structural probing of 6S RNA with trace amounts of 5'-endlabelled 6S RNA Lane 1: 9 µM 6S RNA was subjected to the annealing procedure in 5 µL 1x TN buffer and loaded onto the gel; lane 2 and 3: 9 µM 6S RNA without (lane 2) or with 50 µM pRNA 15-mer (lane 3) was subjected to the annealing procedure in 5 µL 1x TN buffer before lead probing at room temperature; lane 4: limited RNase T1 digestion under high temperature conditions (T1 ladder); lane 5: alkaline hydrolysis ladder of 6S RNA (85 nt);lane 6 and 7: 9 µM 6S RNA without (lane 6) or with 50 µM pRNA 15-mer (lane 7) was subjected to the annealing procedure in 5 µL 1x TN buffer before limited RNase T1 digestion at room temperature. (B) Structural probing using trace amounts of 3'-endlabelled 6S RNA. Lane 1: 9 µM 6S RNA was subjected to the annealing procedure in 5 µL 1x TN buffer and loaded onto the gel; lane 2 and 3: 9 µM 6S RNA without (lane 2) or with 50 µM pRNA 15-mer (lane 3) was subjected to the annealing procedure in 5 µL 1x TN buffer before lead probing at room temperature; lane 4: limited RNase T1 digestion under high temperature conditions (T1 ladder); lane 5 and 6: 9 µM 6S RNA without (lane 5) or with 50 µM pRNA 15-mer (lane 6) was subjected to the annealing procedure in 5 µL 1x TN buffer before limited RNase T1 digestion at room temperature; lane 7: alkaline hydrolysis ladder of 6S RNA (85 nt); lane 8 and 9: 9 µM 6S RNA without (lane 8) or with 50 µM pRNA 15-mer (lane 9) was subjected to the

annealing procedure in 5 µL 1x TN buffer before limited RNase V1 digestion at room temperature (Mg^{2+} added after annealing procedure); lane 10: 9 µM 6S RNA was subjected to the annealing procedure in 5 µL 1x TN buffer (Mg^{2+} added after annealing procedure) and loaded onto the gel (15% PAA, 8 M urea).

In parallel, we probed the structure of the 85-nt 6S RNA variant after annealing of a pRNA-15-mer. The 15-mer, representing the longest pRNA read found by dRNA-seq (Figure 4. 9), was used here to maximize duplex stability with 6S RNA to persistently rearrange the RNA's structure. After pRNA annealing, the following changes in the probing patterns were observed: the entire region from nt 8 to 29 as well as nt 76 became protected from Pb^{2+} cleavage, whereas nt 31-33, the region comprising nt 64-69, and nt 78-81 became more exposed to Pb^{2+}-induced hydrolysis (Figure 4. 11 A, B, lanes 3 vs. 2). Key changes in the RNase T1 cleavage pattern included the protection of G25 to G29 and increased accessibilities of G63, G68 and G78 (Figure 4. 11 B, lanes 6 vs. 5). Annealing of the pRNA 15-mer reduced RNase V1 cleavage in the regions of nt 54-58 and 69-72, whereas cleavage at nt 25 was enhanced (Figure 4. 11 B, lanes 9 vs. 8). These pRNA-induced changes in the hydrolysis patterns are consistent with the structural rearrangement shown in Fig. Figure 4. 12 C. The hallmark of the rearranged structure is the formation of a helix between the 5'- and the 3'-central bulge, termed central bulge collapse helix (CBC helix, nt 24-29/72-77). `RNAfold` analysis (Figure 4. 10 B) also predicts C23 and G78 to base-pair as part of the CBC helix. As we saw some accessibility of nt 78 to Pb^{2+} and RNase T1 hydrolysis (e.g. Figure 4. 11 B, lane 3), we propose some fraying of this terminal bp and have thus indicated it as unpaired in Figure 4. 12 C. The same essentially pertains to the 132-nt variant described in the following.

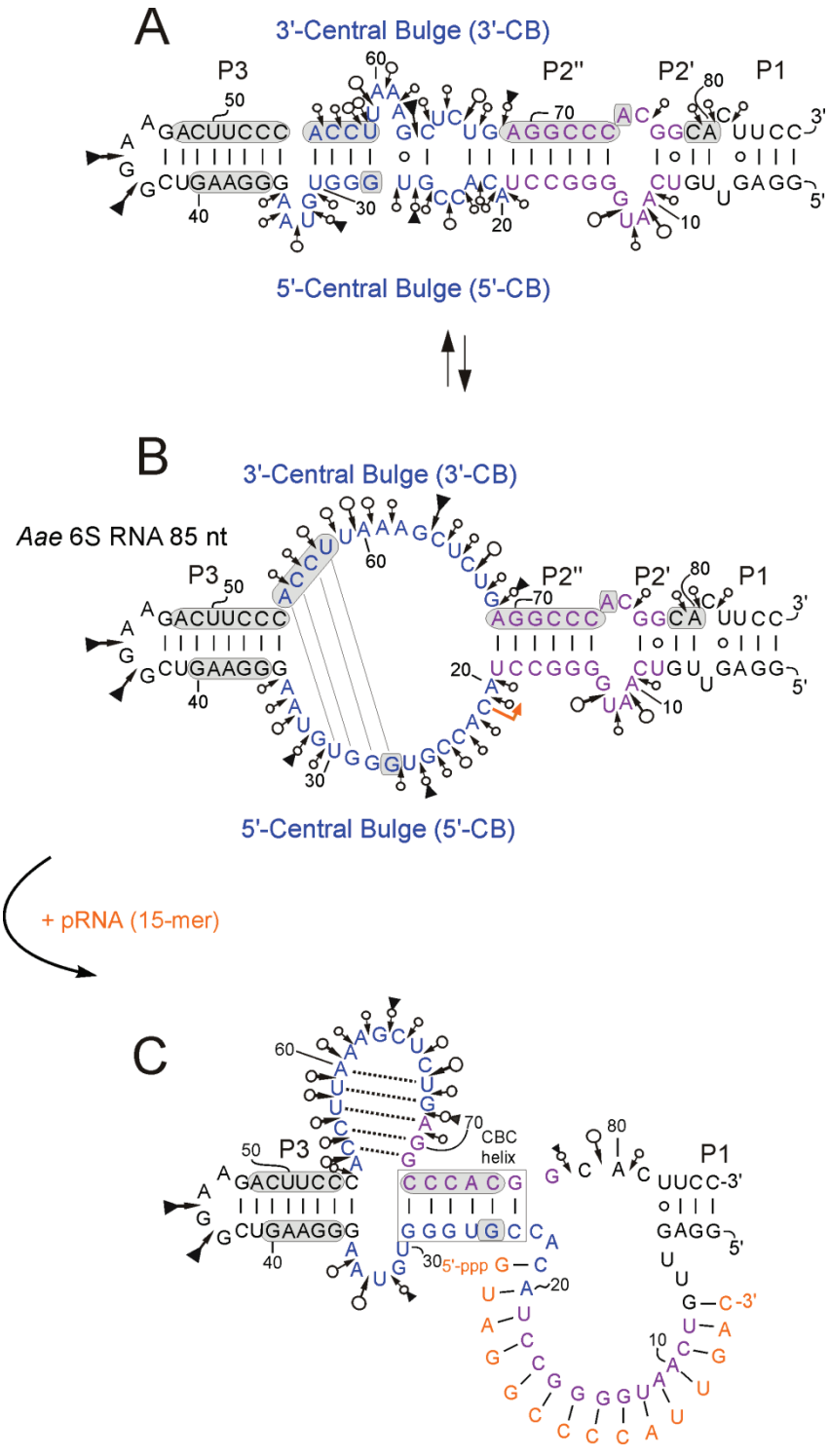

Figure 4. 12 Two dimensional *A. aeolicus* 6S RNA (85 nt) model structures. The 5'-CB and the 3'-CB (central bulge) is illustrated in royal blue. The P2'' and P2' helix marked in magenta become unwind during pRNA transcription. The orange arrow indicates the pRNA transcription starting nucleotide. Pb^{2+} cleavage is indicated by open circles whereas the different sizes are according to the accessibilities of the certain nucleotides. RNase T1 cleavage is marked by filles triangles with different sizes according to the accessibilities of the certain nucleotides. RNase V1 cleavage is illustrated with the light gray elliptic frames (A) The more protected MFE (minimum free energy) structure (top) is shown in balance with (B) the model of 6S RNA (85 nt) in the open bulge form (middle). (C) Model of the pRNA-induced structural rearrangement of the 6S RNA (85 nt) core region (bottom). The structural

rearrangement can be induced by the binding of the pRNA 15-mer (orange letters). The CBC helix (central bulge collapse helix) is annotated by the black box shown after the rearrangement. The exact orientation of the helical elements after the rearrangement is unknown.

Probing of the 132-nt variant of *A. aeolicus* 6S RNA at room temperature, with and without pRNA annealing, resulted in cleavage patterns consistent with those obtained for the 85-nt variant. Nucleotide 42, the region of nt 98-107 and nt 115/116 became more accessible to Pb^{2+} and RNase T1 cleavage (Figure 4. 13, panel A, lanes 1, 2, 4 and 5; panel B, lanes 2, 3, 5 and 6) upon pRNA annealing. Under the same conditions, RNase V1 showed increased cleavage at nt 37/38 and 110-112, supporting the formation of the CBC helix, and decreased hydrolysis in the pRNA:6S RNA duplex region around nt 30 (Figure 4. 13, panel A, lanes 7 and 8; panel B, lanes 8 and 9).

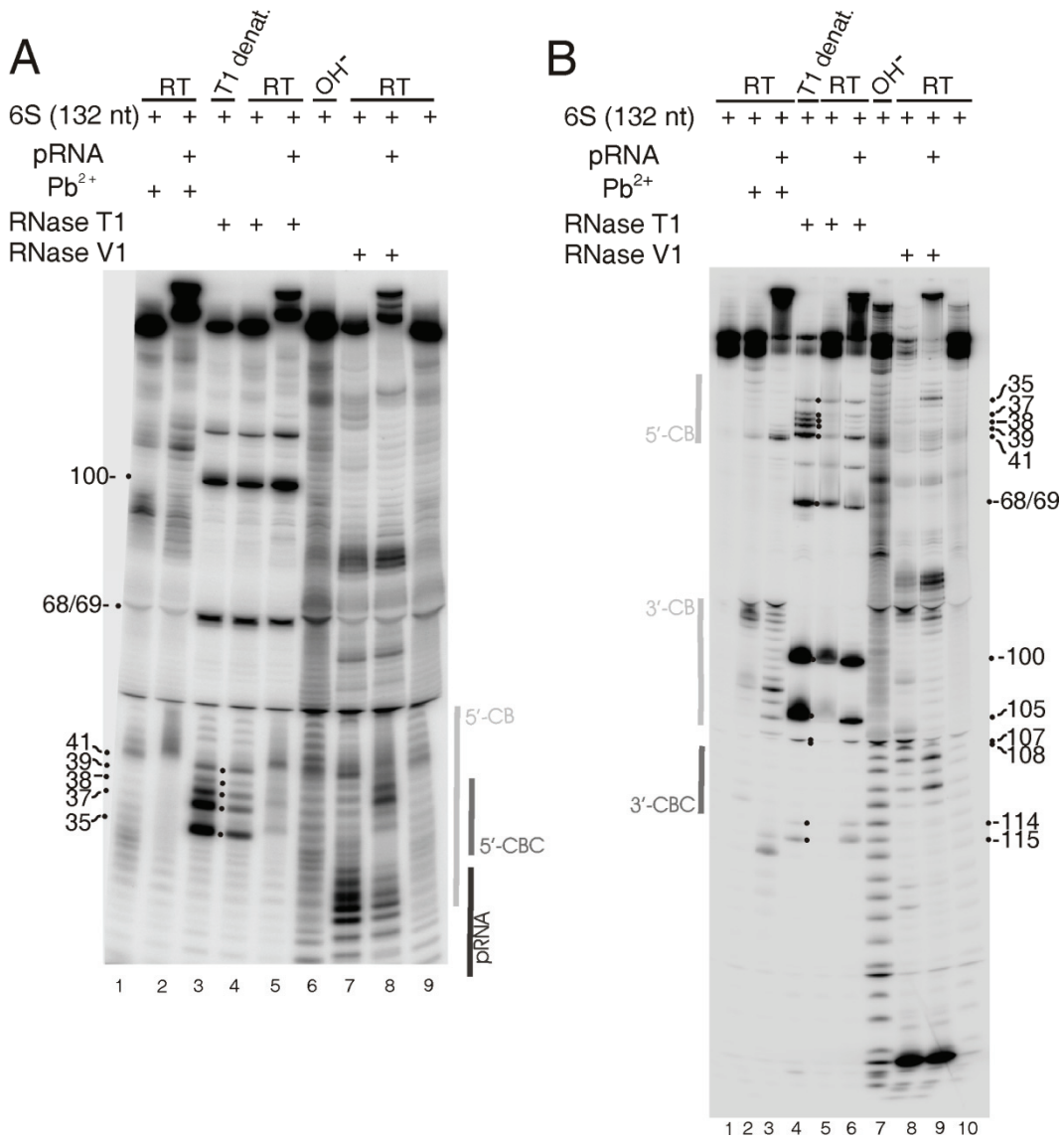

Figure 4. 13 Secondary structure probing of *A. aeolicus* 6S RNA (132 nt). (A) Structural probing using trace amounts of 5'-endlabelled 6S RNA Lane 1 and 2: 9 µM 6S RNA without (lane 1) or with 50 µM pRNA 15-mer (lane 2) was subjected to the annealing procedure in 5 µL 1x TN buffer before lead probing at room temperature; lane 3: limited RNase T1 digestion under high temperature conditions (T1 ladder); lane 4 and 5: 9 µM 6S RNA without (lane 4) or with 50 µM pRNA 15-mer (lane 5) was subjected to the annealing procedure in 5 µL 1x TN buffer before limited RNase T1 digestion at room temperature; lane 6: alkaline hydrolysis ladder of 6S RNA (132 nt); lane 7 and 8: 9 µM 6S RNA without (lane 7) or with 50 µM pRNA 15-mer (lane 8) was subjected to the annealing procedure in 5 µL 1x TN buffer before limited RNase V1 digestion at room temperature (Mg^{2+} added after annealing procedure); lane 9: 9 µM 6S RNA was subjected to the annealing procedure in 5 µL 1x TN buffer (Mg^{2+} added after annealing procedure) and loaded onto the gel (15% PAA, 8 M urea). (B) Structural probing using trace amounts of 3'-endlabelled 6S RNA (132 nt). Lane 1: 9 µM 6S RNA was subjected to the annealing procedure in 5 µL 1x TN buffer and loaded onto the gel; lanes 2 -10 correspond to lanes 1-9 in (A).

At the probing temperatures of 37° and 55° (Figure 4. 14), the Pb^{2+} cleavage pattern did not change significantly relative to room temperature. Little overall cleavage was

observed at 75°C, possibly owing to decreased RNA binding affinity of Pb^{2+} ions at this temperature. The patterns at 37°C and 55°C confirmed the rearranged structure in Figure 4. 15 C: pRNA annealing enhanced Pb^{2+}-induced hydrolysis around nt 15/16, 41-43, 103-107, 115/116, whereas protection was observed at nt 19-24 (pRNA binding region) and approx. 30-37 (including the CBC helix) (Figure 4. 14, panels A and B, lanes 1-6). Noteworthy, retarded gel mobility of the full-length RNA (Figure 4. 14 B, lanes 3, 6 and 9) indicates that the pRNA 15-mer remained stably attached to the 132-nt 6S RNA despite probing temperatures of up to 75°C, sample heating at 95°C in 2x PPF loading buffer and denaturing PAGE. This supports the notion that a tightly bound *A. aeolicus* pRNA 15-mer is able to induce the structural rearrangement even under high temperature (≥ 80°C) conditions.

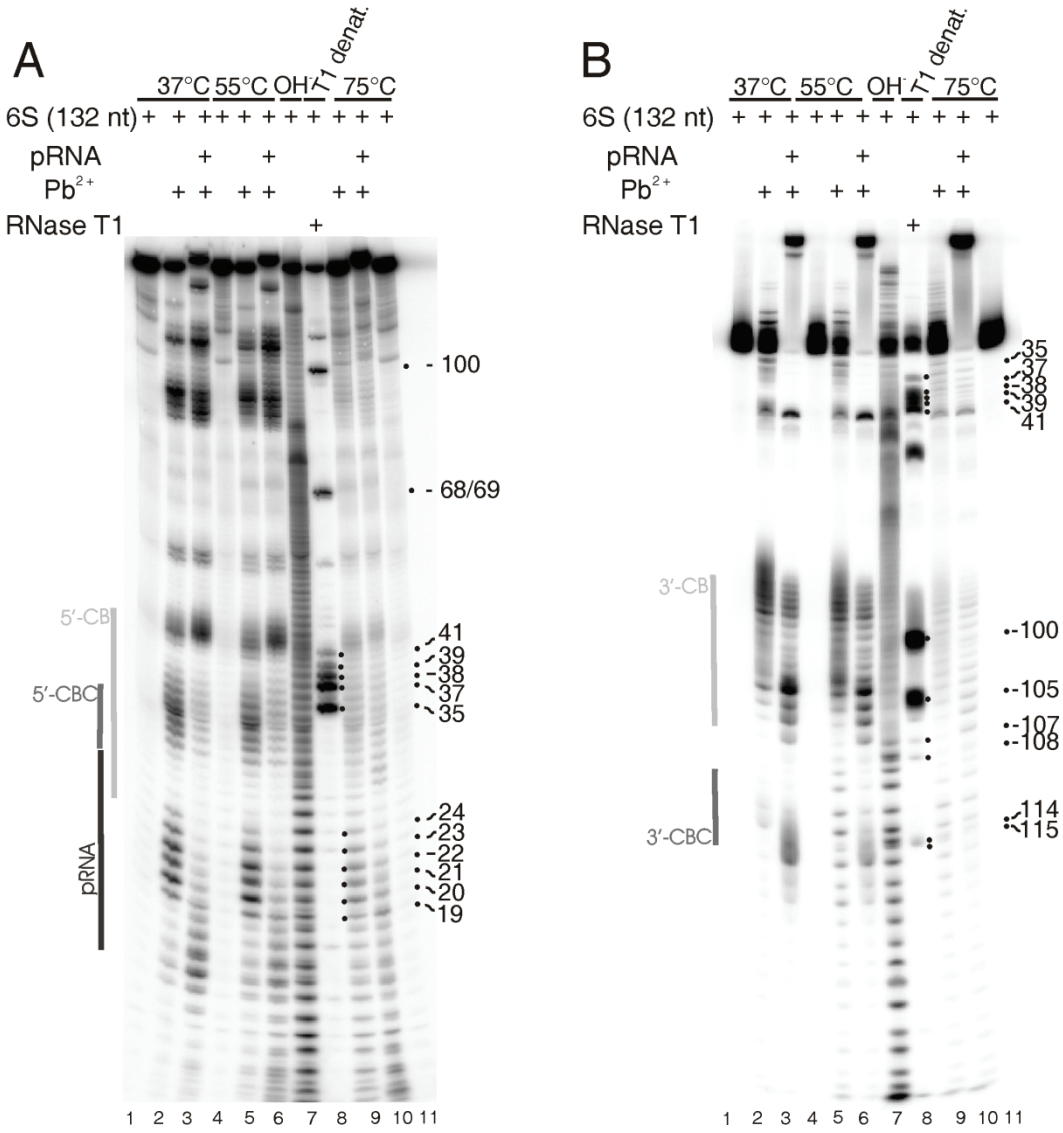

Figure 4. 14 Secondary structure probing of *A. aeolicus* 6S RNA (132 nt) with Pb^{2+} ions at different temperatures. (A) Structural probing using trace amounts of 5'-endlabelled 6S RNA. Lane 1, 4 and 11: 9 µM 6S RNA was subjected to the annealing procedure in 5 µL 1x TN buffer and incubated at 37°C for 4' (lane 1), 55°C for 1'(lane 4) and 75°C for 1' (lane 11); lane 2, 5 and 9: 9 µM 6S RNA was subjected to the annealing procedure in 5 µL 1x TN buffer before lead probing at 37°C for 4' (lane 2), 55°C for

1'(lane 5) and 75°C for 1' (lane 9); lane 3, 6 and 10: 9 µM 6S RNA with 50 µM pRNA 15-mer were subjected to the annealing procedure in 5 µL 1x TN buffer before lead probing at 37°C for 4' (lane 3), 55°C for 1'(lane 6) and 75°C for 1' (lane 10); lane 7: alkaline hydrolysis ladder of 6S RNA (132 nt); lane 8: limited RNase T1 digestion under high temperature conditions (T1 ladder)(15% PAA, 8 M urea). (B) Structural probing using trace amounts of 3'-endlabelled 6S RNA. Lanes 1-11 correspond to lanes 1-11 in (A).

Besides the probing results that confirmed the *A. aeolicus* 6S RNA structure prediction (RNAfold), several differences were observed (Figure 4. 10). For the free 85-nt and 132-nt RNAs, formation of a hairpin in the 3'-CB is predicted at room temperature (indicated by dotted lines in Figure 4. 12 and Figure 4. 15), but not at higher temperatures. However, when the pRNA binding site was blocked for intramolecular base-pairing in RNAfold predictions, formation of this hairpin was predicted at temperatures of up to 75°C (Figure 4. 10 B). In this hairpin, nt 56-60/67-71 of the 85-nt 6S variant would be base-paired. In contrast, nt 56-60 were accessible to Pb^{2+} hydrolysis in the free and pRNA hybrid structure (Figure 4. 11, lanes 2 and 3), and G68 even showed enhanced RNase T1 susceptibility after pRNA annealing (Figure 4. 11 B, lanes 5 and 6). For the 132-nt variant, nt 93-97/104-108 should be base-paired when the hairpin is formed. However, nt 105 was even more accessible to Pb^{2+} and RNase T1 hydrolysis upon pRNA annealing (Figure 4. 13 B, lanes 2, 3, 5 and 6; Figure 4. 14 B, lanes 2 and 3). These findings argue against formation of this hairpin in the 3'-CB region of the rearranged structure, in contrast to the shown RNAfold predictions (Figure 4. 10) and previous suggestions [Beckmann, Hoch *et al*., 2012].

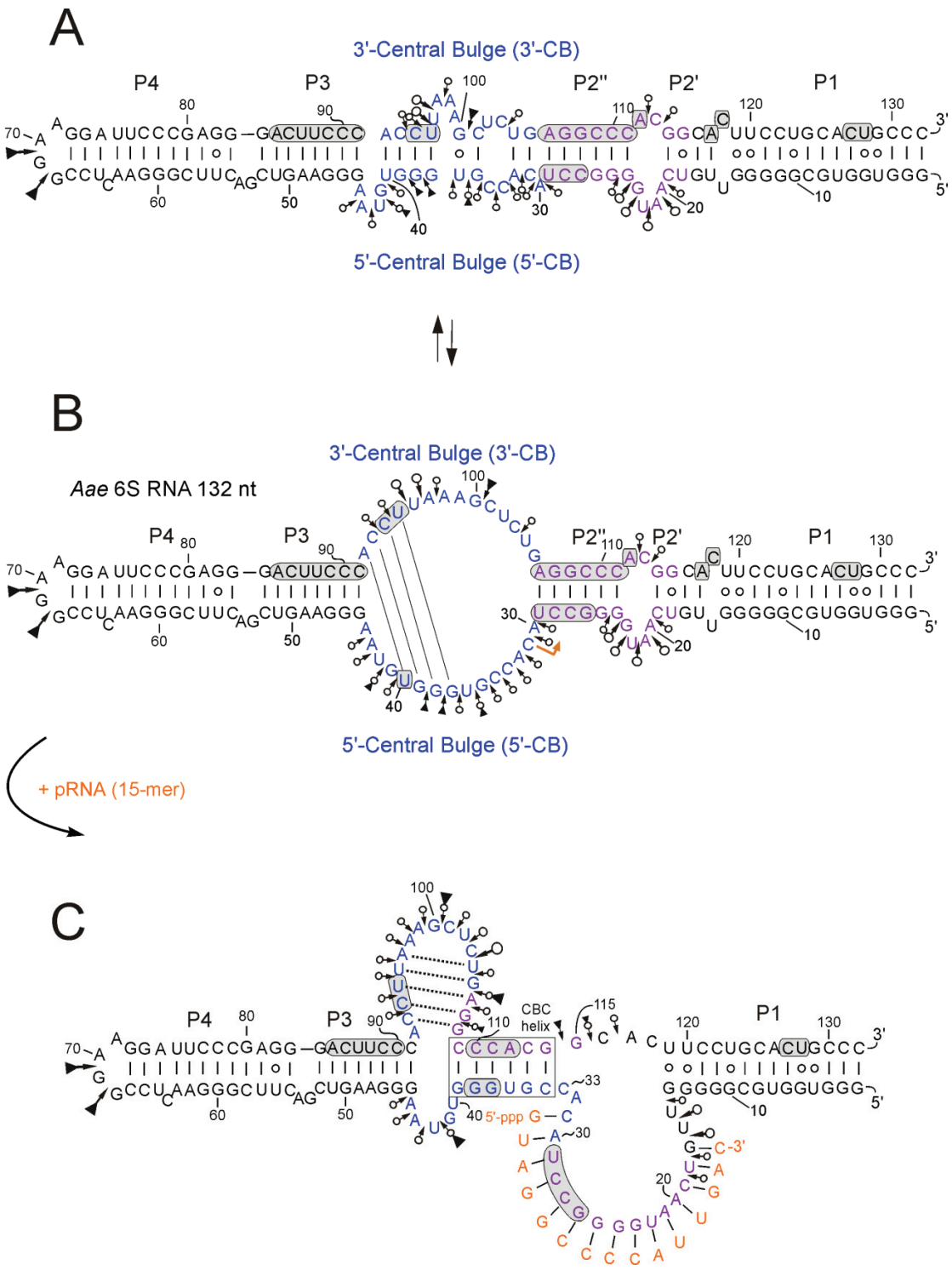

Figure 4. 15 Two dimensional *A. aeolicus* 6S RNA (132 nt) model structures. The 5'-CB and the 3'-CB (central bulge) is illustrated in royal blue. The P2'' and P2' helix marked in magenta become unwind during pRNA transcription. The orange arrow indicates the pRNA transcription starting nucleotide. Pb^{2+} cleavage is indicated by open circles whereas the different sizes are according to the accessibilities of the certain nucleotides. RNase T1 cleavage is marked by filles triangles with different sizes according to the accessibilities of the certain nucleotides. RNase V1 cleavage is illustrated with the light gray elliptic frames (A) The more protected MFE (minimum free energy) structure (top) is shown in balance with (B) the model of 6S RNA (85 nt) in the open bulge form (middle). (C) Model of the pRNA-induced structural rearrangement of the 6S RNA (85 nt) core region (bottom). The structural rearrangement can be induced by the binding of the pRNA 15-mer (orange letters). The CBC helix

(central bulge collapse helix) is annotated by the black box shown after the rearrangement. The exact orientation of the helical elements after the rearrangement is unknown.

We conclude that the pRNA-induced structural rearrangement of *A. aeolicus* 6S RNA involves formation of the CBC helix in addition to the 6S RNA:pRNA hybrid helix, in keeping with `RNAfold` predicting the CBC helix at all temperatures of up to 95°C (Figure 4. 10 B and D).

4.1.11. Secondary structure analysis via NMR

Nuclear magnetic resonance (NMR) spectroscopy is another and direct method to investigate the secondary structure as well as potential tertiary hydrogen bonding interactions of RNA molecules in solution. A special feature of proton NMR measurements is that only stable base-pairings are detectable (sufficiently low proton exchange with bulk water). A potential disadvantage of NMR is the requirement for high RNA sample concentrations (~ 0.5 mM) which may result in artificial interactions between individual RNA molecules.

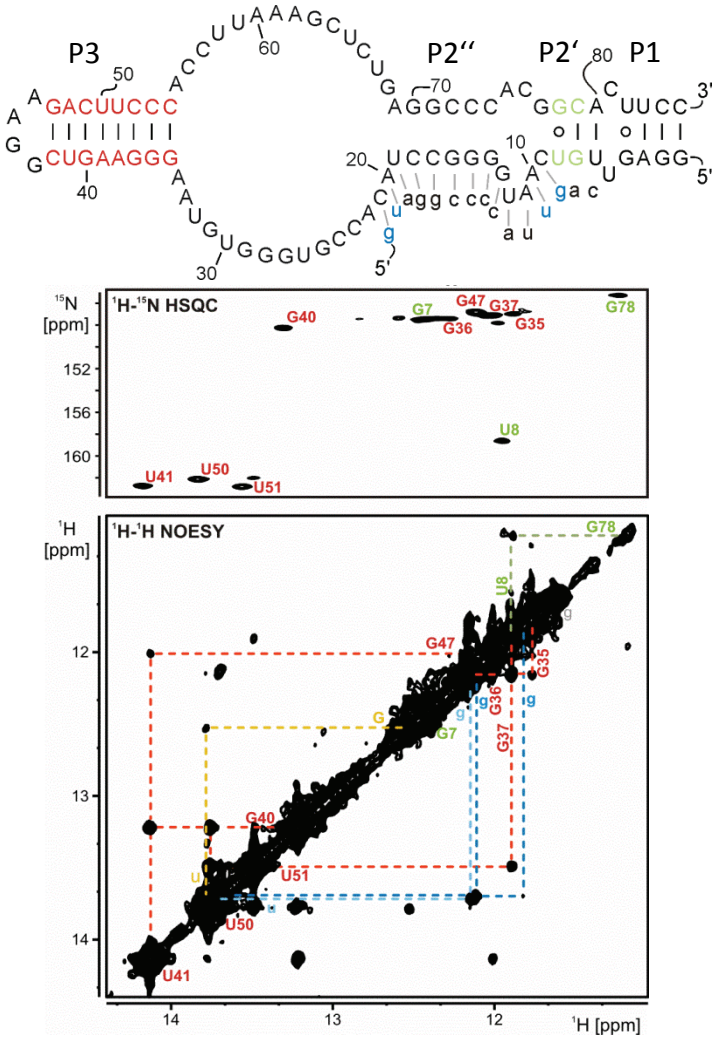

Figure 4. 16 Structural analysis of the 6S RNA 85-nt variant using NMR. Top: Predicted stable base-pairing interactions in the 85-nt 6S RNA variant. Structural elements that can be identified in the NMR spectra are highlighted in different colors according to the assignment in the spectra. Middle and bottom: ^{1}H,^{15}N-HSQC imino spectrum (middle) and ^{1}H,^{1}H-NOESY spectrum (bottom) of ^{15}N-labeled 6S RNA hybridized to an unlabeled pRNA 15-mer specified in the sketch at the top. Base pair type-specific regions for the G and U imino groups are indicated. Assignments are given and colored according to the color scheme given in the secondary structure. In the NOESY spectrum sequential assignments are indicated by dashed lines connecting the respective imino resonances via the NOE cross peaks.

In the ^{1}H,^{15}N-HSQC spectrum (Figure 4. 17, middle) we detected imino groups with characteristic ^{1}H and ^{15}N resonance frequencies, which demonstrate the presence of 4 stable Watson-Crick A:U base pairs, 12 stable Watson-Crick G:C base pairs and 4 stable non-canonical G:U base pairs in the free RNA. The distance information from a ^{1}H,^{1}H-NOESY spectrum of the 6S RNA 132-nt variant (Figure 4. 17, bottom) together with the ^{1}H,^{15}N-HSQC and a ^{1}H,^{1}H-NOESY spectrum of the truncated 85-nt 6S RNA variant in its free state allowed the assignment of all detected A:U and G:U base pairs as well as 6 out of the 12 G:C base pairs (Figure 4. 17, top). Assignment of the remaining G imino resonances is likely disabled by their small spectral dispersion leading to cross peaks close to the diagonal in the ^{1}H,^{1}H NOESY spectrum. The

predicted MFE structure of the 132-nt 6S RNA at 37°C shows some base-pairing between the 5'- and 3'-portion of the central bulge, including 2 G:U pairs (Figure 4. 9 C; Figure 4.14 A). The absence of additional U imino resonances suggest that base-pairing in the CB is not stable enough to be detected by NMR spectroscopy. In addition, also the region between base pairs G11:C122 to U16:A117 appears to be destabilized, since no additional imino resonances of stable G:U or A:U base pairs appeared in the spectrum. Thus, the region between base pairs G24:C111 to U28:A106, which is predicted to be base-paired in the free 6S RNA while its 5'-strand is hybridized to the pRNA in the rearranged state, likely provides the identity of at least 5 of the 6 unassigned G imino resonances. Formation of a hairpin within the 3'-central bulge region of 6S RNA after the pRNA-induced structural rearrangement (dotted lines in Figure 4. 15), as predicted *in silico* (Figure 4. 10 B and D; [Beckmann, Hoch *et al*, 2012]), is not supported by the NMR data. The stem of this hairpin, which is composed of three G-C and two A-U base pairs, would give rise to additional Watson-Crick type U imino resonances, which were, however, not detected in the $^{1}H,^{15}N$-HSQC spectrum. This does not entirely exclude that hairpin formation occurred transiently involving conformational transitions between a structured and unstructured state. However, in this case, one would at best expect broadened imino resonances, as hydrogen bonding needs to be sufficiently protected from solvent exchange to remain detectable by NMR. However, the absence of corresponding imino resonances suggests that the hairpin is too volatile or not formed at all, which is consistent with its low predicted stability (-2.8 kcal/mol for the MFE structure predicted by `RNAfold` using the default parameters).

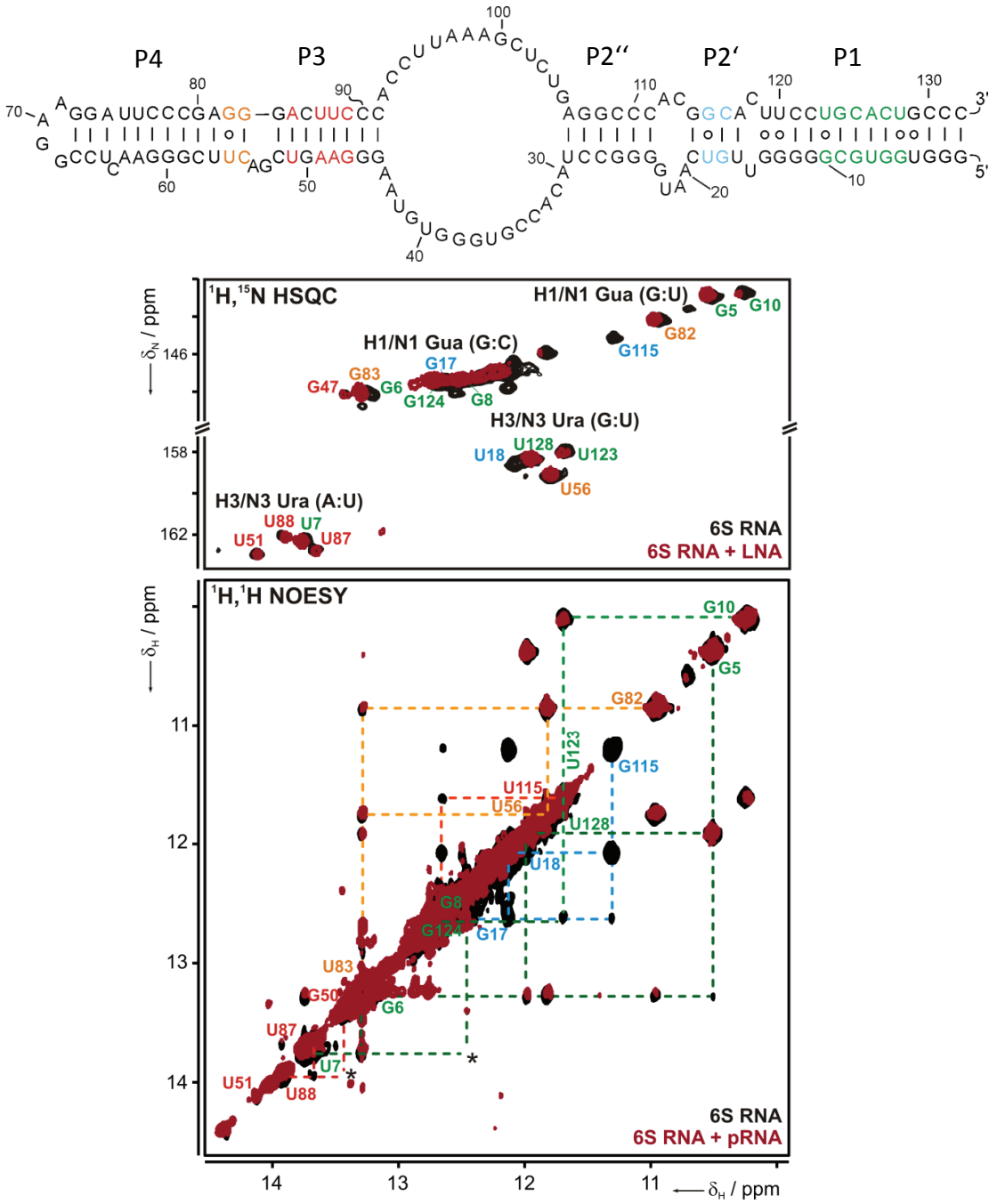

Figure 4. 17 NMR analysis of the *A. aeolicus* 132-nt 6S RNA variant. Top: Predicted secondary structure of the RNA. Structural elements assignable in the NMR spectra are highlighted in different colors according to the assignment in the spectra. Middle and bottom: ^{1}H,^{15}N-HSQC imino spectra (middle) and ^{1}H,^{1}H-NOESY spectra (bottom) of the ^{15}N labeled free 6S RNA (black) and ^{15}N-labeled 6S RNA hybridized to an unlabeled pRNA 15-mer (red signals) specified in the sketch at the top. Base pair type-specific regions for the G and U imino groups are indicated. Base assignments are given and colored according to the color scheme shown in the secondary structure. In the NOESY spectrum, sequential assignments are indicated by dashed lines connecting the respective imino resonances via the NOE cross peaks. *Cross peak visible at lower threshold as displayed.

In order to stably detect the changes in 6S RNA structure upon interaction with maximum resolution and specificity, ^{15}N isotope-labeled 6S RNA was hybridized to an all-LNA analog of the pRNA 15-mer (synthesized by RiboTask, Odense, Denmark).

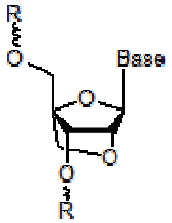

Figure 4. 18 Illustration of a locked nucleic acid (LNA) modification that locks the sugar in the C3'-*endo* conformation via an extra methylene group bridging the O2' and C4' atoms.

LNA residues (Figure 4. 18) lock the sugar moiety in the C3'-*endo* conformation that is typical of RNA-like A-helices. This preorganizes the backbone for base-pairing with RNA and stabilizes stacking interactions, which in turn substantially increases duplex melting temperatures [Kaur *et al*., 2006; Grünweller and Hartmann, 2007].

In addition, a $^{1}H,^{1}H$-NOESY spectrum was obtained for unlabeled 132-nt 6S RNA:pRNA complexes. Comparison with the spectrum of the free 132-nt 6S RNA revealed that structural changes upon pRNA hybridization are confined to the central bulge region and nucleotides in its immediate vicinity. Accordingly, the U18:G115 base pair vanishes in agreement with local unwinding of helices P2' and P2'' upon pRNA hybridization (Figure 4. 15). The assigned stem region between G5 and G10 is still present in the 6S RNA:pRNA duplex, demonstrating that the terminal 6S RNA stem (P1) is not unwound upon annealing of a pRNA 15-mer. Helix P3 flanking the central bulge (G47 to U51) gives rise to similar resonances in free 6S RNA and 6S RNA:pRNA duplexes, supporting the notion that this arm of the 6S RNA is not affected by the pRNA-induced rearrangement. Compared to free 6S RNA, about five unassigned G imino resonances of WC base pairs disappear or decrease in intensity in the 6S RNA:pRNA duplex structure. One explanation for the disappearance of three of these signals is that they belong to G residues in the region between A106 and C116, which are predicted to be base-paired to residues C19, C26 and C27 in free 6S RNA (Figure 4. 17). In 6S RNA:pRNA/pLNA 15-mer complexes, residues 17 to 31 of 6S RNA pair with pRNA/pLNA, which concomitantly displaces the stretch of nt A106 to A117, of which nt 109 to 114 become engaged in forming the CBC helix, as inferred from the probing experiments (Figure 4. 15 C). As the CBC helix was not observed by NMR, we conclude that it is relatively unstable, at least under NMR measurement conditions. In summary, our NMR analyses have identified stem regions on both sides of the central bulge that are particularly stable (Figure 4. 17, colored nt in the secondary structure at the top), thus providing a structural framework for the rod-shaped *A. aeolicus* 6S RNA architecture at elevated temperatures.

Simultaneously, formation of the CBC helix appears as a more dynamic or fine-tuning mechanistic element in the pRNA-induced rearrangement that leads to dissociation of 6S RNA:RNAP complexes. Nevertheless, formation of the CBC helix may well influence the pRNA length pattern and the kinetics and directionality of the structural rearrangement.

4.1.12. pRNA:6S RNA shift experiments

The synthesis of pRNAs of different length *in vivo*, as suggested by our RNA-seq data (Figure 4. 9), raised the question of the minimal pRNA length that confers sufficient stability to form gel-resolvable 6S RNA:pRNA hybrids. To address this, we used chemically synthesized length variants of the pRNA, lacking up to 7 nucleotides from the 3'-end of the reference pRNA 15-mer. These pRNA oligonucleotides were hybridized at different concentrations to one of the 5'-endlabeled 6S RNA variants and then subjected to native PAGE analysis (Figure 4. 19 A and B). For the 85-nt variant, a pRNA 8-mer failed to persistently change the structure at a 1 to 5-molar excess over 6S RNA (10 µM), whereas pRNAs of ≥ 9 nt completely rearranged the structure (as inferred from reduced gel mobility) already at a 1:1 molar ratio (Figure 4. 19 A). A different picture emerged for the 132-nt variant. Here, only the pRNA 10-mer was able to shift the 6S RNA structure, but in a concentration-dependent manner, with little 6S RNA:pRNA complex formation at a 1:1 molar ratio, but > 90% complex formation at a 5:1 ratio (Figure 4. 19 B). Only partial 132-nt 6S RNA:pRNA complex formation was also seen for the longer pRNAs (> 10-mers) at lower molar ratios, and even for the 15-mer at a ratio of 1:1. The results demonstrate that pRNA annealing to 6S RNA is energetically more unfavorable in the context of the structurally more rigid 132-nt RNA that is closely related to the native *A. aeolicus* 6S RNA. An explanation could be that pRNA binding may disrupt the terminal helix of the 85-nt variant, such that the pRNA-bound structure is less constrained and better accessible for pRNA rebinding after transient dissociation in cages of the gel matrix relative to the corresponding 132-nt 6S RNA:pRNA complexes. This also raises the question as to which pRNA length is required *in vivo* to persistently rearrange *A. aeolicus* 6S RNAs for RNAP release at growth temperatures of typically 85°C. As an *A. aeolicus* pRNA 9-mer forms already 7 G-C base pairs with 6S RNA, while a 13- or 14-mer forms only one more G-C bp, a 9-mer may be sufficient to rearrange the structure such that the sigma factor is released as shown for a pRNA 9-mer in the *E. coli* system (Unrau, 2012), also taking into account that RNAP:6S RNA interactions may be weaker at 85°C than in mesophilic bacteria at 37°C.

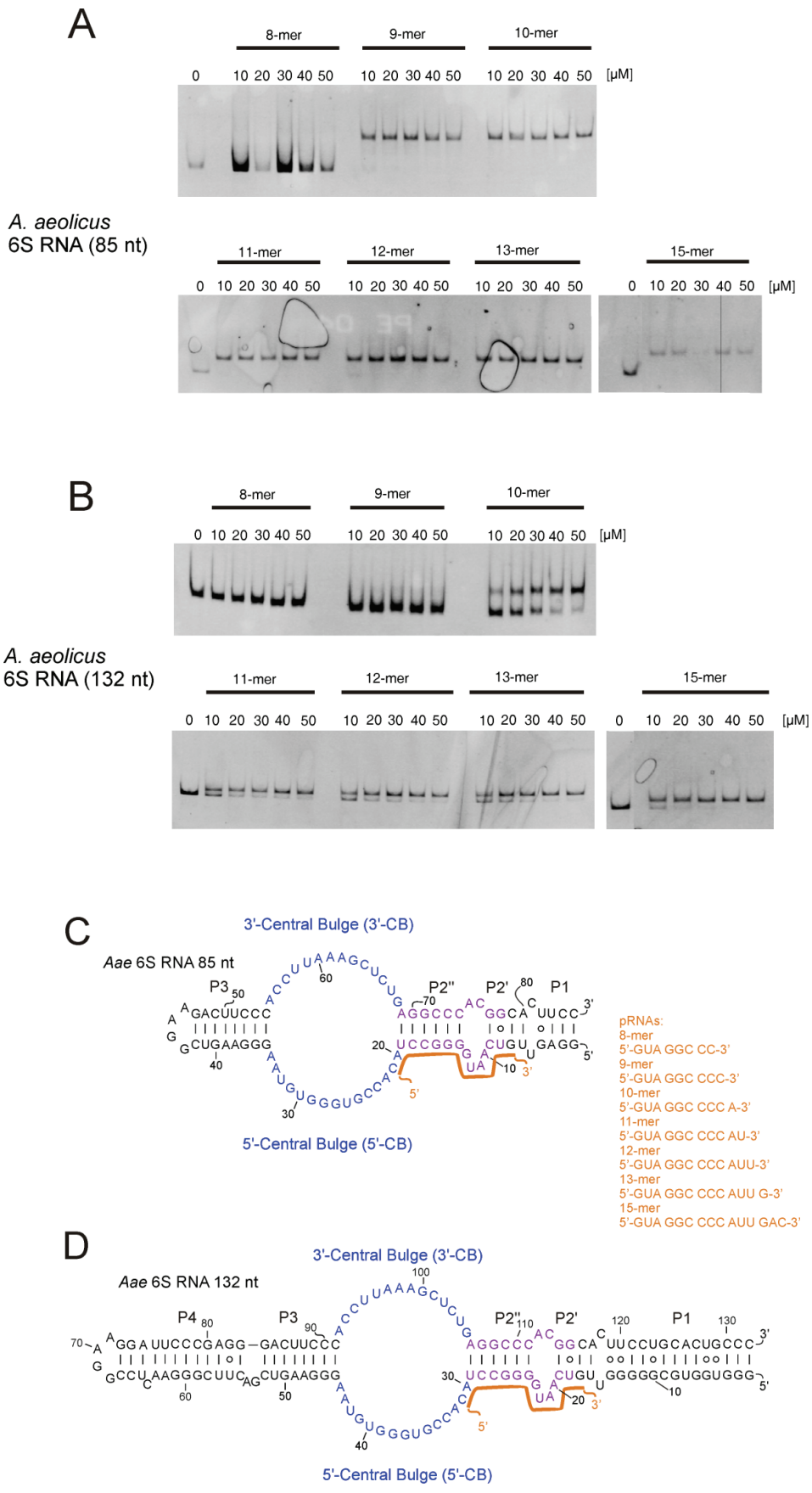

Figure 4. 19 Electrophoretic mobility shift assay (EMSA) to detect pRNA-induced structural changes in 6S RNA (85 nt and 132 nt). (A) 10 μM 6S RNA (85 nt), containing trace amounts of the same 5'-endlabeled 6S RNA, was subjected alone (lanes 0) or in the presence of 10, 20, 30, 40 or 50 μM

pRNA (8 to 15-mers, specified in panel C) to the annealing procedure 1x hybridization buffer (see Materials and Methods). After pRNA annealing, samples were mixed with 2x native loading buffer and directly loaded onto a 10% native PAA gel. (B) As in panel A, but using the 132-nt 6S RNA variant. (C) Open central bulge structure of the 85-nt 6S RNA (left). Nucleotides of the central bulge region are indicated in blue, those of the P2' and P2'' helix disrupted upon pRNA annealing in magenta. The binding site for the longest pRNA 15-mer is marked by the orange line. On the right, the different pRNA length variants (8 to 15-mers) are displayed. (D) Secondary structure of the 132-nt 6S RNA with coloring as described in (C).

4.1.13. *In vitro* transcription of pRNAs from *A. aeolicus* 6S RNA

After we had proven by RNA-seq analysis (chapter 4.1.9) that pRNA transcription takes place in *A. aeolicus* cells, we wanted to investigate if our 85-nt and 132-nt 6S RNA variants serve as templates for *in vitro* transcription. Since the homologous *A. aeolicus* RNAP has not been available we fell back on the well examined RNA polymerase of *B. subtilis*. This decision was also favored by the observation that pRNAs synthesized from *A. aeolicus* 6S RNA and *B. subtilis* 6S-1 RNA are both initiated with G residues (Figure 4. 9; Beckmann *et al*., 2011). No significant pRNA synthesis by *B. subtilis* σ^A-RNAP was seen with the 85-nt variant as template, likely because this truncated 6S RNA bound with low affinity and specificity to σ^A-RNAP. In contrast, pRNA transcripts were obtained with the 132-nt 6S RNA variant, either synthesized in the presence of α-^{32}P-UTP, α-^{32}P-CTP and γ-^{32}P-GTP for detection. Under the applied assay conditions (200 µM of each NTPs, 1 µM σ^A-RNAP, 10 µM 132-nt 6S RNA), predominantly 15 to 17-meric pRNAs but also run off transcripts were observed (Figure 4. 20). Shorter pRNAs (< 8 nt) were seen as well for samples containing α-^{32}P UTP and γ-^{32}P-GTP, but not for those containing α-^{32}P-CTP. This is attributable to the first C residue being incorporated at position 6 of *A. aeolicus* pRNA (Figure 4. 19 C), such that only pRNA 6-mers or longer ones are radiolabeled in the presence of α-^{32}P-CTP, whereas already 2-mers are labeled in the presence of α-^{32}P-UTP. This experiment demonstrated that the mesophilic *B. subtilis* σ^A-RNAP is able to utilize *A. aeolicus* 6S RNA (one of the most stable 6S RNAs known) as a template for pRNA transcription at 37°C, suggesting that 6S RNA-templated pRNA transcription is mechanistically very similar in mesophilic and hyperthermophilic bacteria. We next wanted to examine if these pRNAs synthesized by a heterologous mesophilic RNAP are identical to those synthesized by *A. aeolicus* RNAP *in vivo* (Figure 4. 9). This was done by RNA-seq using RNA prepared from non-radioactive *in vitro* transcriptions of the type shown in Figure 4. 20.

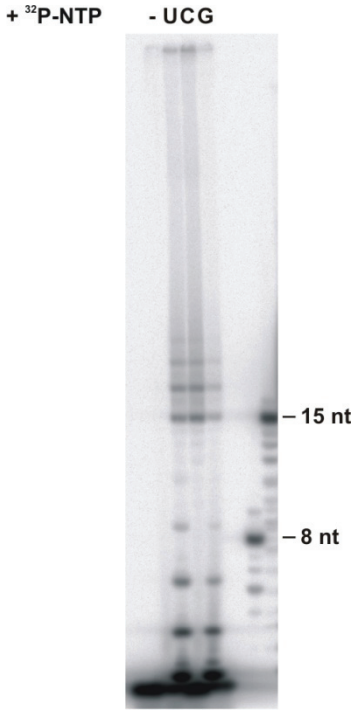

Figure 4. 20 *In vitro* pRNA transcription by *B. subtilis* σ^A-RNAP using *A. aeolicus* 6S RNA (132-nt variant) as template. The assay was performed with radioactively labeled α-^{32}P-UTP (lane U), α-^{32}P-CTP (lane C) or γ-^{32}P-GTP (lane G); (-) represent the control experiment without 6S RNA in the present of α-^{32}P-UTP. For further details see Materials and Methods.

4.1.14. RNA-seq analysis after *in vitro* pRNA transcription

RNA-seq was performed with RNA (114 ng/µl) prepared from non-radioactive *in vitro* transcriptions of the type shown in Figure 4. 20; cDNA libraries were constructed at vertis Biotechnologie AG (Freising, Germany) including 5'-TEX treatment to enrich for pRNAs carrying a 5'-triphosphate.

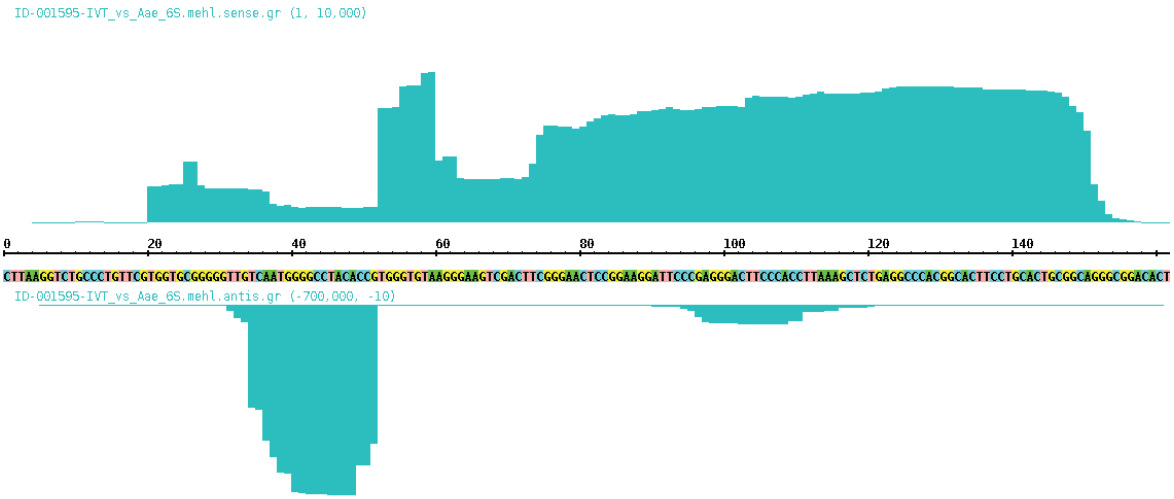

Figure 4. 21 RNA-seq analysis of 5'-TEX-treated RNA from *in vitro* transcriptions catalyzed by *B. subtilis* σ^A-RNAP using *A. aeolicus* 6S RNA (132 nt) as template. Obtained cDNA reads are visualized via the Integrated Genome Browser; reads corresponding to 6S RNA (sense) fragments are displayed at the top, pRNA reads (antisense) at the bottom.

As evident from Figure 4. 21, *B. subtilis* σ^A-RNAP generated two types of pRNA transcripts with different starting points when acting on *A. aeolicus* 6S RNA (132 nt) as template. First, reads for pRNA transcripts complementary to nt 15-34 of 6S RNA were identified in the RNA-seq data. These pRNA reads overlapped the pRNA starting point (C31) identified in the RNA-seq analysis of total RNA from *A. aeolicus* (Figure 4. 9). C31 also seemed to be the predominantly used starting nucleotide during *in vitro* transcription by *B. subtilis* σ^A-RNAP, as most reads had their 5'-terminus at this position. The other reads mapped to pRNAs initiated at C33/34 (Figure 4. 22 A; see Figure 4. 15 for 6S RNA numbering), thus also encoding pRNAs with a 5'-terminal G residue. GTP is most efficiently incorporated by *B. subtilis* σ^A-RNAP as the starting nucleotide [Cabrera-Ostertag *et al.*, 2013]. The finding of varying 5'-initiation sites indicates that the enzyme acts somewhat less precisely on the heterologous 6S RNA. On the other hand, the length distribution of pRNA reads (Figure 4. 22 B) was quite similar to that observed for the *in vivo* RNA-seq data (Figure 4. 9). Thus, it seems that 6S RNA binding to RNAP and pRNA transcription are very similar in the mesophile *B. subtilis* and the hyperthermophile *A. aeolicus*. A second smaller peak (9-fold less reads) of pRNA reads could be assigned to the opposite 3'-CB region. These alternative pRNAs were predominantly initiated at C93, but also at C91 and to a minor extent at C94, again yielding pRNAs with a favorable 5'-terminal G residue (Figure 4. 23). This second type of pRNA transcripts indicates that *A. aeolicus* 6S RNA was bound by the *B. subtilis* RNAP in two orientations, resulting in pRNA transcripts initiated at opposite sites in the central bulge. This phenomenon has also been observed to occur *in vivo* in various bacteria, such as *Helicobacter pylori* [Sharma *et al.*, 2010], *E. coli, B. subtilis or Listeria monocytogenes* [Wehner *et al.*, 2014].

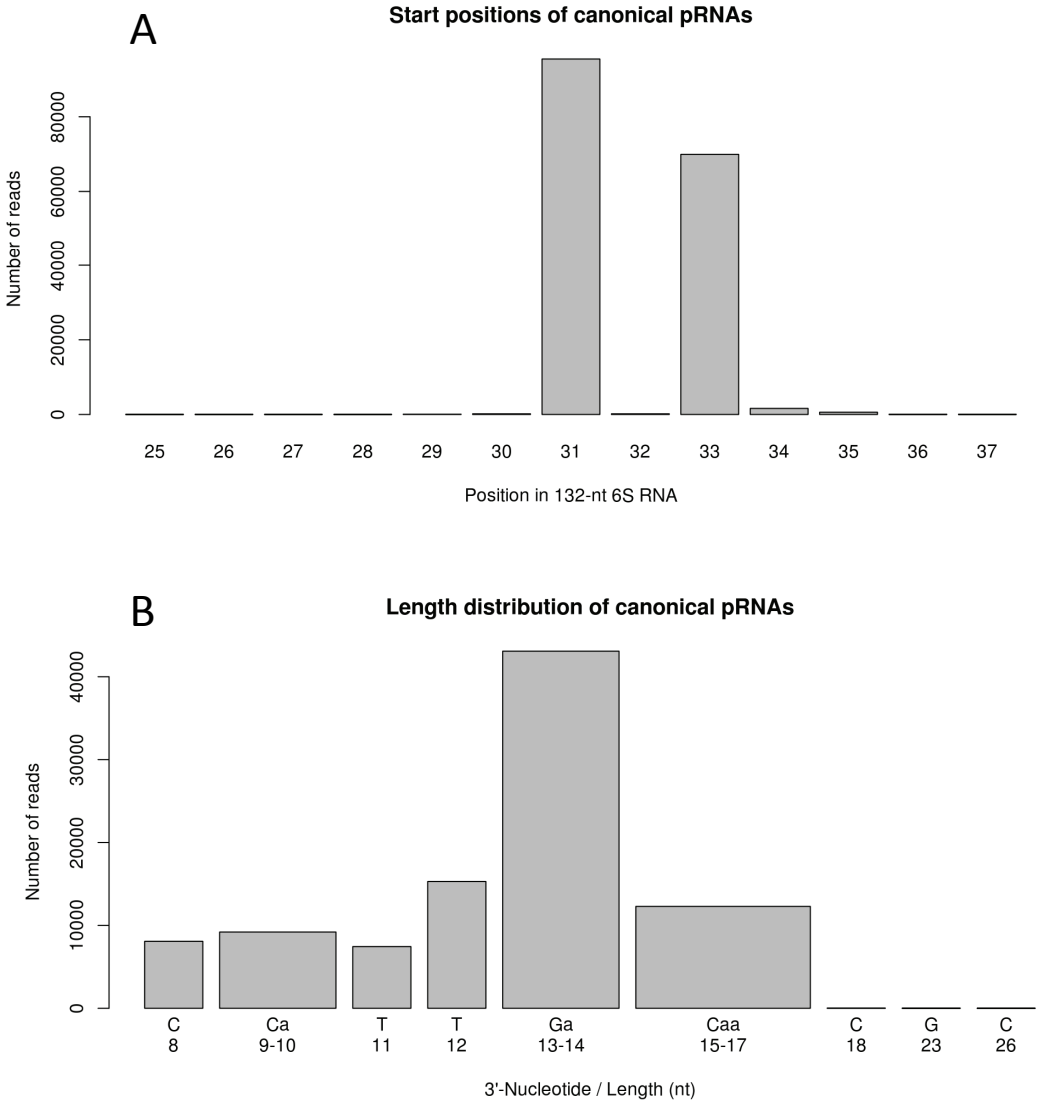

Figure 4. 22 Analysis of RNA-seq data obtained from *in vitro* transcription of pRNAs by *B. subtilis* σ^A-RNAP using *A. aeolicus* 6S RNA (132 nt) as template. Here, only canonical pRNAs initiated in the 5'-CB were considered. (A) The start position for such canonical pRNAs initiated in the 5'-CB is indicated (for 6S RNA numbering, see Figure 4. 15). Only reads containing no more than one mismatch (sequencing error), and no nucleotide gaps or inserts, were considered. Position 31 corresponds to the pRNA starting nucleotide found *in vivo* (Figure 4. 9). (B) Length distribution of canonical pRNA reads. Reads corresponding to pRNAs with a 3'-terminal adenosine were combined with the next shorter pRNA(s), as the poly(A) tailing procedure used for deep sequencing did not allow an unequivocal assignment of 3'-terminal A residues to the original pRNA. All pRNA reads did not match to 6S RNA fragments in the cDNA library.

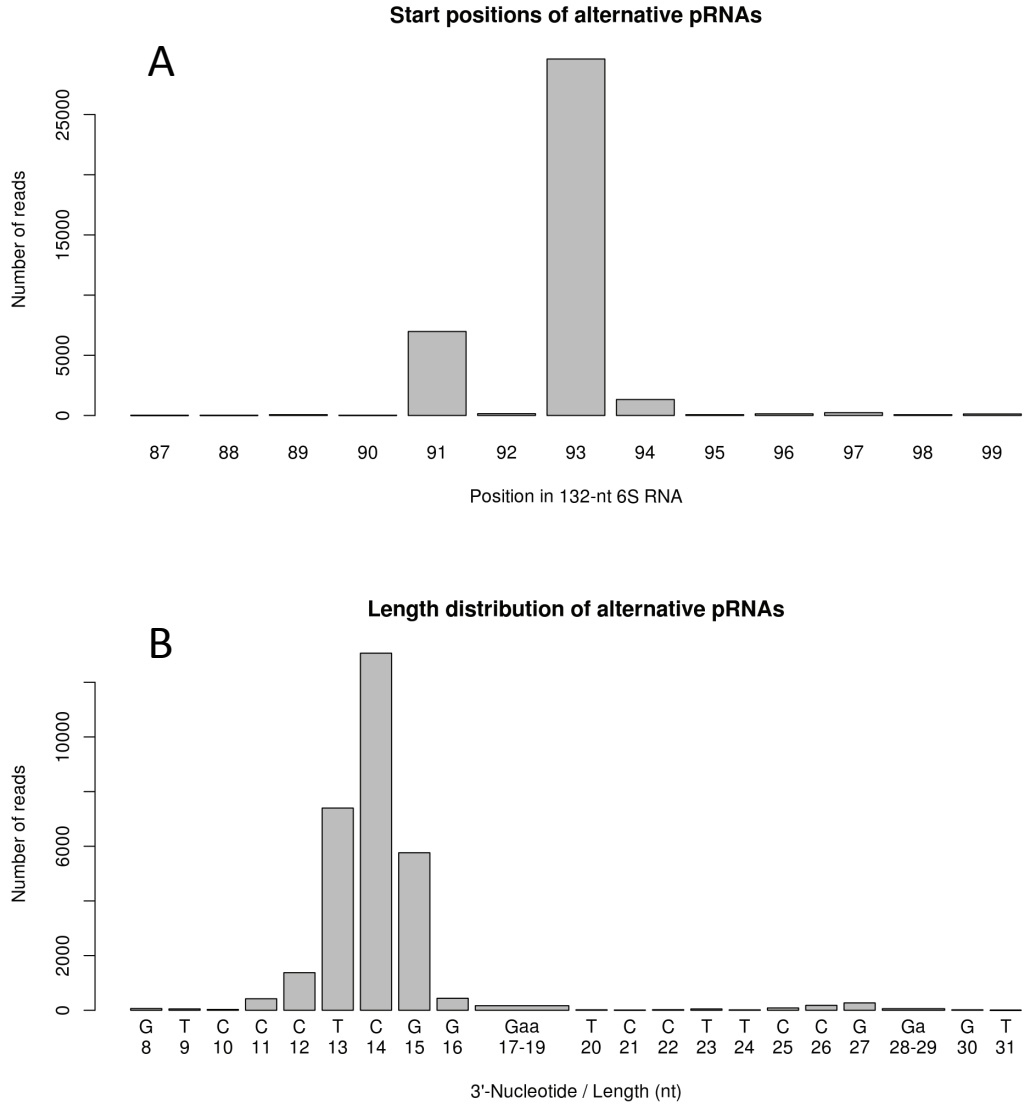

Figure 4. 23 Analysis of RNA-seq data obtained for alternative pRNAs initiated by *B. subtilis* σ^A-RNAP in the 3'-CB of *A. aeolicus* 6S RNA (132 nt) *in vitro*. (A) The start position for such alternative pRNAs initiated in the 3'-CB is indicated (for 6S RNA numbering, see Figure 4. 15). Only reads containing no more than one mismatch (sequencing error), and no nucleotide gaps or inserts, were considered. Position 93 corresponds to C93 in the 3'-CB of A.aeolicus 6S RNA (132 nt; see Figure 4. 15). (B) Length distribution of alternative pRNA reads. Reads corresponding to pRNAs with a 3'-terminal adenosine were combined with the next shorter pRNA(s), as the poly(A) tailing procedure used for deep sequencing did not allow an unequivocal assignment of 3'-terminal A residues to the original pRNA. All pRNA reads did not match to 6S RNA fragments in the cDNA library.

4.1.15. Analysis of 6S RNA:RNAP complexation

After having demonstrated that *B. subtilis* σ^A-RNAP is able to utilize *A. aeolicus* 6S RNA as a template for pRNA transcription (Figure 4. 20, Figure 4. 21), we further analyzed the formation of *A. aeolicus* 6S RNA : *B. subtilis* RNAP complexes and their disruption upon pRNA annealing. This was done with σ^A-RNAP and *A. aeolicus* 6S RNA

(132 nt) as well as *B. subtilis* 6S-1 RNA representing the homologous system. σ^A-RNAP indeed formed gel-resovable complexes with both 6S RNAs (Figure 4. 24 A, lanes 5 and 14). Preannealing of the specific pRNA 15-mer to *A. aeolicus* 6S RNA and a corresponding pRNA 14-mer to *B. subtilis* 6S-1 RNA decreased specific complex formation (Figure 4. 24 A, lanes 6 and 15).

We next addressed the question whether disruption of the helical structure adjacent to the central bulge (magenta nucleotides in Figure 4. 24 B and C) by a pRNA invading the structure from the 3'-CB side may also shift the 6S RNA structure and thus impair complex formation with RNAP. However, in this case formation of the CBC helix would be prevented (Figure 4. 15 and Figure 4. 24 B, C). Thus, this type of experiment may shed light on the role of the CBC helix in the rearrangement process. The 3'-CB pRNAs were designed to form duplexes that are roughly equally stable as the respective duplexes formed with the canonical 5'-CB pRNAs (Figure 4. 24 B, C). The *A. aeolicus* 6S RNA-specific 3'-CB pRNA changed gel mobility to the same extent as the canonical 5'-CB pRNA (Figure 4. 24 A, lanes 2 and 3), whereas the 3'-CB pRNA designed for *B. subtilis* 6S-1 RNA bound inefficiently under the tested conditions and the complex with 6S-1 RNA migrated differently from the one annealed to the 5'-CB pRNA (Figure 4. 24 A, lanes 11 and 12). Accordingly, disruption of the 6S-1 RNA:RNAP complex by the 3'-CB pRNA was barely detectable (Figure 4. 24 A, lane 16 vs. 15). In the case of *A. aeolicus* 6S RNA, annealing of the 3'-CB pRNA appeared to even increase complex formation with RNAP, but in a non-specific manner as inferred from a smear above the specific 6S RNA:RNAP complex (Figure 4. 24 A, lane 7). A control pRNA with the same sequence as the *A. aeolicus* 6S RNA-specific 3'-CB pRNA but reversed polarity neither affected complex formation of σ^A-RNAP with *A. aeolicus* 6S RNA nor with the homologous *B. subtilis* 6S-1 RNA (Figure 4. 24 A, lanes 8 and 17). It is concluded that such 3'-CB pRNAs can induce conformational changes in 6S RNA structure, the efficiency depending on the particular 6S RNA. Although the mobility shift of 6S RNA was the same with the 5'- and 3'-CB pRNAs in the case of *A. aeolicus* 6S RNA, RNAP release was blocked after 3'-CB pRNA annealing and rather non-specific gel-resovable complexes with RNAP were observed. This finding suggests that strand specificity of the pRNA duplex and/or formation of the CBC helix (prevented in case of the 3'-CB pRNA) are crucial for the RNAP release process. Thus, the pRNA-induced RNAP release mechanism has been evolutionarily optimized for pRNAs whose synthesis is initiated in the 5'-CB.

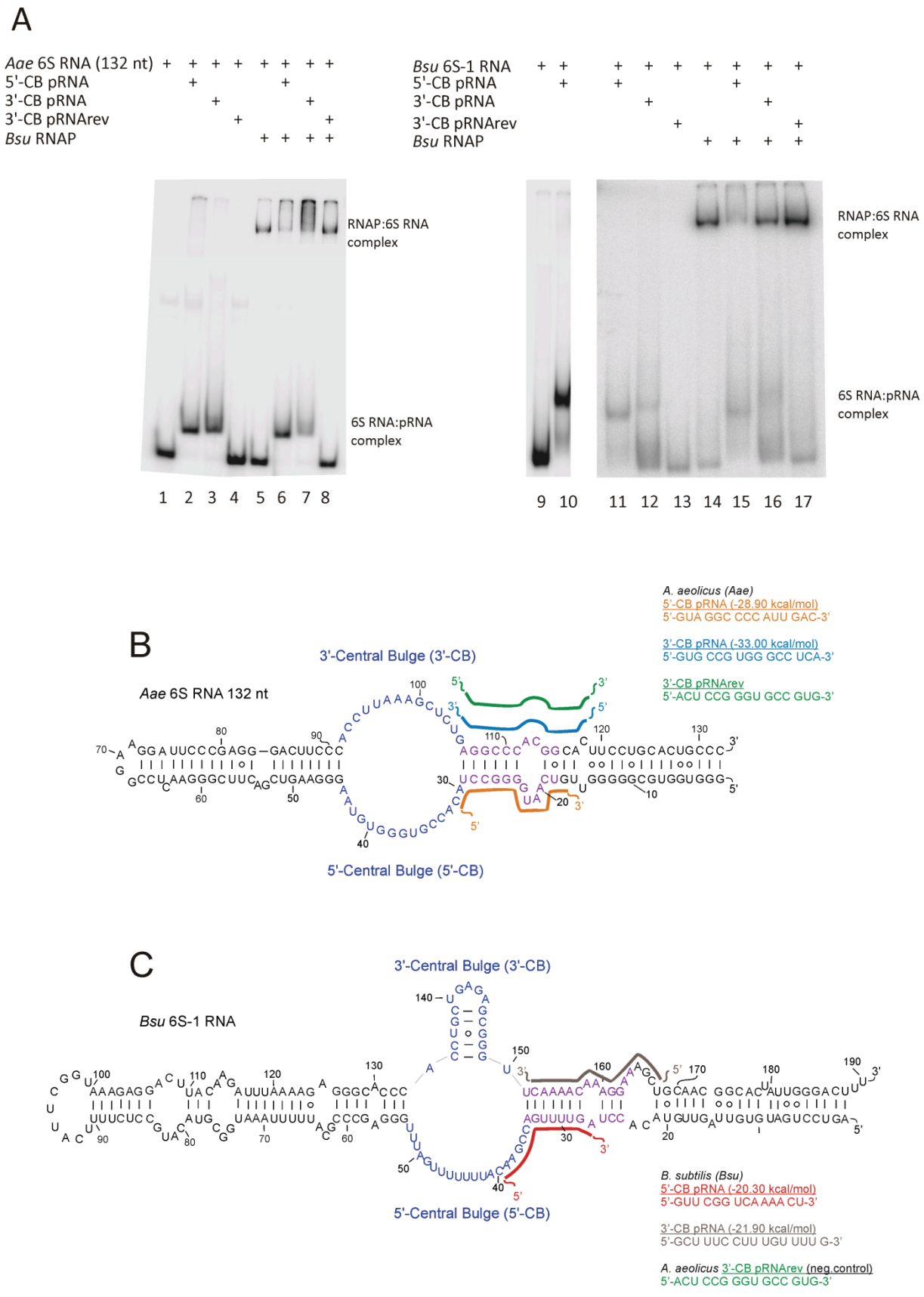

Figure 4. 24 EMSA of *A. aeolicus* 6S RNA (132 nt) and *B. subtilis* 6S-1 RNA alone and hybridized to different pRNA oligonucleotides to analyze binding to and release from *B. subtilis* σ^A-RNAP. (A) 6S RNAs (f.c. 0.24 µM, containing trace amounts of the same 5'-^{32}P-labeled 6S RNA), in the presence or absence of pRNA oligonucleotide (f.c. 2.4 µM), were incubated in 1x hybridization buffer

at 95°C for 10 min, followed by stepwise cooling to 37°C (90, 80, 70, 60, 50 and 40°C each for 5 min, and 10 min at 37°C). Afterwards, all samples were supplemented with buffer LM (40 mM Tris-HCl pH 8.0, 5 mM $MgCl_2$, 160 mM KCl, 1 mM DTT) and heparin (f.c. 8 ng/µL); to samples 5-8 and 13-16, *B. subtilis* σ^A-RNAP (f.c. 2.2 µM) was added, and all samples (final vol. 8.5 µL) were incubated for 30 min at 37°C. Samples were then supplemented with 1 volume of 2x native loading buffer and loaded onto a 7.5% native PAA gel (1x TBE as electrophoresis buffer). (B) and (C) Secondary structures of (B) *A. aeolicus* (*Aae*) 6S RNA (132 nt) and (C) *B. subtilis* (*Bsu*) 6S-1 RNA is illustrate the used pRNA oligonucleotides and their respective target sites. The 3'-CB pRNArev 15-mer has the same sequence as the *A. aeolicus* 6S RNA-specific 3'-CB pRNA but with reversed polarity. Stabilities (minimal free energies, in kcal/mol) of the individual pRNA:6S RNA duplexes are given in parentheses (calculated with RNAcofold of the Vienna RNA package).

In summary, we were able to define the solution secondary structure of *A. aeolicus* 6S RNA in its ground state as well as after the pRNA-induced structural rearrangement using structure probing and NMR. The RNA adopts the canonical rod-shaped architecture with little structure formation in the central bulge already at moderate temperatures. We demonstrate that pRNA invasion into the 6S RNA structure leads to formation of a new central bulge collapse helix, similar to what has been observed for *B. subtilis* 6S-1 RNA [Beckmann, Hoch *et al*., 2012]. The computationally predicted additional formation of a hairpin in the 3'-CB upon pRNA binding (Figure 4. 10 D), was neither indicated by the probing data nor the NMR measurements. Hairpin formation in the 3'-CB is a hallmark of the pRNA-induced rearrangement in a subgroup of proteobacterial 6S RNAs including the one from *E. coli* (Figure 1. 16).

We further demonstrated that *A. aeolicus* 6S RNA mechanistically behaves as a genuine 6S RNA, serving as a template for pRNA synthesis *in vivo*, and remarkably also *in vitro* in reactions catalyzed by the σ^A-RNAP of the mesophile *B. subtilis*. Binding of pRNA to *A. aeolicus* 6S RNA blocks formation of 6S RNA:RNAP complexes, a typical feature of 6S RNAs. The RNA-seq analysis using total RNA from *A. aeolicus* suggested that pRNAs of up to 15 nt in length are synthesized *in vivo*, and we showed for the pRNA 15-mer that it forms an extraordinarily stable duplex with *A. aeolicus* 6S RNA which even resists the denaturing PAGE treatment. All these findings suggest that *A. aeolicus* 6S RNA mechanistically functions as other bacterial 6S RNAs in its *A. aeolicus* host at temperatures around 85°C.

It has been observed in RNA-seq *in vivo* analyses [Wehner *et al*., 2014] as well as in this work (Figure 4. 21) that 6S RNAs can bind RNAP molecules to some extent in reverse orientation giving rise to pRNA synthesis initiated in the 3'-CB. However, as shown here, canonical pRNAs with their 5'-end mapping to the 5'-CB (5'-CB pRNAs) tend to be more efficient and specific than 3'-CB pRNAs with respect to the structural rearrangement and RNAP release. In conclusion, the mechanism of pRNA-induced

disruption of 6S RNA:RNAP complexes has been evolutionarily optimized for transcriptional pRNA initiation in the 5'-CB.

4.1.16. *B. subtilis* 6S-1 RNA

4.1.17. Secondary structure analysis via NMR

So far, the pRNA-induced structural rearrangement of *B. subtilis* 6S-1 RNA was characterized by secondary structure probing [Beckmann, Hoch *et al.*, 2012]. To verify these results, a shorter circularly permuted variant of *B. subtilis* 6S-1 RNA (Figure 4. 25) was prepared and used for NMR experiments.

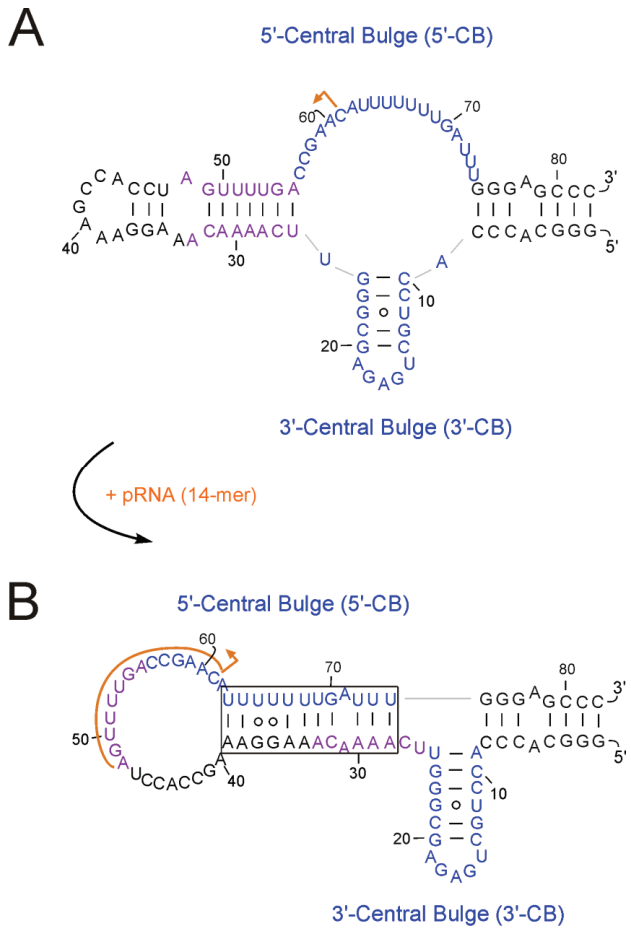

Figure 4. 25 Illustration of the secondary structure of the shortened 82 nt long and circularly permuted (cp) variant of *B. subtilis* 6S-1 RNA. The orange arrow indicates the pRNA transcription starting point. The nucleotides marked in blue represent the region of the central bulge (CB). The nomenclature of the bulge regions (3'-Central Bulge and 5'-Central Bulge) is according to the full-length 6S-1 RNA. The purple region marks the helix which is unwound during pRNA transcription. (A) Predicted ground state structure of the 82-nt_cp variant. (B) pRNA:82-nt_cp hybrid structure. The orange line visualizes the pRNA binding site. The central bulge collapse helix is indicated by the box.

The lower thermodynamic stability (higher proportion of A:U base pairs) of *B. subtilis* 6S-1 RNA relative to *A. aeolicus* 6S RNA was disadvantageous for NMR analyses at high resolution. Besides the advantage of being reduced in size, the 82-nt_cp variant had its closing loop on the side of helix disruption and pRNA duplex formation (Figure 4. 25), which prevented the formation of dangling 5'- and 3'-ends and thus enhanced structural flexibility. The 82-nt_cp variant was shown to bind to σ^A-RNAP and to serve as a template for pRNA transcription *in vitro* (data not shown), demonstrating that this shortened RNA is a functional 6S-1 RNA mimic.

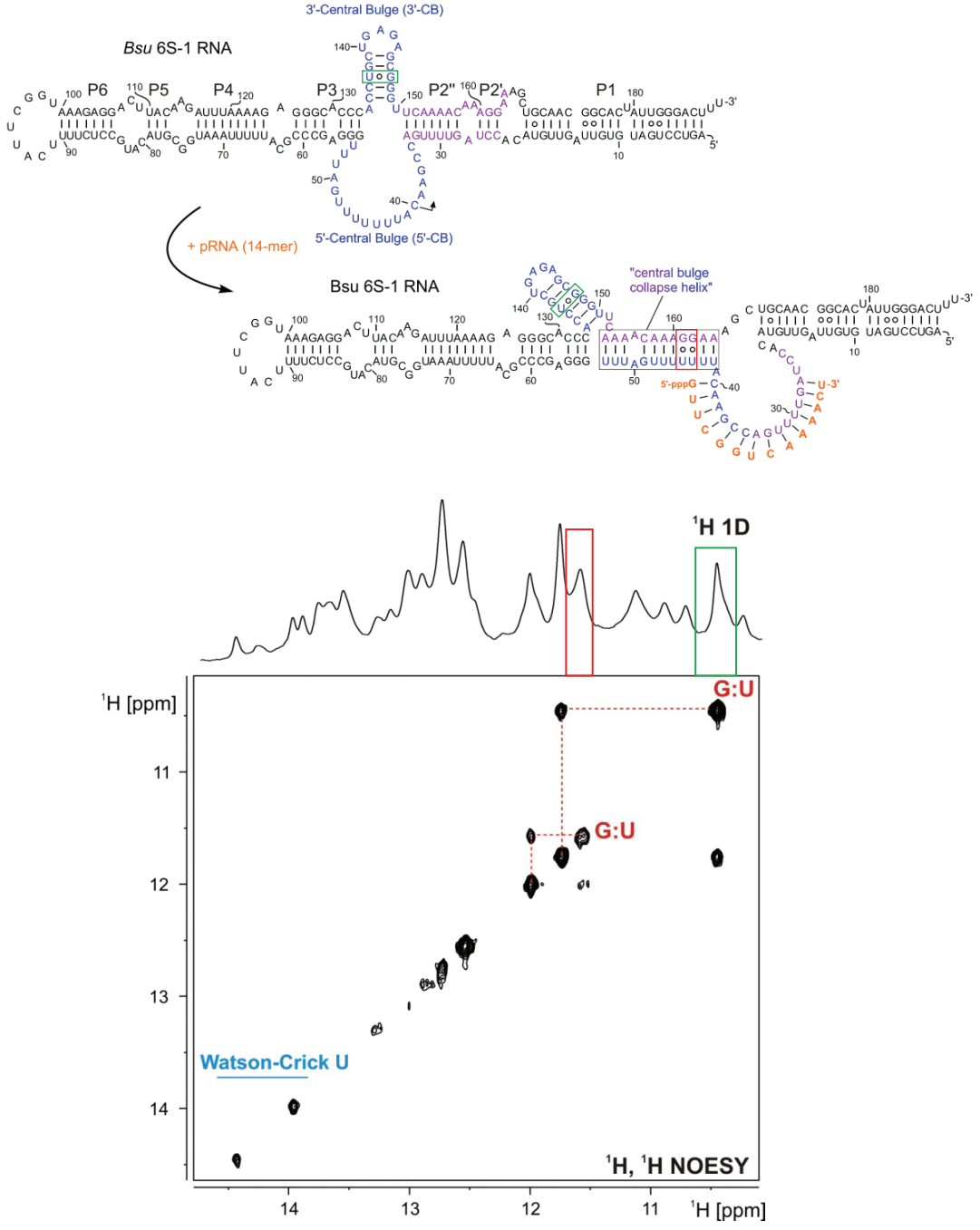

Figure 4. 26 ^{1}H,^{1}H-NOESY spectrum of *the B. subtilis* pRNA:6S-1 RNA (190 nt) hybrid structure at 950 MHz at 350 K (32°C). The pRNA (14 nt) was identical to the 5'-CB pRNA specified in Figure 4. 24 C. Two identified G:U base pairs are highlighted in red in the two-dimensional presentation of the spectrum.

One signal (red box in the one-dimensional spectrum at the top) could be assigned to one of the two adjacent G:U pairs in the central bulge collapse helix (correspondingly marked by a red box in the rearranged secondary structure above). The second signal (green box) was assignable to the G:U pair in the hairpin formed in the 3'-CB. Imino proton signals of uridines involved in Watson-Crick A:U base pairs are found below the blue line (~ 13.9 to 15 ppm region).

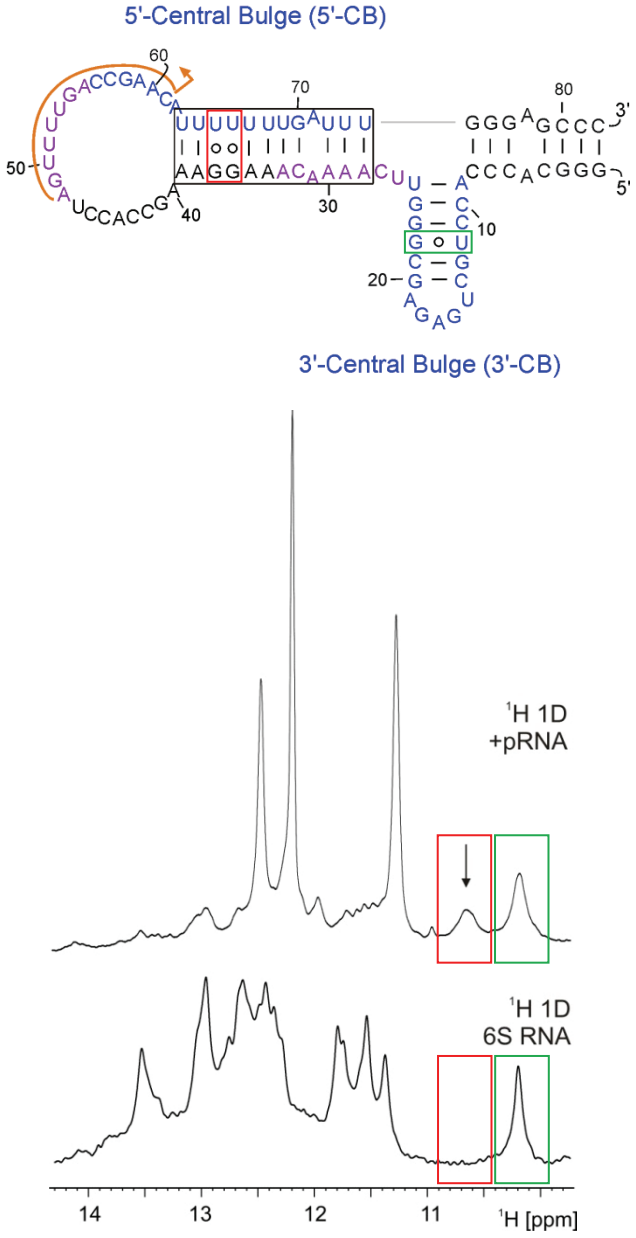

Figure 4. 27 1D-1H spectra of the *B. subtilis* 82-nt_cp variant, either in its ground state (bottom) or in complex with 5'-CB pRNA 14-mer (top). Spectra were recorded at 950 MHz and 283 K (10°C). The signal corresponding to G:U pair in the 3'-CB hairpin and the new signal appearing upon pRNA hybridization are indicated by green and red boxes, respectively, in the spectra and the corresponding secondary structures at the top. Increased peak heights seen after pRNA annealing are indicative of background signals owing to the presence of pRNA in excess over 82-nt_cp RNA (82-nt_cp: 856 µM with tenfold excess of pRNA during hybridization; after annealing, the pRNA excess amounts were partly removed by buffer exchange using Amicon Ultra-0.5 30K filter devices (Merck Millipore) before NMR measurement). One possibility is that uncomplexed pRNAs form intramolecular or dimeric structures leading to these pronounced signals.

The comparison of NMR spectra for *B. subtilis* full-length 6S-1 RNA in its ground state and in complex with pRNA revealed one significant change (Figure 4. 26). In the spectrum for the 6S-1 RNA:pRNA hybrid, an additional signal appeared which could be assigned to a newly formed G:U wobble pair. This nicely correlates with the formation of two adjacent G:U pairs in the CBC helix. Basically the same result was obtained with the shortened 82-nt_cp variant of B. subtilis 6S-1 RNA (Figure 4. 27). Thus, our NMR measurements verified the formation of the CBC helix that was previously inferred from probing experiments [Beckmann, Hoch *et al*., 2012].

Although the NMR analyses on *B. subtilis* 6S-1 RNA did not yield high resolution spectra, they nevertheless provided independent evidence for the formation of the CBC helix involving two adjacent G:U wobble base pairs.

5. Outlook

To further investigate the cleavage reaction mechanism of RNase P, especially before and during cleavage (crystal structure presented by Reiter *et al*., 2010 shows RNase P:pre-tRNA complex after cleavage reaction), more stable short substrates have to be tested. In combination with Ca^{2+} ions the complex can be formed, but no cleavage reaction takes place. By using Mn^{2+} ions the RNA-metal ion interactions on each side (RPR and substrate) should be observable.

Further electromobility shift experiments with pRNAs of different length at higher temperature conditions during PAGE could address the question if the shorter pRNA transcripts only act as abortive pRNA transcripts or if they are able to induce the structural rearrangement even under high temperature conditions.

It should also be investigated if only a lower binding affinity of the 3'-CB pRNA designed for *B. subtilis* 6S-1 RNA was responsible for the inefficient structural rearrangement. To test this, pRNA derivates (all-LNA or RNA/LNA mixmers) can be annealed to the structure to gain more evidence that the formation of the CBC helix is crucial for the release of the 6S RNA:pRNA hybrid from RNAP.

The three-dimensional orientation of the terminal and the initial stem of *A. aeolicus* 6S RNA by NMR studies may be revealed using Pf1 phages which force 6S RNA to orientate alongside the phages in the magnetic field. Such experiments are currently in progress.

Furthermore, Förster/fluorescence resonance energy transfer (FRET) studies using fluorophore pairs at both ends may also deepen our understanding of the spatial changes of 6S RNA structure upon pRNA annealing. Finally, atomic force microscopy (AFM) is as well suited to investigate the aforementioned issue.

6. References

Alifano, P., Rivellini, F., Piscitelli, C., Arraiano, C. M., Bruni, C. B., & Carlomagno, M. S. (1994). Ribonuclease E provides substrates for ribonuclease P-dependent processing of a polycistronic mRNA. *Genes & development*, 8(24), 3021–3031. doi:10.1101/gad.8.24.3021

Altman, S., Baer, M. F., Bartkiewicz, M., Gold, H., Guerrier-Takada, C., Kirsebom, L. A., Lumelsky, N., *et al*. (1989). Catalysis by the RNA subunit of RNase P--a minireview. *Gene*, 82(1), 63–64. doi:10.1016/0378-1119(89)90030-9

Altman, S., Kirsebom, L., & Talbot, S. (1993). Recent studies of ribonuclease P. *The FASEB journal: official publication of the Federation of American Societies for Experimental Biology*, 7(1), 7–14. Retrieved from http://www.ncbi.nlm.nih.gov/pubmed/7916700

Altman, S., & Smith J.D. (1971). Tyrosine tRNA Precursor Molecule Polynucleotide Sequence. *Nature new biology*, 233(36), 35-39.

Altman, S., Wesolowski, D., Guerrier-Takada, C., & Li, Y. (2005). RNase P cleaves transient structures in some riboswitches. *Proceedings of the National Academy of Sciences of the United States of America*, 102(32), 11284–11289.

Barrick, J. E., Sudarsan, N., Weinberg, Z., Ruzzo, W. L., & Breaker, R. R. (2005). 6S RNA is a widespread regulator of eubacterial RNA polymerase that resembles an open promoter. *RNA (New York, N.Y.)*, 11(5), 774–784.

Beckmann, B. M., Burenina, O. Y., Hoch, P. G., Kubareva, E. A., Sharma, C. M., & Hartmann, R. K. (2011). In vivo and in vitro analysis of 6S RNA-templated short transcripts in *Bacillus subtilis*. *RNA Biology*. doi:10.4161/rna.8.5.16151

Beckmann, B. M., Hoch, P. G., Marz, M., Willkomm, D. K., Salas, M., & Hartmann, R. K. (2012). A pRNA-induced structural rearrangement triggers 6S-1 RNA release from RNA polymerase in *Bacillus subtilis*. *The EMBO Journal*. doi:10.1038/emboj.2012.23

Berg, J. M., Tymoczko, J. L., & Stryer, L. (2007). *Stryer Biochemie*. *Biochemistry textbook* (p. 1120). Retrieved from http://books.google.com/books?id=jQKGAAAACAAJ

Biswas, R., Ledman, D. W., Fox, R. O., Altman, S., & Gopalan, V. (2000). Mapping RNA-protein interactions in ribonuclease P from *Escherichia coli* using disulfide-linked EDTA-Fe. *Journal of molecular biology*, 296(1), 19–31. doi:10.1006/jmbi.1999.3443

Bothwell, A. L., Stark, B. C., Altman, S. (1976). Ribonuclease P substrate specificity: Cleavage of a bacteriophage phi80-induced RNA. *Proc Natl Acad Sci U S A* 73, 1912–6.

Brownlee G.G. (1971). Sequence of 6S RNA of *E. coli. Nature*, 229 (5), 147-9.

Buck, A. H., Kazantsev, A. V, Dalby, A. B., & Pace, N. R. (2005). Structural perspective on the activation of RNAse P RNA by protein. *Nature structural & molecular biology*, 12(11), 958–964. doi:10.1038/nsmb1004

Burenina, O. Y., Hoch, P. G., Damm, K., Salas, M., Zatsepin, T. S., Lechner, M., Oretskaya, T. S., Kubareva, E. A., Hartmann, R. K. (2014). Mechanistic comparison of *Bacillus subtilis* 6S-1 and 6S-2 RNAs-commanalities and differences. *RNA* 20(3), 348-59.

Cabrera-Ostertag, I. J., Cavanagh, A. T., Wassarman, K. M. (2013). Initiating nucleotide identity determines efficiency of RNA synthesis from 6S RNA templates in *Bacillus subtilis* but not *Escherichia coli*. *Nucleic Acids Res., 41(15), 7501-11.*

Cavanagh, A. T., Klocko, A. D., Liu, X., & Wassarman, K. M. (2008). Promoter specificity for 6S RNA regulation of transcription is determined by core promoter sequences and competition for region 4.2 of sigma^{70}. *Molecular microbiology*, 67(6), 1242–1256. doi:10.1111/j.1365-2958.2008.06117.x

Cavanagh, A. T., Sperger, J. M., & Wassarman, K. M. (2012). Regulation of 6S RNA by pRNA synthesis is required for efficient recovery from stationary phase in *E. coli* and *B. subtilis*. *Nucleic acids research*, 40(5), 2234–46. doi:10.1093/nar/gkr1003

Cavanagh, A. T., & Wassarman, K. M. (2013). 6S-RNA function leads to a delay in sporulation in *Bacillis subtilis*. *J Bacteriol*, 195, 2079-86; PMID:23457253

Chae, H., Han, K., Kim, K., Park, H., Lee, J., & Lee, Y. (2011). Rho-dependent termination of ssrS (6S RNA) transcription in *Escherichia coli*: implication for 3' processing of 6S RNA and expression of downstream ygfA (putative 5-formyl-tetrahydrofolate cyclo-ligase). *The Journal of biological chemistry*, 286(1), 114–122.

Chen, Y., Li, X., & Gegenheimer, P. (1997). Ribonuclease P catalysis requires Mg^{2+} coordinated to the pro-R(P) oxygen of the scissile bond. *Biochemistry*, 36(9), 2425–2438.

Cho, S., Cho, Y., Lee, S., Kim, J., Yum, H., Kim, S. C. and Cho, B.-K. (2013). Current Challenges in Bacterial Transcriptomics. *Genomics Inform.,* 11(2), 76-82.

Cuzic, S., & Hartmann, R. K. (2005). Studies on *Escherichia coli* RNase P RNA with Zn^{2+} as the catalytic cofactor. *Nucleic Acids Research*, 33(8), 2464–2474.

Evans, D., Marquez, S. M., & Pace, N. R. (2006). RNase P: interface of the RNA and protein worlds. *Trends in Biochemical Sciences*.

Faucher, S.P., Friedlander, G., Livny, J., Margalit, H., Shuman, H.A. (2010). *Legionella pneumophila* 6S RNA optimizes intracellular multiplication. *Proc Natl Acad Sci U S A*; 107, 7533-8; PMID:20368425.

Forster, A. C., & Altman, S. (1990). External guide sequences for an RNA enzyme. *Science (New York, N.Y.)*, 249(4970), 783–786. doi:10.1126/science.1697102

Forti, F., Sabbattini, P., Sironi, G., Zangrossi, S., Deho, G., Ghisotti, D. (1995). Immunity determinant of phage–plasmid P4 is a short processed RNA. *J Mol Biol* 249, 869–78.

Fürtig, B., Richter, C., Wöhnert, J., & Schwalbe, H. (2003). NMR spectroscopy of RNA. *Chembiochem: a European journal of chemical biology*, 4(10), 936–62. doi:10.1002/cbic.200300700

Geissen, R., Steuten, B., Polen, T., Wagner, R. (2010). *E. coli* 6S RNA: a universal transcriptional regulator within the centre of growth adaptation. *RNA Biol*, 7, 564-8; PMID:20930516.

Gildehaus, N., Neusser, T.,Wurm, R.,Wagner, R. (2007). Studies on the function of the riboregulator 6S RNA from *E. coli*: RNA polymerase binding, inhibition of *in vitro* transcription and synthesis of RNA-directed *de novo* transcripts. *Nucleic Acid Res*, 35, 1885-96; PMID:17332013.

Gobert, A., Gutmann, B., Taschner, A., Gössringer, M., Holzmann, J., Hartmann, R. K., Rossmanith, W., *et al*. (2010). A single Arabidopsis organellar protein has RNase P activity. *Nature structural & molecular biology*, 17(6), 740–744. doi:10.1038/nsmb.1812

Griffey, R. H., Poulter, C. D., Bax, A., Hawkins, B. L., Yamaizumi, Z., & Nishimura, S. (1983). Multiple quantum two-dimensional ^{1}H--^{15}N nuclear magnetic resonance spectroscopy: chemical shift correlation maps for exchangeable imino protons of *Escherichia coli* tRNAMetf in water. *Proceedings of the National Academy of Sciences of the United States of America*, 80(19), 5895–5897.

Gruber, T. M., & Gross, C. A. (2003). Multiple sigma subunits and the partitioning of bacterial transcription space. *Annual review of microbiology*, 57, 441–466. doi:10.1146/annurev.micro.57.030502.090913

Grünweller, A. and Hartmann, R. K. (2007). Locked nucleic acid oligonucleotids: the next generation of antisense agents? *BioDrugs*, 21(4), 235-43.

Guerrier-Takada, C., Gardiner, K., Marsh, T., Pace, N., & Altman, S. (1983). The RNA moiety of ribonuclease P is the catalytic subunit of the enzyme. *Cell*, 35(3 Pt 2), 849–857. doi:10.1016/0092-8674(83)90117-4

Guerrier-Takada, C., Haydock, K., Allen, L., & Altman, S. (1986). Metal ion requirements and other aspects of the reaction catalyzed by M1 RNA, the RNA subunit of ribonuclease P from *Escherichia coli*. *Biochemistry*, 25(7), 1509–1515.

Haas, E. S., Banta, A. B., Harris, J. K., Pace, N. R., Brown, J. W.(1996). Structure and evolution of Ribonuclease P RNA in Gram-positive bacteria. *Nucleic Acids Res.,* 24(23), 4775-82.

Haas, E. S., & Brown, J. W. (1998). Evolutionary variation in bacterial RNase P RNAs. *Nucleic Acids Research*.

Hansen, S., Lewis, K., Vulié, M. (2008) Role of global regulators and nucleotide metabolism in antibiotic tolerance in *Escherichia coli*. *Antimicrob Agents Chemother*, 52, 2718-26; PMID:18519731

Harbers, M., & Kahl, G. (2012). *Tag-Based Next Generation Sequencing*. Wiley-VCH.

Hartmann, R K, Heinrich, J., Schlegl, J., & Schuster, H. (1995). Precursor of C4 antisense RNA of bacteriophages P1 and P7 is a substrate for RNase P of *Escherichia coli*. *Proceedings of the National Academy of Sciences of the United States of America*, 92(13), 5822–5826.

Hartmann, R. K., Göringer, M., Späth, B., Fischer, S., & Marchfelder, A. (2009). Chapter 8 The Making of tRNAs and More - RNase P and tRNase Z. *Progress in Molecular Biology and Translational Science*.

Hindley, J. (1967). Fractionation of ^{32}P-labelled ribonucleic acids on polyacrylamide gels and their characterization by fingerprinting. *Journal of molecular biology*, 30(1), 125–136. doi:10.1016/0022-2836(67)90248-3

Holm, P. S., & Krupp, G. (1992). The acceptor stem in pre-tRNAs determines the cleavage specificity of RNase P. *Nucleic acids research*, 20(3), 421–423.

Holzmann, J., Frank, P., Löffler, E., Bennett, K. L., Gerner, C., & Rossmanith, W. (2008). RNase P without RNA: Identification and Functional Reconstitution of the Human Mitochondrial tRNA Processing Enzyme. *Cell*, 135(3), 462–474.

Hsieh, J., Koutmou, K. S., Rueda, D., Koutmos, M., Walter, N. G., & Fierke, C. A. (2010). A divalent cation stabilizes the active conformation of the *B. subtilis* RNase P:Pre-tRNA complex: A role for an inner-sphere metal ion in RNase P. *Journal of Molecular Biology*, 400(1), 38–51.

Jovanovic, G., Lloyd, L.J., Stumpf, M.P, Mayhew, A.J., Buck, M. (2006). Induction and function of the phage shock protein extracytoplasmic stress response in *Escherichia coli. J Biol Chem*, 281, 21147-61.

Jovanovic, G., Engl, C., Mayhew, A. J., Burrows, P. C., Buck, M. (2010). Properties of the phage-shock-protein (Psp) regulatory complex that govern signal

transduction and induction of the Psp response in *Escherichia coli. Microbiol.* 156(10), 2920-2932.

Karginov, F. V., & Hannon, G. J. (2010). The CRISPR System: Small RNA-Guided Defense in Bacteria and Archaea. *Molecular Cell*.

Kaur, H., Arora, A., Wengel, J., & Maiti, S. (2006). Thermodynamic, counterion, and hydration effects for the incorporation of locked nucleic acid nucleotides into DNA duplexes. *Biochemistry*, 45(23), 7347–7355.

Kikovska, E., Svärd, S. G., Kirsebom, L. A. (2007). Eukaryotic RNase P RNA mediates cleavage in the absence of protein. *Proc Natl Acad Sci U S A*, 104(7), 2062-7.

Kim, K. S., & Lee, Y. (2004). Regulation of 6S RNA biogenesis by switching utilization of both sigma factors and endoribonucleases. *Nucleic Acids Research*, 32(20), 6057–6068.

Kirsebom, L. A., & Svärd, S. G. (1992). The kinetics and specificity of cleavage by RNase P is mainly dependent on the structure of the amino acid acceptor stem. *Nucleic acids research*, 20(3), 425–432.

Klocko, A. D., & Wassarman, K. M. (2009). 6S RNA binding to Esigma(^{70}) requires a positively charged surface of sigma(^{70}) region 4.2. *Molecular microbiology*, 73(2), 152–164.

Kondo, J., Dock-Bregeon, A. C., Willkomm, D. K., Hartmann, R. K., & Westhof, E. (2013). Structure of an A-form RNA duplex obtained by degradation of 6S RNA in a crystallization droplet. *Acta Crystallographica Section F: Structural Biology and Crystallization Communications*, 69(6), 634–639.

Kufel, J., & Kirsebom, L. A. (1998). The P15-loop of *Escherichia coli* RNase P RNA is an autonomous divalent metal ion binding domain. *RNA (New York, N.Y.)*, 4(7), 777–788.

Kugel, J.F., Goodrich, J.A. (2007). An RNA transcriptional regulator template its own regulatory RNA. *Nat Chem Biol*, 3, 89-90; PMID:17235345.

Kurz, J. C., Niranjanakumari, S., Fierke, C. A. (1998). Protein component of *Bacillus subtilis* RNase P specifically enhances the affinity for precursor-tRNAAsp. *Biochemistry*, 37(8), 2393-400.

Kurz, J. C. and Fierke, C. A. (2002). The affinity of magnesium binding sites in the *Bacillus subtilis* RNase P x pre-tRNA complex is enhanced by the protein subunit. *Biochemistry*, 41(30), 9545-58.

Lee, S.Y., Bailey, S.C., Apirion, D. (1978). Small stable RNAs from *Escherichia coli*: evidence for the existence of new molecules and for a new ribonucleoprotein partivle containing 6S RNA. *J Bacteriol*, 133:1015-23; PMID:342486.

Lee, C. A., Fournier, M. J., & Beckwith, J. (1985). *Escherichia coli* 6S RNA is not essential for growth or protein secretion. *Journal of bacteriology*, 161(3), 1156–1161.

Li, Y., & Altman, S. (2003). A specific endoribonuclease, RNase P, affects gene expression of polycistronic operon mRNAs. *Proceedings of the National Academy of Sciences of the United States of America*, 100(23), 13213–13218.

Loria, A., & Pan, T. (1998). Recognition of the 5' leader and the acceptor stem of a pre-tRNA substrate by the ribozyme from Bacillus subtilis RNase P. *Biochemistry*, 37(28), 10126–10133.

Mans, R. M., Guerrier-Takada, C., Altman, S., & Pleij, C. W. (1990). Interaction of RNase P from *Escherichia coli* with pseudoknotted structures in viral RNAs. *Nucleic acids research*, 18(12), 3479–3487.

Massire, C., Jaeger, L., & Westhof, E. (1998). Derivation of the three-dimensional architecture of bacterial ribonuclease P RNAs from comparative sequence analysis. *Journal of molecular biology*, 279(4), 773–793. doi:10.1006/jmbi.1998.1797

Medini, D., Serruto, D., Parkhill, J., Relman, D. A., Donati, C., Moxon, R., Falkow, S. (2008). Microbiology in the post-genomic era. *Nature reviews. Microbiology*, 6(6), 419–430. doi:10.1038/nrmicro1901

Neusser, T., Gildehaus, N., Wurm, R., Wagner, R. (2008). Studies in the experssion of 6S RNA from *E. coli*: involvement of regulators important for stress and growth adaptation. *Biol Chem*, 389, 285-97; PMID:18177266.

Neusser, T., Polen, T., Geissen, R., Wagner, R. (2010). Depletion of the non-coding regulatory 6S RNA in *E. coli* causes a surprising reduction in the expression of the translation machinery. *BMC Genomics*, 11, 165; PMID:20222947.

Nicol, J. W., Helt, G. A., Blanchard, S. G., Raja, A., Loraine, A. E.(2009). The Integrated Genome Browser: free software for distribution and exploration of genome-scale datasets. *Bioinformatics*, 25(20):2730–2731.

Niranjanakumari, S, Stams, T., Crary, S. M., Christianson, D. W., & Fierke, C. A. (1998). Protein component of the ribozyme ribonuclease P alters substrate recognition by directly contacting precursor tRNA. *Proceedings of the National Academy of Sciences of the United States of America*, 95(26), 15212–15217.

Niranjanakumari, S., Day-Storms, J. J., Ahmed, M., Hsieh, J., Zahler, N. H., Venters, R. A., & Fierke, C. A. (2007). Probing the architecture of the *B. subtilis* RNase P holoenzyme active site by cross-linking and affinity cleavage. *RNA (New York, N.Y.)*, 13(4), 521–535.

Pace, N., & Brown, J. (1995). Evolutionary perspective on the structure and function of ribonuclease P, a ribozyme. *J. Bacteriol.*, 177(8), 1919–1928. Retrieved from http://jb.asm.org/cgi/content/long/177/8/1919

Pan, T., Loria, A., & Zhong, K. (1995). Probing of tertiary interactions in RNA: 2'-hydroxyl-base contacts between the RNase P RNA and pre-tRNA. *Proceedings of the National Academy of Sciences of the United States of America*, 92(26), 12510–12514.

Panchapakesan, S.S., & Unrau, P.J.E. (2012). *E. coli* 6S RNA release from RNA polymerase requires σ^{70} ejection by scrunching and is orchestrated by a conserved RNA hairpin. *RNA*, 18, 2251-9; PMID:23118417.

Pascual, A., & Vioque, A. (1996). Cloning, purification and characterization of the protein subunit of ribonuclease P from the cyanobacterium *Synechocystis sp.* PCC 6803. *European journal of biochemistry / FEBS*, 241(1), 17–24.

Peck-Miller, K. A., & Altman, S. (1991). Kinetics of the processing of the precursor to 4.5 S RNA, a naturally occurring substrate for RNase P from *Escherichia coli. Journal of molecular biology*, 221(1), 1–5. doi:10.1016/0022-2836(91)80194-Y

Persson, T., Cuzic, S., & Hartmann, R. K. (2003). Catalysis by RNase P RNA: unique features and unprecedented active site plasticity. *The Journal of biological chemistry*, 278(44), 43394–43401. doi:10.1074/jbc.M305939200

Pichon, C., & Felden, B. (2005). Small RNA genes expressed from *Staphylococcus aureus* genomic and pathogenicity islands with specific expression among pathogenic strains. *Proceedings of the National Academy of Sciences of the United States of America*, 102(40), 14249–14254.

Reiter, N. J., Osterman, A., Torres-Larios, A., Swinger, K. K., Pan, T., & Mondragón, A. (2010). Structure of a bacterial ribonuclease P holoenzyme in complex with tRNA. *Nature*, 468(7325), 784–789.

Repoila, F. & Darfeuille, F. (2009). Small regulatory non-coding RNAs in bacteria: physiology and mechanistic aspects. *Biol Cell.,* 101(2),117-31.

Sanger, F., & Coulson, A.R. (1975). A rapid method for determining sequences in DNA by primed synthesis with DNA polymerase. *J Mol Biol*, 94(3), 441-8; PMID:1100841

Sanger, F., Nicklen, S., Coulson, A. R. (1977). DNA sequencing with chain-termination inhibitors. *Proc Natl Acad Sic U S A*, 74(12), 5463-7; PMID:271968.

Schlüter, J.-P., Reinkensmeier, J., Daschkey, S., Evguenieva-Hackenberg, E., Janssen, S., Jänicke, S., Becker, J. D., *et al*. (2010). A genome-wide survey of sRNAs in the symbiotic nitrogen-fixing alpha-proteobacterium *Sinorhizobium meliloti*. *BMC genomics*, 11, 245.

Sharkady, S. M., & Nolan, J. M. (2001). Bacterial ribonuclease P holoenzyme crosslinking analysis reveals protein interaction sites on the RNA subunit. *Nucleic acids research*, 29(18), 3848–3856.

Sharma, C. M., Hoffmann, S., Darfeuille, F., Reignier, J., Findeiss, S., Sittka, A., Chabas, S., *et al*. (2010). The primary transcriptome of the major human pathogen *Helicobacter pylori*. *Nature*, 464(7286), 250–255.

Sharma, U. K., Chatterji, D. (2010). Transcriptional switching in *Escherichia coli* during stress and starvation by modulation of sigma activity. *FEMS Microbiol Rev*, 34, 646-57.

Sinapah, S., Wu, S., Chen, Y., Pettersson, B. M. F., Gopalan, V., & Kirsebom, L. A. (2011). Cleavage of model substrates by archaeal RNase P: Role of protein cofactors in cleavage-site selection. *Nucleic Acids Research*, 39(3), 1105–1116.

Sittka, A., Lucchini, S., Papenfort, K., Sharma, C. M., Rolle, K., Binnewies, T. T., Hinton, J. C. D., *et al*. (2008). Deep sequencing analysis of small noncoding RNA and mRNA targets of the global post-transcriptional regulator, Hfq. *PLoS Genetics*, 4(8).

Smith, D., & Pace, N. R. (1993). Multiple magnesium ions in the ribonuclease P reaction mechanism. *Biochemistry*, 32(20), 5273–5281.

Sprinzl, M., Horn, C., Brown, M., Loudovltch, A., & Steinberg, S. (1998). Compilation of tRNA sequences and sequences of tRNA genes. *Nucleic Acids Research*, 26(1), 148–153.

Stams, T., Niranjanakumari, S., Fierke, C. A., Christianson, D. W. (1998). Ribonuclease P protein structure: Evolutionary origins in the translational apparatus. *Science*, 280, 752-5.

Steuten, B., Hoch, P. G., Damm, K., Schneider, S., Köhler, K., Wagner, R., & Hartmann, R. K. (2014). Regulation of transcription by 6S RNAs: Insights from the *Escherichia coli* and *Bacillus subtilis* model systems. *RNA Biology*, 11(5), 1-14. doi:10.4161/rna.28827

Steuten, B., Setny, P., Zacharias, M., & Wagner, R. (2013). Mapping the spatial neighborhood of the regulatory 6S RNA bound to *Escherichia coli* RNA polymerase holoenzyme. *Journal of Molecular Biology*, 425(19), 3649–3661.

Trotochaud, A. E., & Wassarman, K. M. (2004). 6S RNA function enhances long-term cell survival. *Journal of bacteriology*, 186(15), 4978–4985.

Trotochaud, A. E., & Wassarman, K. M. (2005). A highly conserved 6S RNA structure is required for regulation of transcription. *Nature structural & molecular biology*, 12(4), 313–319. doi:10.1038/nsmb917

Trotochaud, A. E., & Wassarman, K. M. (2006). 6S RNA regulation of pspF transcription leads to altered cell survival at high pH. *J Bacteriol*, 188, 3936-43. PMID:16707685.

Tsai, H.-Y., Masquida, B., Biswas, R., Westhof, E., & Gopalan, V. (2003). Molecular modeling of the three-dimensional structure of the bacterial RNase P holoenzyme. *Journal of molecular biology*, 325(4), 661–675. doi:10.1016/S0022-2836(02)01267-6

Veeman, W. S. (1997). Nuclear magnetic resonance, a simple introduction to the principles and applications. *Geoderma*. doi:10.1016/S0016-7061(97)00054-2

Vitreschak, A. G., Rodionov, D. A., Mironov, A. A., & Gelfand, M. S. (2004). Riboswitches: the oldest mechanism for the regulation of gene expression? *Trends in genetics: TIG*, 20(1), 44–50. doi:10.1016/j.tig.2003.11.008

Wagner, S. D., Yakovchuk, P., Gilman, B., Ponicsan, S. L., Drullinger, L. F., Kugel, J. F., & Goodrich, J. a. (2013). RNA polymerase II acts as an RNA-dependent RNA polymerase to extend and destabilize a non-coding RNA. *The EMBO journal*, 32(6), 781–90. doi:10.1038/emboj.2013.18

Walker, S. C., & Engelke, D. R. (2008). A Protein-Only RNase P in Human Mitochondria. *Cell*.

Warnecke, J. M., Fürste, J. P., Hardt, W. D., Erdmann, V. A., & Hartmann, R. K. (1996). Ribonuclease P (RNase P) RNA is converted to a $Cd^{(2+)}$-ribozyme by a single Rp-phosphorothioate modification in the precursor tRNA at the RNase P cleavage site. *Proceedings of the National Academy of Sciences of the United States of America*, 93(17), 8924–8928.

Wassarman, K M, & Storz, G. (2000). 6S RNA regulates *E. coli* RNA polymerase activity. *Cell*, 101(6), 613–623. doi:S0092-8674(00)80873-9 [pii]

Wassarman, K. M., & Saecker, R. M. (2006). Synthesis-mediated release of a small RNA inhibitor of RNA polymerase. *Science (New York, N.Y.)*, 314(5805), 1601–1603. doi:10.1126/science.1134830

Wassarman, K. M. (2007). 6S RNA: a small RNA regulator of transcription. *Current Opinion in Microbiology*.

Watanabe, T., Sugiura, M., & Sugita, M. (1997). A novel small stable RNA, 6Sa RNA, from the cyanobacterium *Synechococcus sp*. strain PCC6301. *FEBS Letters*, 416(3), 302–306.

Waters, L. S., & Storz, G. (2009). Regulatory RNAs in Bacteria. *Cell*.

Wehner, S., Damm, K., Hartmann, R. K. and Marz, M (2014). Dissemination of 6S RNA among Bacteria, RNA Biology, in press

Willkomm, D. K., & Hartmann, R. K. (2005). 6S RNA - an ancient regulator of bacterial RNA polymerase rediscovered. *Biological chemistry*, 386(12), 1273–1277. doi:10.1515/BC.2005.144

Willkomm, D. K., Minnerup, J., Hüttenhofer, A., & Hartmann, R. K. (2005). Experimental RNomics in *Aquifex aeolicus*: identification of small non-coding RNAs and the putative 6S RNA homolog. *Nucleic acids research*, 33(6), 1949–1960.

7. Appendix

Publications arising from this work

Köhler K, Duchardt-Ferner E, Wöhnert J, and Hartmann RK: Mechanistic and structural analyses of *Aquifex aeolicus* 6S RNA.

Biochimie 2014 September; Manuscript in preparation

Hoch PG, Köhler K, and Hartmann RK: Advanced mechanistic studies on the transcript-induced structural rearrangement of *Bacillus subtilis* 6S-1 RNA.

Manuscript in preparation

Steuten B, Hoch PG, Damm K, Schneider S, Köhler K, Wagner R, Hartmann RK: Regulation of transcription by 6S RNAs: Insights from the *Escherichia coli* and *Bacillus subtilis* model systems.

RNA Biol. 2014 Apr 23; 11(5). [Epub ahead of print]

Gößringer M, Helmecke D, Köhler K, Schön A, Kirsebom LA, Bindereif A and Hartmann RK: Chapter 1. Enzymatic RNA Synthesis Using Bacteriophage T7 RNA Polymerase

In: Handbook of RNA Biochemistry: Second, Completely Revised and Enlarged Edition; Wiley-VCH 2014 Mar 28. (eds. Hartmann RK, Bindereif A, Schön A and Westhof E)

Acknowledgments

I would like to thank…

…Prof. Dr. Roland K. Hartmann for the possibility to do my PhD in his laboratory and his great supervision.

…Prof. Dr Jens Wöhnert for the possibility to get time and knowledge of you and your group to measure my samples and for reviewing my PhD work.

…Prof. Dr. Klaus Reuter for taking the chair of my examination commission.

…Prof. Dr. Marc Schneider for participating in my examination commission.

…Dr. Elke Duchardt-Ferner for all the efforts and time, the knowledge and great ideas and not least the friendship arisen.

…Philipp for his great ideas, time discussing and mutual understanding.

…Maren and Julia for all the motivation and constructive critic.

…Marcus, Dominik, Dennis W., Clemens, Manu and Bene for all the help and fun.

…Katja and Marina for the administrative support.

…the Hartmann lab for a great time and fun.

…the Wöhnert lab for the help and the coffee breaks.

…my family for their support and help, especially for child care.

and finally Alex and Kira for the helpful devices, appreciation, care and love leading through hard times.

List of figures

List of tables

Acronyms

A	Adenosine
α-ATP	gamma- adenosine tri-phosphate
Amp	Ampicillin
APS	Ammonium persulfate
Aae	*Aquifex aeolicus*
bp	Base pair(s)
BPB	Bromophenol blue
Bsu	*Bacillus subtilis*
C	Cytosine
cpm	Counts per minute
denat.	Denatured
DNA	Deoxyribonucleic acid
DNase	Deoxyribonuclease
dNTP(s)	Deoxynucleoside thrphosphate(s)
DTT	Dithiothreitol
E	Extinction
Ecat	E. coli RNase P RNA catalytic domain
Eco	*Escherichia coli*
EDTA	Ethylenediamine tetraacedic acid
Fig.	Figure
g	Gram
G	Guanosine
h	Hour(s)
HCl	Hydrogen chloride
HEPES	N-2-Hydroxyethylpiperazin-N'-2-ethane sulfonic acid

HOAc	Acetic acid
IPTG	Isopropyl β-D-1-thiogalactopyranoside
kb	Kilo bases
KN	Knut Nierhaus buffer
L	Liter
LB	Lysogeny broth
M	Molar [mol/L]
M1 RNA	*E. coli* RNase P RNA
mA	Milliampere
min	Minute(s)
nm	Nanometer
nt(s)	Nucleotide(s)
NTP	Ribonucleoside triphosphate
OAc	Acetoxy group
$OD_{(600)}$	Optical density (at 600 nm)
ON	overnight
p.a.	pro analysis
PAA	Polyacrylamide
[5‘-P32]pCp	[5‘-P32] Cytidine 3‘,5‘-bisphosphate
PCR	Polymerase chain reaction
pRNA	product RNA (derived from 6S RNA)
RNase	Ribonuclease
RNAP	RNA polymerase
rpm	Revolutions per minute
RT	Room temperature
s	Second

T	Thymine
TB	Terrific Broth
TBE	Tris-Borat-EDTA buffer
TE	Tris-EDTA buffer
Tm	Melting temperature
Tris	Tris-hydrosymethylaminomethane
U	Unit(s) (for enzyme activity)
U	Uracil
XCB	Xylene cyanol blue

Semantics:	G	Giga (10^{9})
	M	Mega (10^{6})
	k	Kilo (10^{3})
	m	Milli (10^{-3})
	µ	Mikro (10^{-6})
	n	Nano (10^{-9})
	p	Pico (10^{-12})
	f	Femto (10^{-15})

Scientific curriculum vitae

Name	Köhler
First Name	Karen
Date of birth	February 25th, 1981
Place of birth	Marburg, Germany
Nationality	German

Education

2008-2014	Ph.D. studies, *Institute of Pharmaceutical Chemistry*, Philipps University Marburg.
2000-2006	Studies in Chemistry (Diploma), Philipps University Marburg. Main topic: Biochemistry

Diploma thesis

Title	"Strukturelle Charakterisierung der Bindung kleiner Liganden und Fragmente an die Metalloenzyme Carboanhydrase II und Thermolysin."
Supervisor	Prof. Dr. G. Klebe (Philipps University Marburg)

Ph.D thesis

Title	"Mechanistic and structural analyses of different non-coding RNAs in bacteria."
Supervisor	Prof. Dr. R.K. Hartmann (Philipps University Marburg)

Experience

Field of interest	Molecular biology, RNA biochemistry, Drug design
Teaching	Supervision of students practical courses and undergraduate students lab courses

Scientific skills and methods

Molecular biology	Work with genetically modified organisms (bacteria); standard DNA technique (preparation/modification); cloning; PCR
RNA methods	*In vitro* transcription (large scale); RNA structural probing; RNA purification; analysis of sRNA-protein binding; structural analysis of RNA by NMR
Protein methods	Recombinant protein expression and purification; protein crystallization alone and in combination with ligands (co-crystallization and soaking); enzyme activity assays (pH-stat and kinetic)
Bioinformatics	Analysis of data (DNA and RNA sequences; Clustal, CLCViewer, etc.); visualization of RNA and protein (CoralDRAW) and their three dimensional structure (Pymol, etc.).

Scientific achievements

Poster presentation	GBM Meeting “RNA Biochemistry & Workshop 'Deep Sequencing and Bioinformatics of RNA'”; September/October 2010, Pforzheim-Hohenwart
	SFB Meeting; September 2012, Bochum
	GBM Meeting “RNA Biochemistry & Workshop 'RNA trafficking'”; October 2012, Bonn
Oral presentation	2nd Meeting “Non-coding RNAs”; March 2009, Hirschegg (Austria)
	6th Meeting “Non-coding RNAs”; April 2013, Hirschegg (Austria)
	7th Meeting “Non-coding RNAs”; April 2014, Hirschegg (Austria)

Publications

Köhler K, Duchardt-Ferner E, Wöhnert J, and Hartmann RK: Mechanistic and structural analyses of *Aquifex aeolicus* 6S RNA. Biochimie 2014 September; Manuscript in preparation

Hoch PG, Köhler K, and Hartmann RK: Advanced mechanistic studies on the transcript-induced structural rearrangement of *Bacillus subtilis* 6S-1 RNA. Manuscript in preparation

Steuten B, Hoch PG, Damm K, Schneider S, Köhler K, Wagner R, Hartmann RK: Regulation of transcription by 6S RNAs: Insights from the *Escherichia coli* and *Bacillus subtilis* model systems. RNA Biol. 2014 Apr 23; 11(5). [Epub ahead of print]

Gößringer M, Helmecke D, Köhler K, Schön A, Kirsebom LA, Bindereif A and Hartmann RK: Chapter 1. Enzymatic RNA Synthesis Using Bacteriophage T7 RNA Polymerase. In: Handbook of RNA Biochemistry: Second, Completely Revised and Enlarged Edition; Wiley-VCH 2014 Mar 28. (Hartmann RK, Bindereif A, Schön A and Westhof E)

Languages

German	Native	
English	Very Good	Ongoing experience in reading English literature, giving talks and writing proposals.
French	Basics	School education for four years
Italian	Basics	School education for one year

Declaration

Ich versichere, dass ich meine Dissertation

„Mechanistic and structural analyses of different non-coding RNAs in bacteria“

selbstständig ohne unerlaubte Hilfe angefertigt und mich dabei keiner anderen als der von mir ausdrücklich bezeichneten Quellen bedient habe.

Die Dissertation wurde in der jetzigen oder einer ähnlichen Form noch bei keiner anderen Hochschule eingereicht und hat noch keinem sonstigen Prüfungszwecken gedient.

Marburg, Juli 2014

_____

Karen Köhler